POLYAMIDE COMPOSITE AGEING CHARACTERIZATION

POLYAMIDE CARBON FIBRE FILLED COMPOSITE AGEING CHARACTERIZATION IN CONVENTIONAL AUTOMOTIVE FLUIDS

By SAMUEL B.N. GRIMSHAW, B.Sc.

A Thesis Submitted to the School of Graduate Studies in Partial Fulfilment of the Requirements for the Degree Master of Applied Science

McMaster University

McMaster University MASTER OF APPLIED SCIENCE (2016) Hamilton, Ontario

(Chemical Engineering)

TITLE:	Polyamide Carbon Filled Composite Ageing Characterization in Conventional Automotive Fluids
AUTHOR:	Samuel B.N. Grimshaw, B.Sc. (Queen’s University)
SUPERVISOR:	Dr. Michael R. Thompson
NUMBER OF PAGES:	xiii, 126

LAY ABSTRACT

The use of carbon fibre-reinforced plastic technology is steadily gaining traction in the modern automotive industry as a lightweight alternative to conventional materials. The versatile chemical resistance of polyamide resins combined with the high strength properties of carbon fibre filler content aims to meet this growing need in the industry. By employing a number of accelerated and amplified ageing techniques, this work assessed the resilience of carbon fibre-reinforced polyamide composites in a variety of foreseeable chemical, temperature, moisture, and stress environments. The composite only showed significant sensitivity to windshield wiper fluid in the tests.

ABSTRACT

The use of carbon fibre-reinforced plastic technology is steadily gaining traction in the modern automotive industry as a lightweight alternative to conventional materials. The versatile chemical resistance of polyamide resins combined with the high strength properties of carbon fibre filler content aims to meet this growing need in the industry. By employing a number of accelerated and amplified ageing techniques, this work hopes to assess the resilience of carbon fibre-reinforced polyamide composites in a variety of foreseeable chemical, temperature, moisture, and stress environments.

The resins included in this characterization study include polyamide-6 (PA6) and polyamide-6,6 (PA6/6). The carbon fibre-reinforced composite specimens are subject to long term immersion in commercial automotive fluids at room and elevated temperatures. Results show that the mechanical properties of both polyamide resins are sensitive to windshield washer fluid exposure, regardless of temperature. The significant drop in glass transition temperature and greater elongation at break confirmed a plasticization effect. The Young’s modulus and tensile strength experienced a loss of approximately 40% at saturation.

Elevated temperatures resulted in increased fluid sorption rates of antifreeze and E-20 gasoline into the PA6 composite specimens. Likewise, a corresponding drop in PA6 composite mechanical properties was noted for the antifreeze and E-20 gasoline at elevated temperatures. The mechanical properties of the PA6/6 composite were largely retained in all tested automotive fluids, except windshield washer fluid, at elevated temperatures. The effect of absorbed fluid on mechanical properties tended to increase with higher fibre loadings for the PA6/6 composite and lower fibre loadings for the PA6 composite.

Finally, a single parameter acoustic emission testing technique was employed to assess internal damage of stressed PA6 composite specimens exposed to different temperature and humidity levels. However, there was no discernible correlation between environmental stress conditions and internal damage for short term exposure times.

ACKNOWLEDGEMENTS

Firstly, I would like to thank my supervisor, Dr. Michael R. Thompson, for his guidance, understanding, and patience during the course of the project. I would also like to thank everyone at General Motors, especially Dr. William R. Rodgers, for their insightful counsel pertaining to the direction and substance of the project. Likewise, I extend thanks to everyone at the Fraunhofer Project Center, notably Dr. Jeff T. Wood, for their role in the preparation and delivery of the polymer composite plates featured in this body of work. Thanks to Ying Fan at the University of Western Ontario for coordinating intermediary material pickup and cross-checking select tensile runs. Special thanks to our machinist, Paul Gatt, for all his work cutting the composite plates at the expense of a good number of saw blades. Thanks to my colleagues for their support and guidance in both life and work hemispheres. Special thanks to Wing Hei Lam for his very active role in fixing the odd malfunctioning humidity sensor, computer drive, HAAKE and SEM work. Finally, I thank my family, both here in Canada and abroad, for their constant love and support.

TABLE OF CONTENTS

LIST OF FIGURES

LIST OF TABLES

LIST OF SYMBOLS AND ABBREVIATIONS

Symbols

d	Fibre diameter
l	Fibre length
l_c	Critical fibre length
σ_f	Fibre strength
$\overline{\sigma}$	Mean fibre strength
τ_i	Interfacial shear stress
V_f	Fibre volume fraction
E	Young's modulus
E_L	Young's modulus in longitudinal direction
E_T	Young's modulus in transverse direction
E_m	Young's modulus of matrix
E_f	Young's modulus of fibre
ε_b	Elongation at break
T_g	Glass transition temperature
T_{gd}	Dry glass transition temperature
T_{gw}	Wetted glass transition temperature
T_m	Melting temperature
M	Moisture content
g	Temperature shift per unit of moisture absorbed
Γ	Gamma function
m	Weibull modulus

m_t	Mass uptake at time ‘t’
m_∞	Mass uptake at equilibrium
k	Constant related to diffusion coefficient and sample thickness
n	Constant related to type of diffusion mechanism
G'	Storage modulus
G''	Loss modulus
η^*	Complex viscosity

Abbreviations

AF	Antifreeze
BR	Brake fluid
PW	Powersteering fluid
MO	SAE 5W-30 motor oil
WW	Windshield washer fluid
GS	E-20 gasoline
PA6	Polyamide-6
PA6/6	Polyamide-6,6
ESC	Environmental stress cracking
HDT	Heat distortion temperature
UTS	Ultimate tensile strength

Chapter 1 INTRODUCTION

1.1. Overview of Long Term Ageing

In the modern automotive industry, the use and application of carbon fibre reinforced polyamide materials are gaining momentum as a light-weight, high strength alternative to conventional support materials. Polyamides and carbon fibres both have well-established physio-mechanical properties that are considered resilient, as separate entities, in a multitude of environments. Figure 1.1 illustrates the projected material composition of the average automobile, with carbon fibres expected to perform a more significant role as reinforcing filler in the future.

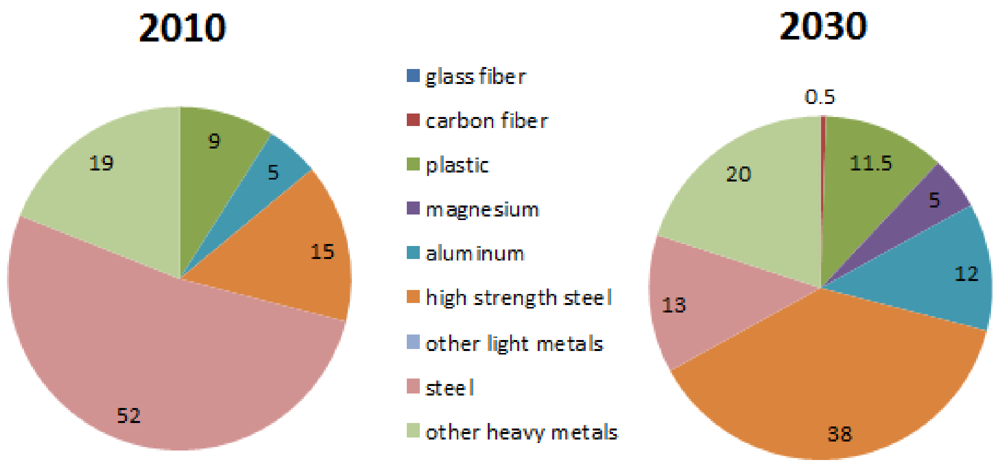

Figure 1.1. Material share for automobile industry in 2010 (left) and projected in 2030 (right) [1].

Despite the appeal that carbon fibre reinforced plastics offer, including the potential weight reduction, strength retention, and chemical resistance, future market penetration is ultimately limited by the part cost associated with the material. Indeed, the cost of using carbon fibres can be between 5-6 times greater than using steel to build a part of equivalent size and function, as depicted in Figure 1.2. While the cost of carbon fibres is projected to come down as the process to produce the fibres is gradually refined and improved overtime, there still remains the issue to justify the use of carbon fibres inside of composite technology today.

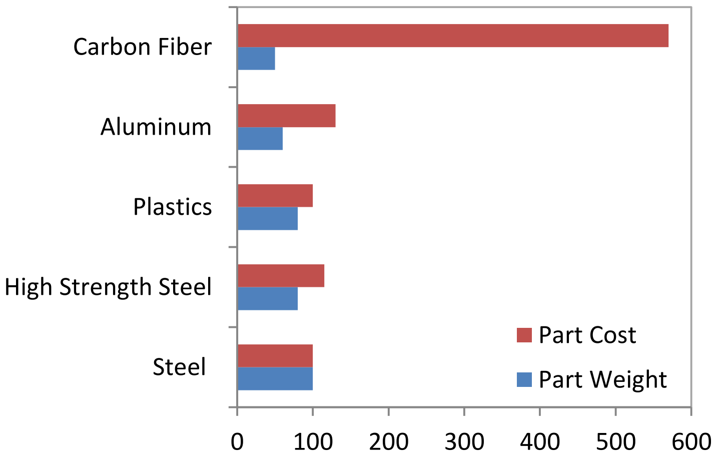

Figure 1.2. Normalized weight and cost of conventional automotive materials [1].

To justify the investment in carbon fibres as reinforcing filler within polyamide matrices for select automotive applications, the original composite properties must be retained in a variety of foreseeable chemical environments for an extended period of time. Polyamides are known to be susceptible to plasticization from small polar molecules, some of which are found in the composition of conventional automotive fluids. Hypothetically, the fibre-dominated properties of the composite may prove to be enough to counter the subsequent ageing effects of the matrix material, assuming the fibres are unaffected by the respective exposure conditions. Difficult-to-incorporate fibre loadings, random fibre orientation and variable length distribution, as well as poor fibre-matrix interfaces may also promote new pathways for fluid absorption compared to the chemical sorption route permitted by the polyamide alone. By employing a number of accelerated and amplified ageing techniques, this work hopes to highlight the potential benefits and limitations of carbon fibres as reinforcement filler in a polyamide matrix with respect to its capacity to resist variable temperatures, moisture content, stress applications, and chemical exposure. The testing standards that were exercised in this work are summarized in the table below:

Table 1.1. Summary of standard methods employed for the characterization and assessment of CF/PA composite ageing across a range of physical and chemical environments.

Measurement	ASTM Testing Standard
Moisture Content	D570
Tensile Testing	D638
Flexural Testing	D790
Carbon Content	D3171
Chemical Reagent Resistance/ESC	D543
Rheological Property Characterization	D4440
Thermal Property Characterization	D3418

1.2. Objectives

The primary intent of this work is to characterize changes, where present, in the physio-mechanical properties of two carbon-filled polyamide composites as it pertains to accelerated ageing techniques which employ chemical immersion, elevated temperature exposure, and short-term environmental stress cracking.

Chapter 2 BACKGROUND

2.1. Composite Physicochemistry

2.1.1. Polyamide Resins

Polymers can be classified in several manners, but the two most general groupings can be distinguished by their thermal processing behavior. Polyamides are an example of a thermoplastic species, which are characterized by long individual chains of repeating monomer units, as shown in Figure 2.1. Since thermoplastics do not possess crosslinks, they allow repeated melting and forming, unlike thermosets. More specifically, polyamides are generally categorized as engineering thermoplastics, given that they have good strength, toughness, abrasion and chemical resistance [2].

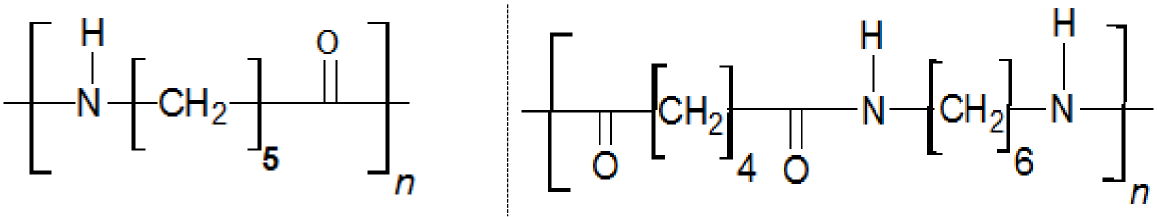

Figure 2.1. Chemical structure for repeating unit found in aliphatic polyamide 6 (left) and polyamide 6,6 (right).

Furthermore, the resins used in this work, polyamide 6 (PA6) and polyamide 6,6 (PA6/6), both have aliphatic chemical structures. The two sub-classes of aliphatic amides, monadic (-AB-) and dyadic (-AABB-) polyamides include PA6 and PA6/6 respectively. The specific structure of PA6/6 allows its chains to align more easily than the PA6 conformation, making their crystallites harder to disrupt, and subsequently results in a lower theoretical solvent uptake and higher melting point. The molecular structures of polyamides are polar, so the attractive forces between them are further increased by hydrogen bonding [3]. These strong intermolecular forces, especially by the stiff amide groups, result in relatively high melting temperatures and act as primary driving forces of crystallization [3, 4]. The two polyamides of this work are therefore, semi-crystalline, meaning that they are comprised of a well-organized, impermeable crystalline phase and an amorphous phase where polymer chains have more freedom of movement (at least above their glass transition temperature). As a result, solvents are more probable to diffuse into the amorphous phase of the polymer matrix. In particular, it is well known that both polyamides are adept at absorbing water, which in-turn leaves the resin susceptible to the effects of plasticization (discussed in 2.2.1) and loss of its dry-state mechanical properties.

2.1.2. Carbon Fibres

The extensive use of carbon fibres in the automotive industry primarily serves to offer a light-weight alternative to metal parts without significant compromises to structural integrity, corrosion, and wear resistance. The mechanical properties of the carbon fibre composite blends can generally be expected to outperform the base polymer matrix by bearing some of the load that would otherwise lead to some mode of material failure. However, the extent of structural reinforcement imparted by this filler material is dependent on a number of factors, including its filler volume content, size and shape, orientation, and wettability by the matrix phases.

Excessively high filler contents (> 30 %vol) intended to maximize thermal, mechanical, and electrical conductivity properties can prove to be detrimental to improving composite performance. For example, Meng and Tjong [5] observed a marked decrease in the break strain with increasing liquid crystal polymer filler content dispersed in a blend of polyamide 6 and maleated polypropylene, which is presumably characteristic of the filler content having a lower break strain than the matrix material. In their case, the structure of the matrix material also appeared to influence the mechanical reinforcement supplied by the filler content volume. When sufficient compatibility existed between the matrix and filler materials, the tensile strength was shown to increase with higher filler concentrations [5], provided that the filler content exhibited a higher breaking strength than the matrix phase. Likewise, the composite tensile strength declines with higher filler concentrations dispersed into a porous-foamy structure because of poor fibre-matrix adhesion [5].

The percolation threshold, a phenomena where there is a sharp rise in electrical conductivity attributed to a critical conductive filler volume dispersed in an otherwise insulative matrix material, may be used to approximate the onset of excessive carbon fibre loadings that will have a limited or undesirable influence on the composite mechanical and rheological properties. For instance, Clingerman et al. [6] noted that the tensile strength and electrical conductivity of a composite containing chopped PAN carbon fibres dispersed into a polyamide 6/6 matrix would plateau near an upper percolation threshold of 20%vol fibre content. Additionally, Motlagh et al [7] observed a marked increase in viscosity near the percolation threshold of 10%vol carbon fibre filler content dispersed in a cyclic olefin copolymer matrix. In terms of achieving optimum processability and performance, with regards to melt flow resistance and tensile strength reinforcement respectively, the carbon loading levels used in this experimental work should attempt to operate near the prescribed percolation threshold.

The fibre geometry, which includes its shape, length, and diameter, influences the distribution of mechanical loading within the filler content dispersed in a polymeric matrix. The cross-section of carbon fibre is circular, but for the sake of a comprehensive discussion this shape is ideal. Indeed, Masoud et al. [8] observed that the circular cross-section of polypropylene fibres dispersed in Portland cement produced the highest flexural strength than compared to equivalent diameter fibres with triangular and hollow cross-sections. Aside from providing a more uniform load distribution [9], round cross-sectional fibres of equivalent diameter have a reduced lateral surface area, which reduces the probability of finding a critical defect along the fibre length [10]. Hence, fibres with smaller diameters are more favorable than compared to thicker fibres in any matrix material. The maximum load transmitted from the matrix to the fibre cannot be achieved unless the fibre length meets or exceeds twice the critical fibre length $\left(l_c\right)$ [11]. The critical length can be determined using equation 1:

$$l_c = \frac{\sigma_f \cdot d}{2 \cdot \tau_i} \tag{1}$$

Equation 1 expresses the critical length as a function of the fibre strength (σ_f), fibre diameter (d), and the interfacial shear stress (τ_i) between the matrix and the fibre. Typically, fibres exceeding 15 times the critical length are regarded as continuous, whereas shorter fibres are labelled as discontinuous. The mean fibre strength can be approximated using equation 2, which utilizes Weibull statistics to model the distribution in fibre strength as a function of fibre length [12]:

$$\bar{\sigma} = \sigma_o \left(\frac{l}{l_o} \right)^{1/m} \Gamma\left(1 + {}^{1}\!/_{m}\right) \tag{2}$$

where l is the fibre length, m is the Weibull modulus, Γ is the gamma function, and σ_0 is the characteristic strength, which is defined as the stress where the probability of the fibre to fail is 0.63. Pardini and Manhani [13] indicated that the PAN-based, high-strength carbon fibre used in their research operated with a dimensionless Weibull modulus between 3.0-3.6 regardless of fibre length, suggesting nearly homogeneous fibre quality where only a few random flaws were responsible for the scatter in fibre strength data. The average fibre strength was also shown to increase as the length of carbon fibre decreased. Within the frameworks of a composite material, longer fibres are more able to promote optimized load transmittance from the matrix material but are likewise more susceptible to premature fracture. Ideally, the longer fibres and subsequent fragments would continue to fracture until the fibre strength of the shorter fragments exceeds the effective transmitted load. As the shorter fibres are no longer capable of relieving the load from the matrix, the composite finally experiences failure itself. Ultimately, the composite material stands to benefit from a larger aspect ratio (l/d), given the need to maximize the fibre length and minimize the fibre diameter.

The orientation of the fibre will have a significant impact on the performance of the final composite product. In simple uniaxial composite layouts, the longitudinal properties are controlled by the fibre, while the transverse properties are controlled by the matrix. The longitudinal Young's modulus can be subsequently estimated using the simple law of mixtures:

$$E_L = V_f E_f + (1 - V_f) E_m \tag{3}$$

where E is the Young's modulus of the fibre (f), matrix (m), and longitudinal composite (L) and V is the respective component volume fraction; the composite strength can likewise be modelled by this simple approach. The law of mixtures in this case assumes uniaxial fibre direction, perfect bonding, negligible void space, and fibre lengths that exceed double the critical length. The transverse modulus (E_T) of the composite may be obtained using the general mathematical expression below, assuming that the fibres are uniform in properties, direction, size, and load transfer [14]:

$$E_T = \frac{1}{\left(\frac{V_f}{E_f} + \frac{1-V_f}{E_m}\right)} \tag{4}$$

With reference to equations 3 and 4, a hypothetical constituent stiffness ratio of $E_f / E_m = 80$ and 25% filler content would result in a transverse modulus that is only 1.33 times the matrix modulus, whereas the ideal longitudinal modulus would be 20.75 times greater than the matrix modulus; both directions will be evaluated in the ageing studies of this work, but it can be seen that strength evaluations in the transverse direction will be more sensitive to changes by solvents on the matrix.

As the angle between the applied stress and fibre direction increases, the mode of failure is increasingly influenced by shear failure in the matrix instead of fibre fracture. Indeed, maximum tensile strength is usually observed for loads applied parallel to the fibre direction, with declining composite performance at intermediate and perpendicular angles respectively [15, 16]. Bakir and Hashem [15] noted that the tensile strength of polyester/fibreglass composites tended to increase with fibre volume fractions up until 30%. This peak filler volume may imply some degree of fibre misalignment, since Jackson and Cratchley [17] found that the tensile strength for metal composites would peak at 20-30% fibre volume content dispersed in random orientations. In polymeric composites, as in the works by Knibbs and Morris [18], carbon fibres that deviated 11° from the parallel load position could expect variances of at least 20% in the composite longitudinal Young's modulus. In contrast, fibre misalignment was less prone to influence the transverse Young's modulus of the composite material considering that the matrix dominated the mode of failure regardless of filler content.

The wettability, which in the context of this work refers to the extent of contact and adhesion of the polymeric matrix to the dispersed fibres, strongly influences the effective load transmittance onto the fibres. The compatibility between the carbon fibres and matrix material is dependent on a number of physical, chemical, and processing conditions. A discontinuous matrix coating enveloping the dispersed fibre network may affect fluid transport through voids and defects along the capillary pathway at the poorly wetted fibre-matrix interface. The interfacial load transfer mechanism is particularly important for discontinuous-fibre composites but also for continuous-fibre composites whose fibres fracture prior to the composite itself [14]. A strong bond between the fibre and matrix mitigates crack propagation along the length of the fibre, increases transverse strength, and potentially improves environmental performance of the composite [14]. Poor fibre-matrix adhesion can be qualitatively assessed by the frequency of clean, striated fibre surfaces pulled from the matrix [19], which may be initiated via cryofracture to retain the original microstructure, under a scanning electron microscope (SEM).

2.2. Ageing Modes and Mechanisms

2.2.1. Chemical Sorption and Degradation

Although plastics generally offer excellent chemical resistance to a wide spectrum of environments, chemical exposure under certain circumstances can gradually impact the physio-mechanical properties of a composite product. In principle, longer periods of exposure can enable chemical interactions with the fibre surface, polymer matrix, and fibre-matrix interfacial regions. The fluid may be drawn into the various regions of the composite material by diffusion through the resin, penetration through defects, cracks, and voids, and by capillary action along the fibre surface. The chemical interactions that subsequently occur may be explicit chemical degradation or conformational changes that subsequently affect the performance of the composite overtime.

The most common mode of chemical attack against polyamides include hydrolytic reactions by water, acid, and alkali, considering the notable susceptibility of the amide and carbonate functional groups. Hydrolysis is, simply put, the condensation reaction set in reverse whereby the polymer chain is slowly fragmented, as illustrated in Figure 2.2.

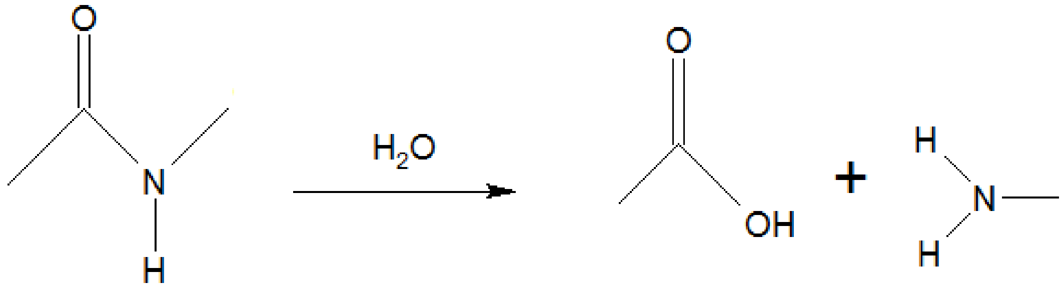

Figure 2.2. General mechanism for hydrolytic attack on amide link resulting in chain scission of bulk polymer chain.

The loss of mechanical properties by hydrolysis may be attributed to a reduction in molecular weight as a result of chain scission. Hydrolysis by water alone is exceptionally slow at room temperature, since polyamides can be repeatedly washed in water without obvious adverse effects [20]. However, the amine functional group can also be easily hydrolyzed from exposure to dilute acid or alkali. Conditions of low (<4) and high (>10) pH will markedly increase the rate of hydrolytic reaction [20]. To be specific, PA6/6 has limited acid resistance compared to its excellent base resistance, but should perform better than its PA6 counterpart [21].

Chemical attack against the carbon fibre component is generally insignificant compared to the inherent strength degradation promoted by the physical defects found along the length of the respective fibre. The hydrophobic nature of carbon fibres would imply limited interaction with water. Wyatt and Ashbee [22] observed that polyester resin swelling in temperate water was insufficient to produce the necessary interfacial tensile stress for any debonding of the carbon fibres to occur. However, it should be noted that the peak dimensional swell of the unfilled polyester resin was only 0.4%, whereas polyamides are known to swell significantly in water. Carbon fibres are, nonetheless, considered stable in a wide spectrum of chemical environments, despite variable susceptibility to a number of oxidizing agents [23]. The effect of the fibre finish, originally intended to improve wettability, damage protection, and/or interfacial strength may also be subject to chemical interaction in exposed environments. For instance, Drzal et al. [24] noted that the interphase region was more brittle in the amine deficient layers created around the carbon fibres of an epoxy composite. Therefore, chemical reagents capable of interacting with this interphase region could potentially interfere with the functionality of beneficial surface groups found on the fibre coating.

Aside from direct chemical attack against the polymer chain, chemical interaction within the polymeric resin may instead take the form of plasticization, which is typically characterized by an increased mobility of the polymer chains located in the amorphous phase. The polar nature of both polyamide resins inherently imply that other polar molecules should be readily absorbed into the amorphous phase of the matrix, as confirmed by the specific solvent uptake in Table 2.1.

Table 2.1. Solvent uptake at sorption equilibrium for exposed polyamide 6/6 specimens as a function of penetrant size and polarity.

Solvent	**Saturated Mass Gain (% w/w)** [25]	**Molar Volume (cm^3/mol)** [25]	**Relative Polarity** [26]
water	9.6	18.0	1.000
methanol	13.2	40.4	0.762
ethanol	11.9	58.3	0.654
ethylene glycol	14.5	55.7	0.790
toluene	1.7	106.1	0.099
p-xylene	2.7	123.3	0.074
n-hexane	1.2	130.7	0.009

There is extensive literature on the effect of water sorption, specifically, and subsequent plasticization of polyamide matrices. Puffr and Šebenda [27] proposed three mechanisms for water to bind to functional groups found in PA6: 1) one water molecule is firmly bound to two different carbonyl groups via two hydrogen bonds, 2) water molecules are loosely bound to an existing hydrogen bond between a carbonyl group and a hydrogen atom of one amide group, and 3) water molecules agglomerate at sites for capillary condensed water, where a water molecule is already bound to either an amide or carbonyl group. The insertion of water, or other small polar molecules, between polymer chains made possible by these hydrogen bonds is generally characterized by increased mobility by the newly spaced out chains. It is common to model the increased chain mobility by tracking the glass transition temperature with respect to moisture uptake, as in equation 5 [23]:

$$T_{gw} = T_{gd} - g \cdot M \tag{5}$$

where T_{gw} is the wetted glass transition temperature, T_{gd} is the dry glass transition temperature, g is the temperature shift per unit absorbed, and M is the percent of absorbed moisture. Plasticized material should exhibit more chain flexibility in the amorphous regions of the polymer than the dry material at the same temperature, so the glass transition temperature is expected to drop with higher levels of known plasticizer uptake.

The rate of solvent uptake into a polyamide matrix depends on a number of factors, which include: the penetrant size, concentration, and polarity; degree of crystallinity; permeability and porosity of the resin; and interfacial strength between the resin and filler materials. Rios de Anda [25], for example, noted that larger sized polar solvents would observe lower rates of mass uptake into PA6/6 resins. Comparatively higher rates of peak solvent uptake for small alcohols were observed for PA6 resins [28], which may be attributed to the higher amide concentration found in PA6 polymer chains. The absorption rates provided in Table 2.1 confirm preferential affinity towards polar solvents and limited mass uptake of the non-polar solvents. Non-polar solvents lack the preferential sites for polar interaction with either polyamide resin for any appreciable rate of mass uptake, and hydrogen bonds formed between amide functions could act as physical crosslinks and deter non-polar solvents from swelling [25].

The transport of small organic solvent molecules across a concentration gradient between the resin surface and enveloping fluid is primarily concerned with diffusion as the mode of fluid uptake into the composite. The polar alcohols listed in Table 2.1 are sufficiently small to diffuse into polyamide membranes, as noted for example by Fillot et al. [28] who found an increased rate of permeability into PA6 membranes as the ethanol content in biofuel mixtures was increased. The nature of the diffusion mechanism for thin film (< 1 mm) planar geometries is best described using equation 6 [29], derived from Fick's law:

$$\frac{m_I}{m_\infty} = 1 - \exp\left[-7.3 \cdot \left(\frac{D_x \cdot t}{h^2}\right)^{0.75}\right] \tag{6}$$

where m is the mass uptake at any time (t) and equilibrium (∞), D_x is the through-thickness diffusion coefficient, h is the sample thickness, and t is the time. Equation 7 may estimate the diffusion coefficient as a function of the fibre volume fraction and unfilled resin diffusion coefficient D_m, assuming unidirectional fibre orientation and that the diffusion by the fibre content is negligible compared to the matrix.

$$D_x = \left(1 - 2\sqrt{\frac{V_f}{\pi}}\right) D_m \tag{7}$$

Fickian diffusion (case I) observes steady mass transfer across a static boundary where the change in mass is proportional to the square root of the penetrant time. Non-Fickian diffusion (case II) is characterized by a transient boundary layer with linear sorption kinetics. Unfortunately, solvent diffusion into solid polymers rarely behaves as case I diffusion. Indeed, the sigmoidal sorption curves of ethanol diffusing into PA6 would suggest predominately case II diffusion [28, 30]. The progressively plasticized polymer layer near the surface presumably forms the transient barrier that is characteristic of case II diffusion.

It is conceivable that capillary action along the fibre-matrix interface may contribute to anomalous diffusion in carbon fibre reinforced composites. Benavente et al [31] adapted the Washburn equation to predict capillary imbibition while subsequently correcting for pore shape and tortuosity. The expression is simplified into the form equation 8, wherein the liquid mass absorbed by capillary action is proportional to the square root of the imbibition time.

$$m_{II} = \phi \cdot \rho \cdot A \cdot \sqrt{\frac{r \cdot \delta \cdot \gamma \cdot \cos\theta}{2 \cdot \eta \cdot \tau} \cdot t} = k\sqrt{t} \tag{8}$$

According to equation 8, the absorption coefficient (k) depends on the composite properties such as the porosity (ϕ), wetted cross-sectional area (A), capillary radius (r), pore shape factor (δ), and tortuosity (τ) as well as fluid properties including the fluid density (ρ), interfacial tension (γ), contact angle (θ), and fluid viscosity (η). Therefore, the absorption coefficient would be expected to reflect the differences in carbon fibre loading and type of fluid that is absorbed by the polyamide composite specimens.

It should be noted that absorption is not strictly dictated by diffusive mechanisms, especially since composites can be markedly influenced by fluid penetration via cracks, voids, and the interface between the fibre and matrix material. Results reported by Paulidou and Papaspyrides [32] showed that strong interfaces between the matrix and filler content would correlate with matrix-dominant absorption behavior, such as a diffusion-controlled rate of uptake. Likewise, weak interfaces could provide an accessible route for solvent penetration and be considered a form of interface-dominant absorption. For example, Zhang et al. [33] declared that the interlaminar shear strength for carbon/epoxy composites decreased by 35% when void content increased from 0 to 4% while noting distinctly higher absorption coefficients and porosity. In terms of poor wettability, it can be inferred that the fibre-matrix interfacial region can be used as a pathway for significant fluid absorption.

2.2.2. Thermal Ageing

Considering that many of the fluid sorption mechanisms are temperature dependent, it should be expected that exposure to elevated temperatures will amplify and/or accelerate the ageing observed by a composite product. The temperature will also influence the organization and mobility of polymer chains, since the polymer chains in amorphous regions of a polyamide matrix will induce less of a hard, brittle ‘glassy’ state with increasing temperature. Thermo-oxidative degradation which refers to the propagation of free radical species in the presence of oxygen to cleave weak bonds along the polymer chains, is typically related to the formation of chromophores in the visible UV spectra. The subsequent ‘yellowing’ of exposed polyamides in literature is well-established, and is an adequate indicator of the extent of thermal ageing taking place over time.

With regards to chemical sorption and degradation, elevated temperatures are expected to immediately influence the rate of diffusion and radical induced damage, respectively. Indeed, Kumar et al. [34] observed an increased rate of solvent uptake, rate of diffusion, and permeation with increasing temperature for high density polyethylene blends. The same modes of mass transfer are likewise applicable to polyamide composites. Changes in color and texture, indicative of some degree of chemical interaction, are also known to amplify according to exposure conditions. For instance, Thompson et al. [35] noticed an imparted discoloration on polyethylene samples immersed in biodiesel blends at 23°C, which became more prominent at the elevated temperature of 80°C. The end loss in stiffness was analogous, but the mechanical properties would plateau more rapidly from exposure at elevated temperatures. Since no additional loss of mechanical properties were observed at higher temperatures, which would usually be expected for temperature dependent chemical degradation reactions, the subsequent plateau shift may be interpreted as an indication of the equilibrium state of plasticization.

The effect of temperature on carbon fibre composites, notably on the interlaminar shear strength, is also an area of interest pertaining to carbon filled polyamide composites. For instance, the interlaminar shear strength of graphite fibres in an epoxy matrix remained relatively stable for temperatures between -50°C and 80°C, but rapidly declined to zero for temperatures exceeding 170°C [36]. Likewise, Agster [37] observed that PA6 fibres, like the interlaminar shear strength of graphite fibres from the previous example, would begin to experience significant losses in strength for temperatures exceeding 80°C. According to Ramazani et al [38], changes in PA6 and PA6/6 tensile properties following 16 hour heat treatment cycles between 50-100°C could be partially attributed to annealing in the amorphous phase, subsequently resulting in higher degrees of crystallinity, more brittle character, and lower breaking loads. It was also noted that the mechanical strength declines for temperatures above the heat distortion temperature (HDT), which is generally used to infer the point of initial softening [38]. The respective HDT values (see Table 3.1) imply that PA6 resins are more likely to permanently deform at elevated temperatures compared to PA6/6 resins.

The discoloration linked to thermo-oxidative degradation of the polyamide resin is also worth noting as an indicator of thermal ageing, provided that it is attributed to the polymer and not an absorbed solvent. It is agreed that the general mechanism for thermo-oxidation in polyamides is for oxygen to attack the N-vicinal methylene group to form a new radical which ultimately results in chain scission, consumption of amide groups, and the formation of carbonyl and carboxyl end groups [39, 40]. Karstens and Rossbach [39] proposed that the UV/VIS active chromophores were produced by chemical structures resulting from a chain reaction pertaining to azomethine (-CH=N-) groups instead of the degradation products. The azomethine mechanism stops once the amine end groups are consumed, which required approximately two hours of exposure at 160°C [39]. However, for the present experimental work, elevated temperature condition will not exceed 80°C, and so the concentration of chromophores, if any, is anticipated to be low, despite long term exposure.

2.2.3. Environmental Factors

Although temperature is a prominent ageing mechanism in all polymers, it is important to also consider the effects of other sources of fatigue, wear and degradation. Atmospheric moisture content, environmental stress cracking (ESC), and even light exposure can all potentially contribute to the mode of failure in composite materials. Erosion of the plastic due to mechanical damage initiated by long term contact with a fluid in motion containing suspended solids, different phases, or at high velocities is assumed to be negligible in the following series of ageing studies. The well-established abrasion resistance of most polyamides generally supports this early assumption. Instead, the static environmental exposure techniques employed in this work assures that the degradation mechanisms, if present, limits the mean effect of an erosion component.

As discussed earlier, the uptake of moisture content generally causes the mechanical properties of the composite material to decline, regardless of the existence of chemical degradation. As the polymer chains in the amorphous regions exhibit increased mobility due to solvent uptake, mechanical properties dependent on the crystallinity of the polymer, like stiffness and tensile strength, are subject to deteriorate. The increased flexibility of the polymer chains can also result in higher elongations of the composite material until it breaks. Fibre-dominated, longitudinal material properties are less sensitive to the effect of plasticization than compared to matrix-dominated, transverse properties. In some instances, residual stresses leftover from the initial composite curing process are relieved through moisture plasticization in the polymer, which results in a sudden increase in the elastic modulus and tensile strength [23]. Aside from residual stresses, the fabrication process may also imprint pre-existing damage, such as inherent surface fibre defects and matrix microcracks, onto the composite material prior to exposure testing.

Crack initiation and propagation are keystone indicators of mechanical damage. Failure usually begins with one or more cracks, commonly found on the surface of the material. Microcracks developed from processing conditions may also be a site for future crack propagation. Certainly, an increase in microcrack density is known to increase the probability of delamination and consequently, fibre breakage thereafter [41]. Stress that is applied to the composite material is magnified at the crack tip [36], until it begins to widen and expand. External stress may be applied to a composite material by fixing it to a three-point flexural rig. Additionally, Reis et al [42] postulated that a combination of severe ageing conditions, with a pre-existing stress field and temperature spike would be sufficient to induce crack propagation for an aliphatic polyamide. Higher stresses may promote greater polymer chain alignment in amorphous regions of the polymer, potentially leaving the material more susceptible to degradative conditions [43]. For example, the magnitude of tensile stress applied to the polymer is known to increase the rate of photodegradation, whereas compressive stress inhibits photodegradation [43].

The mechanisms of photo-degradation are often pre-determined by extraneous groups and/or impurities in the polymer that absorb light quanta to form excited states that ultimately result in chain cleavage [43]. However, the effect of photodegradation is often restricted to the surface, since many polymers form an oxidized surface layer that absorbs the UV/Vis light and prevents further penetration. Nonetheless, Pillay et al [44] observed considerable yellowing of CF/PA6 composites after 600 hours of exposure to UV light, although there was no other evidence to support deterioration in the physico-mechanical properties. However, there was some degree of recrystallization and increased molecular mobility post-exposure, but only for a penetration depth up to 50-60 μm [44]. This means that photo-degradation can be difficult to quantify and has a disputable impact on final aged properties. Photo-degradation was not considered in this thesis.

Chapter 3 MATERIALS AND METHODS

3.1. Materials

The composite plates used in this body of work were supplied by the Fraunhofer Project Center for Composites Research. There are two polymer resins used as the matrix material, including BASF Ultramid A3W PA 6/6 and BASF Ultramid 8202 HS PA6. Each matrix material was reinforced with Zoltek-Panex 35 PAN-based carbon fibres.

Table 3.1. Summary of constituent mechanical properties for composite blends used in experimental work, as quoted by the supplier.

Property	**Ultramid 8202 HS PA6** [45]	**Ultramid A3W PA6/6** [46]	**Zoltek PX 35 Carbon Fibre** [47]
Tensile Modulus (GPa)	2.70	3.00	242
Tensile Strength (MPa)	75	85	4137
Saturated Water Absorption (% w/w)	9.5	8.5	n/a
Density (g/cm^3)	1.13	1.13	1.81
Melting Temperature (°C)	220	260	n/a
Heat Distortion Temperature @ 1.8 MPa (°C)	60	75	n/a

For the PA6 composite study, 25%, 30%, and 50 wt% carbon loadings were subject to long term immersion ageing. The same PA6 composite carbon loadings were used in the environmental stress cracking trials, but also include an intermediate loading level at 40 wt%. The PA6/6 composite characterization work was consistent with carbon fibre loadings at 35%, 40%, and 45 wt% levels. Fibre loadings were confirmed by the Fraunhofer Project Center using thermogravimetric analysis (TGA). The carbon fibres were isolated from the polymeric matrix in accordance with ASTM D3171 Procedure G, such that the composite coupons of various carbon loadings were subject to a partial burn-off of the matrix material at 600°C for 15 minutes within a muffle furnace. A small sample (< 2 mg) of the partial burn-off product was carefully placed on a microscope slide and dispersed using fine tweezers in a transparent silicone oil medium to help separate individual fibre lengths from the char. A series of micrographs tracing the length of the longest visible fibres were superimposed to estimate the carbon fibre length distribution of the respective carbon fibre loading. The lengths of other fibres visible in the superimposed micrographs were also recorded. The partial burn-off product from two other replicate composite coupons of the same fibre loading were likewise analyzed in order to yield a total count ranging between 50-100 individual fibre lengths. The final partial burn-off products were used to estimate the carbon fibre length distribution, shown in Figure 3.1, for the range of experimental carbon loading levels.

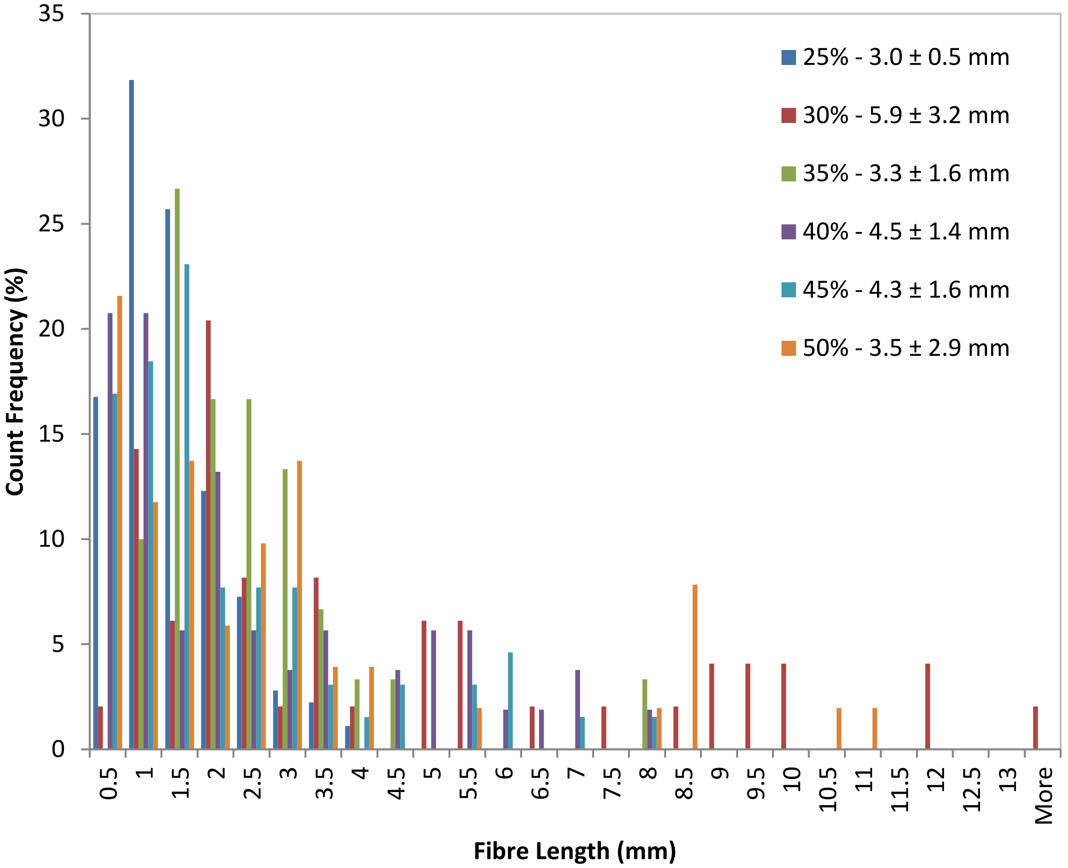

Figure 3.1. Carbon fibre length distributions for partial burn-off products from PA6 composite loadings. Legend gives the weight percent carbon fibre loading of a PA6 composite as well as its nominal fibre length as L_{50} ± standard deviation.

There were six conventional automotive fluids used in the immersion ageing case studies, each of commercial brands, including: 1. Pennzoil® Platinum SAE 5W-30 Motor Oil, 2. Dex-Cool Prestone® Long Life Antifreeze, 3. Prestone® Synthetic Brake Fluid DOT3, 4. Prestone® Power Steering Fluid, 5. Windex™ -40°C Windshield Wash, and 6. E-20 Gasoline (winter grade). The approximate compositions, adapted from relevant SDS/MSDS sheets, of the fluids used in the immersion based ageing trials are summarized in Table 3.2.

The average pH values of the automotive fluids are also provided, which were measured using a VWR sympHony pH probe.

Table 3.2. Main chemical composition of automotive fluids used in immersion-based ageing experiments.

Automotive Fluid	pH	Concentration (% w/w)
Motor Oil [48]	7.50	➢ 0-90% interchangeable low viscosity base oil (< 20.5 cST at 40°C) ➢ 1-5% alkaryl amine ➢ 1-2% alkylated phenol ester ➢ 1-2.4% zinc dialkyldithiophosphate
Antifreeze [49]	8.93	➢ 80-95% ethylene glycol ➢ 0-5% diethylene glycol ➢ 1-5% 2-ethyl hexanoic acid, sodium salt ➢ 1-5% neodecanoic acid, sodium salt
Brake Fluid [50]	10.01	➢ 10-30% diethylene glycol ➢ 10-30% poly(oxy-1,2-ethanediyl), α-butyl-ω-hydroxy- ➢ 7-13% 3,6,9,12-tetraoxahexadecan-1-ol ➢ 7-13% diethylene glycol monobutyl ether ➢ 3-7% poly(oxy-1,2-ethanediyl), α-methyl-ω-hydroxy- ➢ 1-5% diethylene glycol monoethyl ether ➢ 1-5% diethylene glycol monomethyl ether
Powersteering Fluid [51]	7.50	➢ 60-100% highly refined petroleum oils ➢ <1% zinc compounds ➢ <1% proprietary additive
Windshield Wash	10.30	➢ 38.2 ± 0.2% methanol[1] ➢ 61.8 ± 0.2% water
E-20 Gasoline	7.25	➢ 20 ± 2%vol anhydrous ethanol ➢ 80 ± 2%vol premium 91 octane ethanol-free gasoline

---

[1] Windshield wash composition is derived from density measurements at room temperature of an ideal binary methanol-water mixture which assumes negligible influence by any unlisted proprietary components.

3.2. Ageing Conditioning

All CF/PA6 composite test specimens were machined from plates and followed ASTM D638 Type IV dimensions. These specimens were prepared in the transverse direction (90°), such that the load applied during the tensile testing procedure would be perpendicular to the carbon fibre direction. In contrast, the CF/PA6/6 composite specimens were machined from plates according to ASTM D638 Type I dimensions. The CF/PA6/6 composite specimens were prepared in both in the longitudinal (0°) and transverse (90°) flow directions, such that the load applied during tensile testing would be parallel and perpendicular to the carbon fibre direction. To counter the significant level of water absorption by the polyamide matrix material, the composite test specimens were dried for a minimum of 8 hours at 70°C under 15 mm Hg of vacuum before long term static immersion in one of the six automotive fluids.

Room temperature, static immersion involved placing the composite test specimen in a one litre clear plastic canning jar filled with one of the automotive fluids. Each jar would only contain a single fibre loading concentration at any given time. Furthermore, the composite test specimens were marked by physical etches placed on the grip surface faces of the dogbone specimens to distinguish between replicates, cut direction, and the length of time that a sample had been immersed in solution. The jar was subsequently sealed and stored in a laboratory fumehood cabinet for the duration of the prescribed immersion cycle at 20 ± 5°C and 40 ± 10% relative humidity. Three replicate samples per carbon loading level were removed from each fluid at any given immersion time interval. The composite test specimens were sampled after 1, 2, 3, 5, 10, and 20 weeks of storage in a fluid. Once taken out, the test specimen was briefly washed with distilled water for a maximum of 1-2 minutes, and then gently dried with paper towels.

The elevated temperature, static immersion experiments involved placing the pre-dried, marked composite coupons in one of the configurations illustrated in Figure 3.2. The volatility and viscosity of the automotive fluid would ultimately decide whether a heated, circulating fluid bath or a reactor vessel with an overhead water chilled condenser was employed in the elevated temperature immersion runs. The windshield washer fluid and E-20 gasoline mixture, for example, were prone to vaporize at elevated temperatures compared to the other automotive fluids. This tendency could only be countered with good sealing and an overhead chilled condenser. Other fluids were heated in the reactor vessel simultaneously using a circulating bath. Following this procedure, three fluids were tested simultaneously at elevated temperatures for a period of six consecutive weeks.

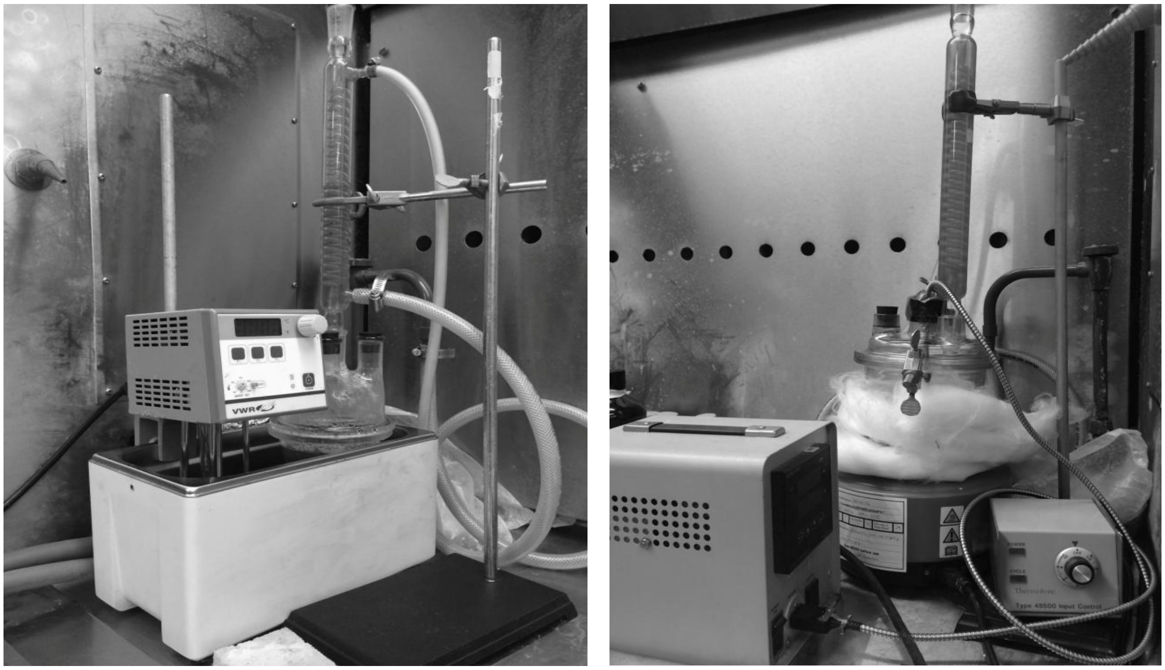

Figure 3.2. Elevated temperature apparatus for long term immersion-based ageing in a temperature controlled circulating bath (left) and reactor vessel with electric heating mantle (right).

The fluid temperature was raised and maintained at 70 ± 5°C for a period of six weeks for each automotive fluid except the notably more volatile E-20 gasoline, which was set to 50 ± 5°C. The liquid level would be periodically renewed for the heated windshield washer and E-20 gasoline in order to retain consistent fluid contact against the immersed composite coupon surfaces. Three replicate samples per carbon loading level were removed from each fluid at any given immersion time interval. For the elevated temperature immersion runs, the composite test specimens would be sampled every week for six weeks. Once taken out of solution, a composite test specimen was briefly washed with distilled water for a maximum of 1-2 minutes, and then gently dried with paper towels.

3.3 Environmental Stress Cracking

A select number of the pre-dried PA6 composite test specimens, which included 25, 30, 40, and 50% carbon fibre loadings, were set aside for short term environmental stress cracking (ESC) conditioning instead of the long term immersion ageing trials. The environmental stress cracking conditions attempted to stimulate an accelerated ageing effect on the composite material through exposure to various levels of heat and humidity while under strain provided by a symmetrical three-point beam deflection apparatus, shown in Figure 3.3. The maximum deflection, regardless of carbon loading, was determined to be 5 mm in order to induce 80% of the flexural stress observed for the tensile dogbone specimens at break. The flexural stress at 5 mm deflection was estimated using an equivalent fraction of the break strain for four rectangular (125 mm x 12.7 mm) specimens at the 25% and 50% fibre loadings in the transverse direction according to ASTM D790 for a span-to-depth ratio of 32:1. For instance, a deflection of 5 mm corresponded to 70% of the flexural break strain for the 25% CF/PA6 composite dogbone specimens. The flexural stress at 70% of the strain at break was 188.3 ± 6.3 MPa for the 25% CF/PA6 rectangular specimens. The flexural strength was nearly 80% of the stress observed at break, which was subsequently 231.0 ± 8.1 MPa for the 25% CF/PA6 rectangular composite specimens. It is assumed that this same loading was applied on the tensile dogbone specimens once deflected by 5 mm at the centre of the beam. Likewise, the presumed flexural stress for the 50% CF/PA6 composite dogbone specimens deflected by 5 mm was determined to be 171.1 ± 13.0 MPa. Again, the conditioned flexural stress was 80% of the flexural stress at break, which was 207.5 ± 37.2 MPa for the 50% CF/PA6 rectangular composite specimens. The flexural stress applied to the 30 % CF/PA6 dogbone specimens was interpolated to yield 184.9 ± 17.4 MPa at 5 mm deflection, using the flexural test data for the 25% and 50% PA6 composite specimens. The flexural stress applied to the 40% CF/PA6 composite specimens was interpolated to yield 178.0 ± 14.2 MPa. In any case, the 5 mm deflections of the dogbone specimens are assumed to operate within 80% of the maximum flexural stress prior to breaking.

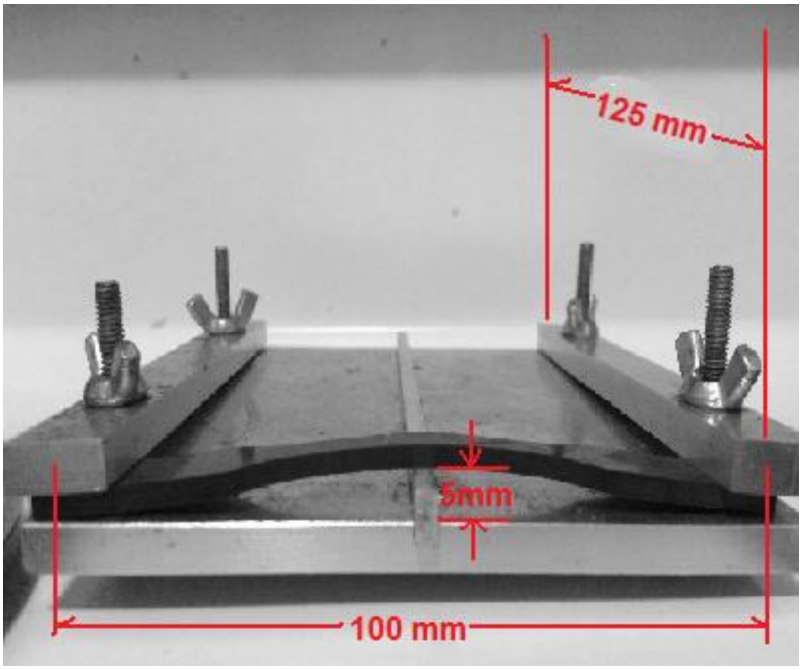

Figure 3.3. Three-point strain device with 5 mm deflection bar used to bend PA6 composite dogbone specimens in conjunction with environmental stress cracking (ESC) conditioning.

Three to five replicate pre-dried PA6 composite dogbone samples simultaneously mounted into the beam deflection apparatus were placed in a freezer for an hour so that the system temperature equilibrated to -30°C as the initial condition for environmental stress cracking. After an hour, the deflected specimens were quickly pre-heated under a thermoformer to the desired surface temperature, then moved into a nearby horizontal air flow oven, shown in Figure 3.4, already at the desired operating temperature and humidity levels. There were nine ESC conditions tested within the oven chamber, which included surface temperatures at 50, 60, and 70°C and relative humidity levels at 5, 25, and 50% respectively. The temperature was tracked by a thin-wire J-type thermocouple attached to the surface of one of the deflected samples. The relative humidity was monitored by a capacitance hygrometer suspended over the deflected samples within the oven chamber.

Figure 3.4. Makeshift apparatus used to control temperature and humidity settings for short term environmental stress cracking tests.

The deflected samples would remain in the oven for an hour, so that steady state temperature and humidity conditions had been attained. A personal cool mist humidifier connected to the oven was used to partially control humidity levels within the chamber. A small motorized fan inside the connecting funnel tubing further adjusted the water vapor level into the oven chamber, as required. Multiple open glass jars filled with hot tap water were also inserted into the oven chamber to reach higher humidity levels at the higher operating temperatures. An overlapping pattern of wax paper was used to minimize loss in relative humidity within the oven chamber, especially during the transfer stage from the preheater. After an hour of exposure at the designated ESC condition, the deflected samples would be immediately returned to the freezer to rapidly bring the specimens back to room temperature and potentially induce some form of thermal shock on the system. Once at room temperature, the PA6 composite samples are released from the deflection bar apparatus and are set for the successive characterization study.

Characterization first included visual inspection of the deflected specimens under a reflected light microscope for signs of surface matrix cracking that were not present prior to ESC conditioning. Next, two ultrasonic sensors would be coupled to opposite grip ends on the test specimens. The reflected acoustic emission signal is compared to the wave signature produced prior to ESC conditioning. More specifically, the peak amplitude variance was used to quantify potential internal damage. Finally, the deflected test specimens were mechanically tested following the procedure outlined in section 3.4.3 to note any significant shifts in the ultimate tensile strength that could be attributed to the ESC conditions.

3.4. Apparatus Testing Procedure

3.4.1. Macroscopic Analysis

The macroscopic analyses encompassing the characterization of physical attributes of the composite test specimen, including sample mass, thickness, and colour. The physical attributes of samples preceding environmental conditioning were compared to average values from a control batch of material not subject to any of the aforementioned ageing techniques. The mass of the dry tensile coupon was measured and reported to the nearest 0.001 g. The dimensions of each tensile specimen were measured using a micrometer that was capable of reporting to the nearest 0.001 mm. With regards to the immersion trials, any potential gains in sample mass and thickness were attributed to solvent uptake by the composite material overtime. The mass uptake and swelling of the test specimens were estimated with respect to the average weight and thickness measurements of pre-dried specimens at a given carbon loading.

The specimen colour was measured after it was removed from an immersion jar, but prior to mechanical testing, using a PocketSpec ColorQA colour reader. Three independent colour readings were recorded per specimen from the two end grips and middle area of the narrow cross-section of the dogbone. The colour data are presented in CIE 1932 X-Y chromaticity units, in order to illustrate any potential yellowing trends in the 2D color scale while immersed in the various automotive fluids at room and elevated temperatures.

3.4.2. Microscopic Analysis

Microscopic analyses involved the characterization of surface topography of the bulk composite sample, quantification of carbon fibre sizes, and the qualitative evaluation of the fibre-matrix interface. Surface roughness scans were conducted for a number of select PA6 and PA6/6 composite specimens using the Zygo NewView 5000 White Light Interferometer at 2X magnification. With regards to the environmental stress cracking tests for the PA6 composite specimens, a Nikon AZ100 Multizoom reflected light microscope was used to detect any prominent surface microcracks found at the area of maximum flexural deflection before and after exposure to the variable temperature-humidity settings. A VWR VistaVision transmission light microscope was used to measure the carbon fibre length distribution of the partial burn-off products of the PA6 composite coupons. The fibres were suspended in transparent silicone mineral oil, to help deter the formation of aggregate fibre clusters. Finally, a JEOL JSM-7000F scanning electron microscope (SEM) equipped with a Schottky Field Emission Gun discharging an electron beam at 10keV was used to assess the quality of the fibre-matrix interface for the PA6 composites. Dry samples designated for SEM analysis were briefly chilled in liquid nitrogen to mitigate carbon fibre dislocation in the matrix during the subsequent manual break event. The fracture zone of the individual composite samples was the targeted area for SEM work pertaining to the characterization of the fibre-matrix interface.

3.4.3. Mechanical and Acoustic Testing

Mechanical testing monitored the change in the Young's moduli, ultimate tensile strength, and elongation at break as a function of ageing conditions. Strain was determined using the extension reading automatically recorded by the mechanical tester, divided by the gauge length (25 mm for PA6 composite and 50 mm for PA66 composite). At least three dry 50% CF/PA6 composite tensile specimens utilized an extensometer to record the true strain at the gauge length. The true strain was compared to the strain recorded by the mechanical tester such that the true extension was approximated as 35.5% of the measured extension for all PA6 composite specimens in order to normalize the data pertaining to the elastic moduli and strain at break. The elastic moduli and strain at break for the unexposed PA6/6 composite specimens were normalized with respect to the given mechanical data for the same composite loadings to accommodate the difference in strain readings from the mechanical tester. For instance, the elastic modulus was multiplied by a factor of 2.94, 3.57, 2.56, and 3.33 for the 35% longitudinal, 40% longitudinal, 40% transverse, and 45% longitudinal fibre loadings. The same factor correction was applied to exposed PA6/6 composite specimens. Likewise, the strain at break was corrected by a factor of 0.23, 0.22, 0.19, and 0.21 for the 35% longitudinal, 40% longitudinal, 40% transverse, and 45% longitudinal fibre loadings respectively. Tensile tests for the PA6 composite specimens were conducted using an Instron 3366 Mounted Mechanical Testing System with a 5 kN load cell at a crosshead rate of

3 mm/min until material failure was observed. The larger PA6/6 composite specimens were tested using a MTS Criterion Model 43 mechanical testing system with a 50 kN load cell at a crosshead rate of 5 mm/min.

A single-parameter acoustic emission testing (AET) technique was employed to distinguish any potential internal damage to the dispersed fibres from the surface matrix cracking as a result of the ESC conditioning of the PA6 composite specimens. The AE monitoring system comprised of two sensors, including a F30α 150-750 kHz High Sensitivity Flat Frequency response sensor and a Panametrics-NDT C604 2.25 MHz Standard Contact transmission sensor, whose signals were pre-amplified to 40 dB and sampled with a 10 MHz 12-bit four channel simultaneously-poling data acquisition card connected to a computer running LabView™ v.2013. The transmitter and receiver AE sensors were fastened onto opposite grip ends of the PA6 composite test specimens using high vacuum grease couplant before and after ESC conditioning. Hit detection would register a significant AE event for any signal exceeding the threshold value of 2 mV. Data would be subsequently sampled at a rate of 2 MHz.

3.4.3. Thermal and Rheological Characterization of Composite Films

The inherent variability between tensile dogbone cuts made it difficult to accurately assess the specific rates of fluid uptake using a bulk average method. To overcome this problem, the mass uptake and thickness swell/shrinkage of PA6 composite films (0, 25, and 50 wt% CF content) immersed in antifreeze, brake, and windshield washer fluid was tracked to simulate the characteristic fluid absorption in the original composite test specimens. The composite films were made from virgin PA6 resin and Zoltek-35 carbon fibre that was mixed together according to the desired carbon weight fraction using a Thermo Haake Rheocord at 240°C. The solidified mixture was then ground into a fine aggregate powder using a pelletizer, before being hot pressed into a film. The film thickness did not exceed 0.25 mm for the unfilled and 25% carbon loadings and was under 0.50 mm for the 50% carbon loading.

The PA6 composite films used in the specific fluid studies were weighed and measured to track the rate of fluid of absorption and swelling, then examined using a Thermo Fisher Scientific Nicolet 6700 FTIR with a smartiTR diamond ATR to check the film composition post-immersion after 1, 3, 5, and 10 weeks of room temperature fluid exposure. The thermal properties were assessed according to ASTM D3418 with a Digital Scanning Calorimeter Q200. Approximately 6-8 mg was cut from one of the exposed composite films in order to run a modulated heat ramp test from 20°C to 250°C at a scan rate of 4°C/min and nitrogen purge of 50 mL/min.

The PA6 composite mixtures originally prepared for the fluid-film study were also molded into 25 mm diameter discs to characterize the general rheological properties using a Rheometric Scientific ARES parallel plate rheometer. The critical strain level is estimated from a dynamic strain sweep test run from 0.1 to 100% strain at 225°C and 275°C for the PA6 and PA6/6 specimens respectively. A dynamic frequency sweep from 0.1 to 100 rad/s was then ran at the same temperature conditions and the predetermined critical strain level to further characterize the molecular structure of the melt flow.

Chapter 4 LONG TERM STATIC IMMERSION

4.1. Room Temperature Immersion

The physico-chemical ageing study involved the long term static immersion of 25, 30, and 50% CF/PA6 composite specimens in antifreeze, brake, power steering, motor oil, windshield washer, and E-20 gasoline fluids for a period of 20 weeks. The focus of the characterization in this chapter is to note significant post-exposure changes in physical, thermal, and mechanical properties for aged specimens. The rheological properties and fibre-matrix interfaces of unexposed composite specimens will also be compared in order to appreciate the effect of carbon loading content on the matrix. To assess the mode and mechanism of solvent uptake, a number of PA6 composite films were immersed in select automotive fluids to model the possible mass transfer occuring for the thicker, tensile dogbone specimens used in the long term immersion tests.

4.1.1. Polyamide 6 Composite Film Case Study

The shear-thinning character of the PA6 composites prepared by batch mixer is depicted in Figure 4.1; these fibres will be shorter in length than in the plaques from FPC but since the purpose of this work was aging effects, the results were only considered comparative. The complex viscosity curves show that the low carbon fibre loading (25 wt%) exhibited a melt flow behavior comparable to the unfilled PA6 specimens. Additionally, the non-Newtonian flow behavior at low frequencies is increasingly perceptible for higher carbon loadings. This is because the low frequency rheological response is more sensitive to the composite structure. The subsequent shear thinning may be attributed to the gradual alignment of fibres within the bulk polymer melt flow. The shear thinning is also present to a lesser degree for the 25% carbon loading, suggesting the onset of a transition away from polymer-dominated melt behavior.

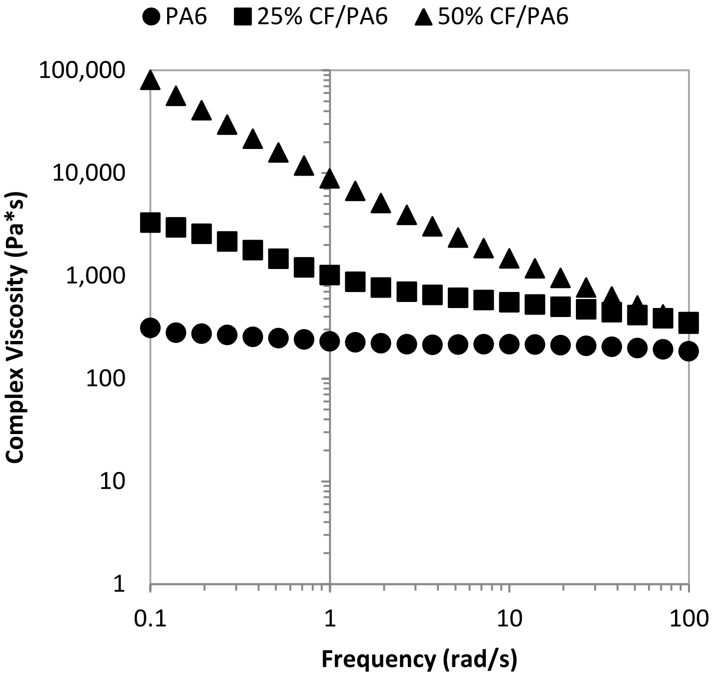

Figure 4.1. Complex viscosity of PA6 composite specimens at 240°C.

Abbasi [52] noted that increasing carbon nanotube filler content for a polycarbonate base would lead to greater fibre-fibre interaction, ultimately restraining the motion of polymer chains. It is possible to infer from Figure 4.1 that increased fibre content will likewise inhibit the flowability of the enveloping polyamide matrix at lower frequencies, especially for carbon filler weight fractions above the 25% threshold.

The increasingly elastic response with higher carbon loadings, manifested by the increasing storage moduli (see in appendix, Figure A.1, Figure A.2, and Figure A.3), suggests the formation of a fibrous percolation network. The increased carbon fibre content would subsequently increase the probability of fibre-fibre contact, leading to the purported network structure that responds elastically at low frequencies. Significant jumps in low frequency properties may indicate a transition from a viscoelastic liquid to solid-like behaviour controlled by the fibre content. Insufficient carbon loadings were evaluated to pinpoint the exact rheological percolation threshold for the PA6 composites. Nonetheless, the percolation threshold is expected to lie just above 25% carbon fibre loading, since the low frequency (20 rad/s) storage moduli at the 50% fibre loading is five times the storage moduli at the 25% fibre loadings (Figure A.4). The mechanical properties would be expected to plateau for carbon loadings above the percolation threshold, assuming ideal wettability of the fibres. Therefore, the unaged mechanical properties of the carbon loadings assessed in this work should not vary significantly for perfect wetting conditions. However, the quality of the fibre-matrix interface is not necessarily independent of the respective carbon loading content.

The poor wettability of the fibre content could hypothetically lead to an accelerated fluid uptake at higher carbon loadings, assuming an interface-dominant absorption mechanism into the composite. The relative solvent uptake of unfilled, 25%, and 50% CF/PA6 composite films are provided in Figure 4.2 over a period of 3 weeks (500 hours) in antifreeze, brake, and windshield washer fluid at room temperature.

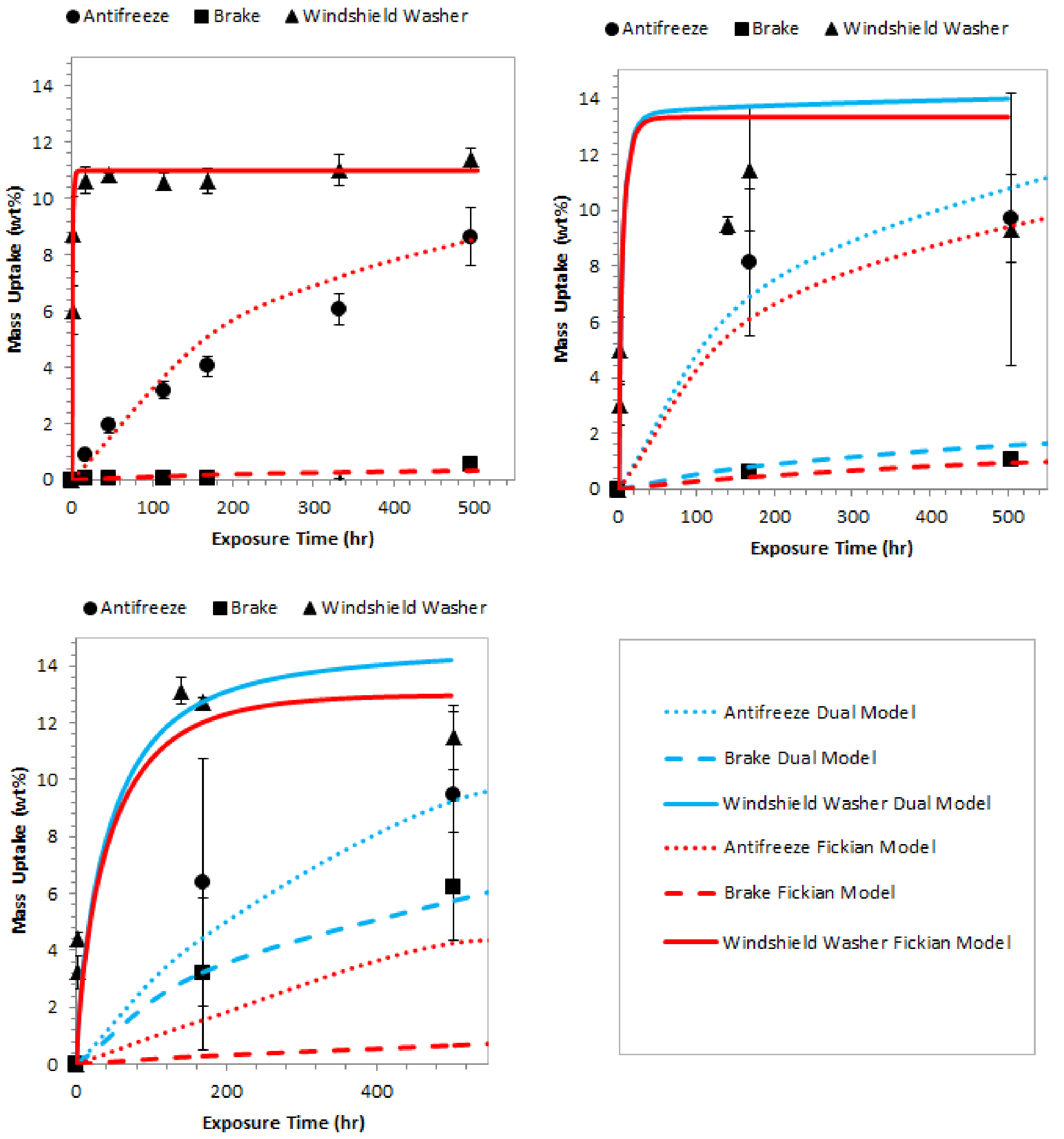

Figure 4.2. Select automotive fluid absorption after room temperature immersion of neat PA6 (top-left), 25% CF/PA6 (top-right), and 50% CF/PA6 films (bottom-left).

The rate of fluid ingress is initially fitted using a Fickian diffusion model (equation 6) in order to approximate the diffusion coefficients for the unfilled resin in antifreeze, brake, and windshield washer fluids at room temperature. The rate of fluid ingress into the 25% and 50% CF/PA6 composite films uses the unfilled diffusion coefficient that is corrected for fibre volume content according to equation 7. Although the Fickian diffusion fluid ingress model appears to be sufficient for the lower 25% carbon fibre loading, Fickian diffusion significantly underestimates the rate of actual fluid ingress into the 50% CF/PA6 composite films. Therefore, a dual-stage transport model comprised of capillary-based convection (equation 8) and Fickian diffusion corrected for fibre volume is used to provide a superior fit to the actual fluid ingress observed at higher fibre loadings. Consequently, the capillary absorption constant was the only fitted variable to the model for the composite samples, assuming only capillary action changes between the composites of different carbon fibre content. The diffusion and capillary-absorption coefficients are summarized below in Table 4.1.

Table 4.1. Specific automotive fluid diffusion coefficients (Dx) and absorption coefficients (k) estimated used to fit Fickian and capillary-based transport models to the fluid ingress observed for the PA6 composite films.

Fibre Loading (wt%)	**0 wt%**		**25 wt%**		**50 wt%**	
	D_x (mm^2/h)	k (g/h$^{1/2}$)	D_x (mm^2/h)	k (g/h$^{1/2}$)	D_x (mm^2/h)	k (g/h$^{1/2}$)
Antifreeze	$2.5\cdot10^{-5}$	0	$1.3\cdot10^{-5}$	$9.0\cdot10^{-5}$	$7.5\cdot10^{-6}$	$5.3\cdot10^{-4}$
Brake Fluid	$5.0\cdot10^{-6}$	0	$2.7\cdot10^{-6}$	$4.5\cdot10^{-5}$	$1.5\cdot10^{-6}$	$5.5\cdot10^{-4}$
Windshield Washer Fluid	$1.5\cdot10^{-3}$	0	$8.0\cdot10^{-4}$	$4.5\cdot10^{-5}$	$4.5\cdot10^{-4}$	$1.5\cdot10^{-4}$

The absorption coefficients indicate a signifcant influence imparted by the capillary action component of the fluid ingress model for the 50% CF/PA6 composite films, which are nearly ten times greater than the fitted absorption coefficients observed for half the fibre loading. The unfilled and 25% CF/PA6 composite films are comparitively dominated by Fickian diffusion. Botelho et al [53] reported circular voids along the fibre-matrix interface in CF/PA laminates, although the overall void content tended to be lower for higher fibre volume fractions. Regardless, the purported higher fluid uptake rate for the filled PA6 composite films may be the result of fluid trapped along this fibre-matrix interface.

The saturated mass uptake is ultimately controlled by the polymer free volume, assuming that the carbon fibres do not absorb nor swell in the various automotive fluids. Since the polymer content decreases with higher carbon loadings, the saturated mass uptake should only be considered as a proportional change relative to the actual amount PA in the composite, not relative to the original total mass of the composite, in order to see trends where absorption is differing from normal penetration into neat PA. Consequently, the saturated mass uptake for the 25% and 50% fibre loadings are corrected with respect to the mass fraction of the polymer matrix to account for the part of the composite that is capable of absorbing the fluid. Hence, the plateau mass of solvent uptake for antifreeze and windshield washer are equivalent for all fibre loadings on a per volume basis of PA6. The saturated mass uptake of brake fluid, though less than the other two fluids, appeared to increase with higher carbon fibre loadings, instead of decrease proportionally with respect to the available polymer volume. The increasingly poor wettability and subsequent voidspace for higher carbon loadings may account for the increased uptake of the brake fluid; the lack of affinity of this fluid with PA may limit its modes of entry by being unable to effectively diffuse into the polymer matrix compared to the small polar compounds found in antifreeze and windshield washer fluid.

According to the model diffusion coefficients, the windshield washer fluid is absorbed the fastest, followed by the antifreeze, then the brake fluid for comparable PA6 composite films. This is attributed to the affinity between the polyamide matrix and the relative differences in the small polar molecules found in the three fluids. The methanol component of windshield washer is most readily absorbed by the polyamide as the relatively small molar volume assures relative ease navigating into the free volume of the adjacent polymer chains. The diols present in antifreeze and brake fluid are notable polar molecules that share an affinity towards the polyamide matrix, but lack the ability to appreciably diffuse into the matrix due to their inherently larger molar volumes. Antifreeze observes higher rates of diffusion relative to brake fluid because of the high concentration of ethylene glycol, a simple polar molecule, in its composition. The complex polar molecules found in brake fluid are considerably larger with respect to molar volume. The reason the diffusion coefficient for brake fluid is comparable to the antifreeze value at the 50% fibre loading is attributed to the increased likelihood of both fluids occupying the void space between the poorly wetted fibres.

The IR spectra of the immersed composite films further shows that solvent absorption is taking place. The IR spectra of the neat automotive fluids are provided in Figure 4.3 and can be easily identified by their characteristic absorption peaks. The characteristic peaks found in antifreeze share a number of absorption bands with ethylene glycol, notably the O-H stretching at 3350 cm^{-1}, C-O stretching at 1040 cm^{-1}, and methylene rocking at 880 cm^{-1} [54]. The brake fluid composition is more ambiguous, but the characteristic peak at 3430 cm^{-1} implies the presence of a complex alcohol or diol group while the intense band at 1100 cm^{-1} suggests the presence of an ether (C-O) group. In methanol, the regions of intense absorption occur at 3682, 2976, 2846, 1467, and 1056 cm^{-1} [55], all of which are accounted for in the IR spectra for the windshield washer fluid. The band broadening around the 3300 and 1600 cm^{-1} peaks may be explained by the overlapping O-H stretching and bending of the water molecules also present in the windshield washer fluid [56].

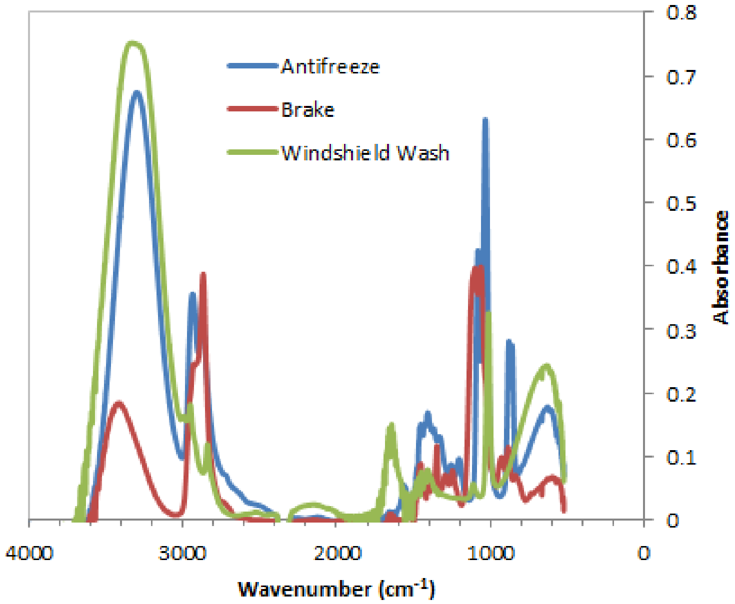

Figure 4.3. IR spectra for antifreeze, brake, and windshield washer fluids.

A fluid is presumably absorbed by the composite if the characteristic absorption peaks of the fluids appear in the IR spectrum of the exposed composite specimens. Figure 4.4 shows the IR spectra of the PA6 composite films after being immersed in antifreeze, brake, and windshield washer fluids for five weeks at room temperature. The characteristic peaks of the composite film specimens exposed to antifreeze and brake fluids, especially at higher fibre loadings, closely resemble the IR spectra of the respective fluid shown in Figure 4.3. The composite film specimens exposed to windshield washer fluid show some band broadening near the 3300 cm^{-1} hydroxyl group region, suggesting some degree of fluid uptake, although the peak intensity does not accurately reflect the significant sorption of the fluid that is known to have occurred. Once taken out of solution, the PA6 composite film specimens may not be able to retain the same volume of absorbed fluid for long periods of time, which may explain the weak peak intensity of the characteristic peaks of the fluid found in the IR spectra of the exposed composite film. The higher volatility of the components found in windshield washer fluid, which partially differentiates it against the antifreeze and brake fluid, may also lend to an accelerated leakage of the absorbed fluid following the allotted immersion time.

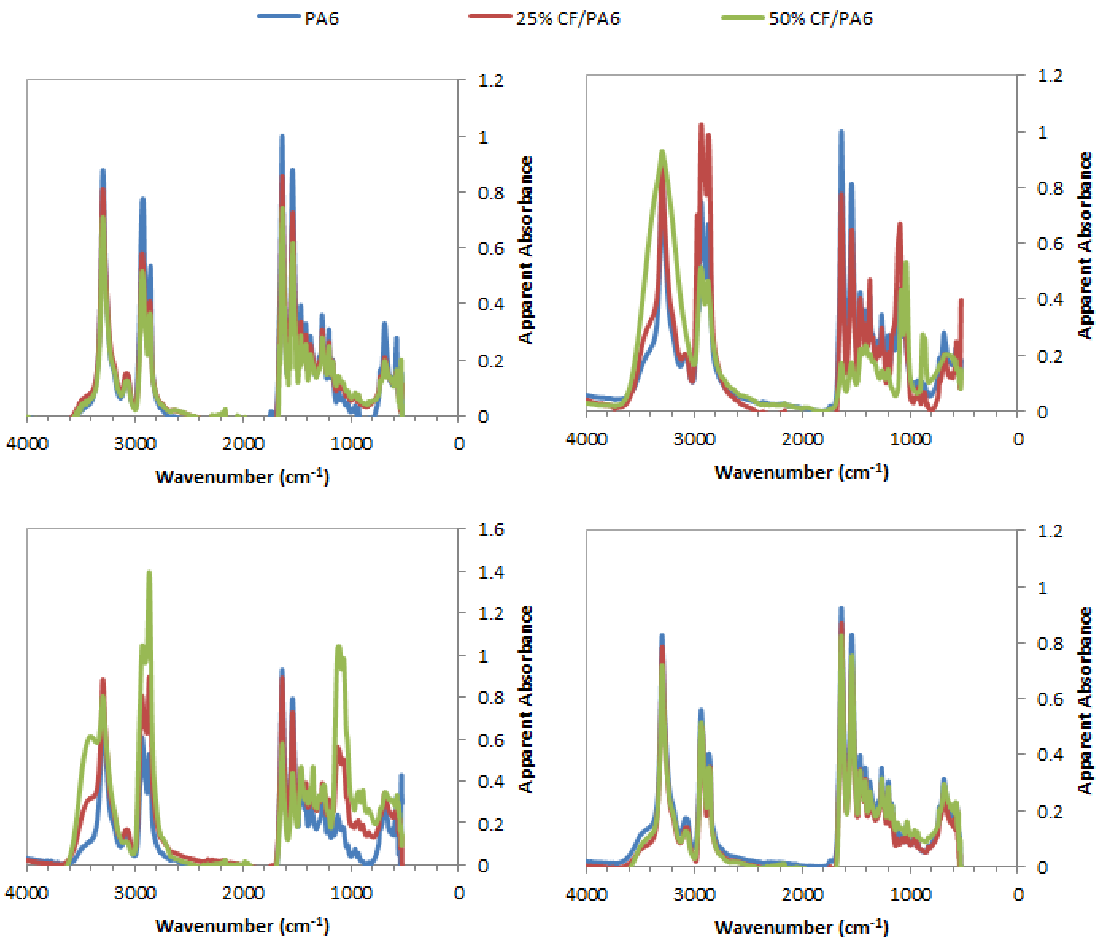

Figure 4.4. IR spectra for unfilled, 25% and 50% CF/PA6 composite films pre-exposure (top-left), after 5 weeks exposure to antifreeze (top-right), after five weeks exposure to brake fluid (bottom-left), and after five weeks exposure to windshield washer fluid.

The characteristic peaks of unfilled PA6 are nearly identical for each carbon loading level. The primary absorption bands of the unexposed (0 wk) PA6 composite films include the N-H stretching at 3290 cm^{-1}, methylene asymmetric stretching at 2920 cm^{-1}, methylene symmetric stretching at 2850 cm^{-1}, C=O stretching at 1630 cm^{-1}, and C-N stretching at 1540 cm^{-1} [21]. It is evident from Figure 4.7 that antifreeze has been absorbed into the PA6 composite films by noting the distinct band broadening of the N-H peak, which is attributed to O-H stretching of the ethylene glycol at 3310 cm^{-1}. The appearance of C-O stretching at 1040-1080 cm^{-1} also supports the presence of the antifreeze in the composite. Interestingly, the IR spectra of the 50% CF/PA6 composite films distinctly resemble the IR spectra of the absorbed fluid. The increasingly anomalous fluid ingress noted at higher fibre loadings, inferred from the absorption coefficients in Table 4.1, may be the result of fluid transport along the fibre-matrix interface via capillary action. This change in IR spectra may be indicative of the probability of the infrared beam detecting isolated pockets of absorbed fluid trapped along the fibre-matrix interface near the surface of the composite film. Wapner and Grundmeier [57] had likewise associated the normalized intensity of the D_2O symmetric stretch band to sites of D_2O concentrations found in discontinuities in a thin layer of adhesive. In the case of this polyamide composite film study, the peak broadening observed for higher fibre loadings may suggest that the absorbed fluid sits along a similar stretch of discontinuities, like the fibre-matrix interface, given the significant void space noted previously for higher carbon loadings. A similar phenomenon is observed for the composite films immersed in the brake fluid and windshield washer regarding the carbon fibre content and shape of the IR spectra.

The glass transition temperature of the PA6 composite film specimens may also be used to assess the extent of solvent aided mobility in the amorphous phases of the polyamide matrix. Considering the significant mass uptake of antifreeze and windshield washer fluids by PA6 film specimens of 10-11% on a polymeric mass fraction basis, these solvents were selected to characterize how they plasticize the polymer matrix. Recall that equation 5 predicts a drop in the wetted glass transition temperature with increased plasticizer uptake. The change in glass temperature for immersed PA6 composite films is depicted below, in Figure 4.5.

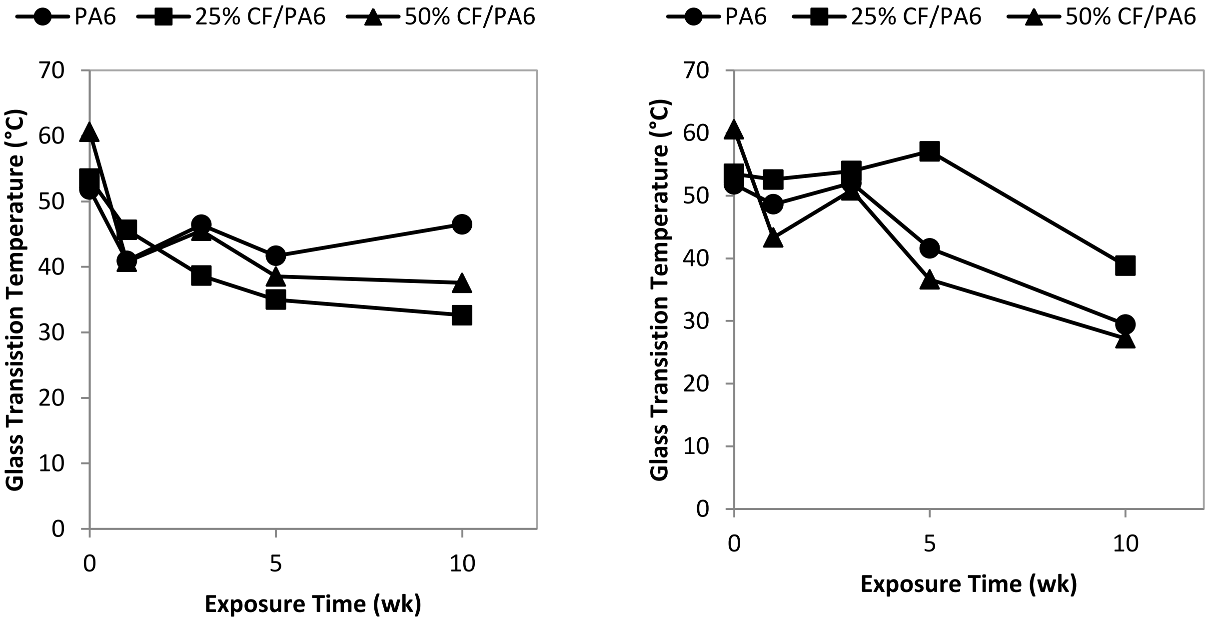

Figure 4.5. Change in glass transition temperature (±20% uncertainty) for PA6 composite films immersed in antifreeze (left) and windshield washer fluid (right) at 23°C.

The glass transition temperature, prior to any fluid exposure, appeared to increase incrementally with higher carbon loadings, from 52°C to 60°C at the unfilled and 50% carbon loadings respectively. This agrees with the expectation that the increased fibre content would restrict polymer chain mobility from various wall effects [58]. The 30-50% drop in glass transition temperature is immediately apparent for PA6 composite specimens immersed in windshield washer fluid.

Likewise, plasticization is inferred from the 10-40% drop in the glass transition temperature observed for carbon loaded film specimens immersed in the antifreeze. The change in glass transition temperature for specimens exposed to brake fluid is not greater than the 20% standard deviation noted for unaged film specimens. Hence, that data was not shown. Both the 25% and 50% carbon fibre loadings experience a 40% drop in the glass transition temperature after 10 weeks of exposure to antifreeze at room temperature. In contrast, the unfilled PA6 composite films immersed in antifreeze for 10 weeks only experienced a 20% drop in the glass transition temperature, which is nearly half the loss reported by the two other loadings despite similar rates of fluid uptake on a polymer volume basis, which may be inferred from Figure 4.2. It would appear that the carbon filler content expedited plasticization of the polyamide matrix with exposure to antifreeze.

Certainly, the 30% and 50% drops in glass transition temperature for the 25% and 50% CF/PA6 composite films exposed to windshield washer for 10 weeks agrees that higher fibre content tends to promote plasticization of the matrix. However, the drop in the glass transition temperature does not appear to reflect the rapid uptake of the windshield washer fluid, which plateaus after 100 hours of immersion according to Figure 4.2. In contrast, the glass transition temperature only begins to significantly shift after 5 weeks (840 hours) of exposure to the windshield washer fluid. Once removed from solution, it is conceivable that the absorbed windshield washer fluid partially evacuated the cavities it once filled via capillary action. Plasticization is likewise reversible and dependent on the content of windshield washer fluid trapped within the boundaries of the composite film. A lower apparent fluid content within the composite film will yield a lower drop in the glass transition temperature. Therefore, the test coupon designated for thermal analysis may not contain the same fluid content as when it was first removed from solution, especially considering that the testing delay could be as long as five hours between measuring the initial fluid content and conducting the thermal analysis test to approximate the glass transition temperature.

While the rate of plasticization are affected by increased fibre loadings, the affinity between the polyamide matrix and the small polar molecules found in the automotive fluids ultimately dictates the magnitude of the drop in T_g. Both methanol and ethylene glycol, found in windshield washer and antifreeze respectively, share relatively similar polarities, but the reduced molar volume of the methanol (given in Table 2.1) may allow it to fit between polymer chains with greater ease than compared to ethylene glycol. Hence, the PA6 composite is more readily plasticized in windshield washer than antifreeze, despite the high concentration of ethylene glycol found in the later solution.

No significant change in the degree of crystallinity or melting temperature was observed with respect to room temperature fluid exposure. However, the degree of crystallinity appeared to decrease with higher carbon loadings, where

27 ± 5%, 26 ± 3%, and 20 ± 2% crystalline volumes were noted for unfilled, 25%, and 50% carbon loadings respectively. Therefore, it could be inferred that higher carbon loadings may be more susceptible to plasticizer content given the higher fraction of amorphous regions within the matrix. The higher diffusivity coefficients (noted in Table 4.1) for higher carbon loadings, attributed to weakening wettability ensure rapid transportation of the plasticizer content to amorphous sites. The IR spectra of higher carbon loadings support the claim that the absorbed solvent sits on the fibres within the interface region, especially in the case of higher carbon loadings given the relationship between the concentration and normalized band intensity. The IR spectra would have been expected to show evidence of minor band broadening of the original PA6 spectra if the fluid diffused into the matrix uniformly. Instead, the characteristic peaks of the absorbed fluids are predominant for the higher carbon loadings, suggesting solvent agglomeration at a site of discontinuity, such as the fibre-matrix interface.

4.1.2. Polyamide 6 Composite Case Study

The quality of the fibre-matrix interfaces for the PA6 composite plaques from FPC with 25, 30, and 50% carbon fibre loadings are shown by SEM images in Figure 4.6, Figure 4.7, and Figure 4.8 respectively. The 25% CF/PA6 specimen shows evidence of good wettability of the fibres, since the matrix is seen to adhere to individual fibre strands. At higher carbon loadings, it is noticed in the images that there is a marked increase of void space between the fibres and matrix.

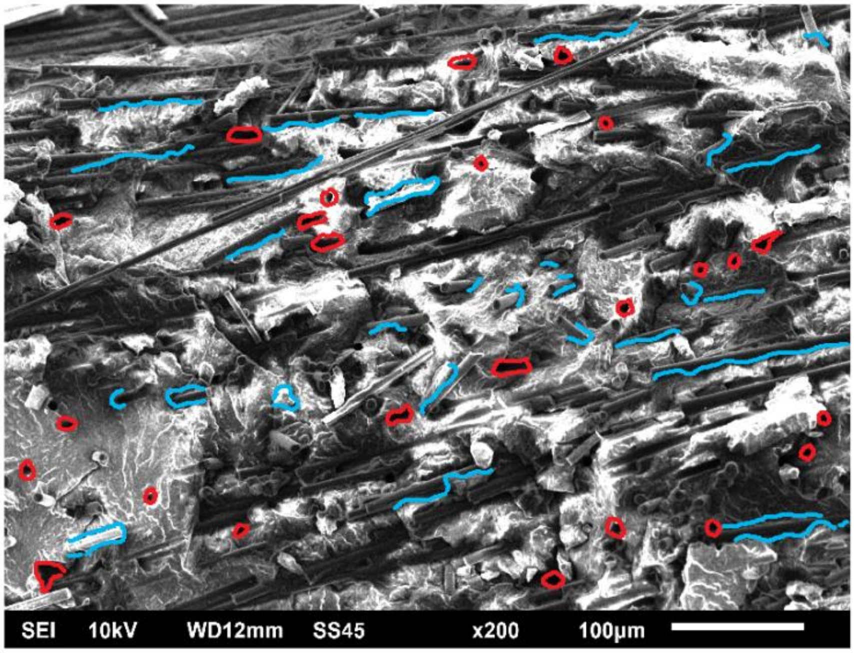

Figure 4.6: SEM micrograph of fibre-matrix interface at fracture surface of a 25% CF/PA6 specimen. Light blue outline highlights good fibre-matrix interface and red outline highlights poor adhesion, voids, and/or sites of fibre pullout.

The relative abundance of clean striated fibres and cavities resembling a fibre pullout (see Figure 4.7) suggests weaker wettability of the carbon fibres for weight loadings above the 25% filler threshold. The fibre-matrix interface is especially poor in the core region of the 50% CF/PA6 specimen (see Figure 4.8).

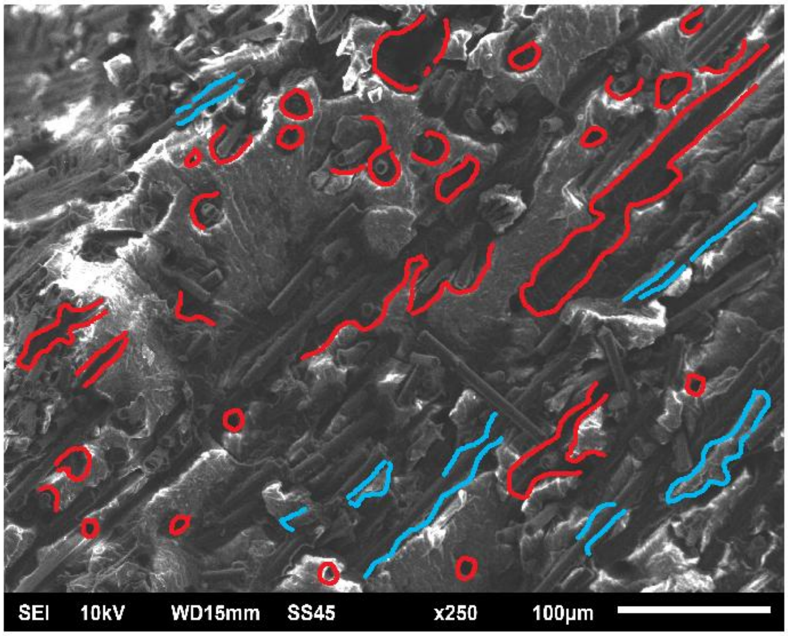

Figure 4.7: SEM micrograph of fibre-matrix interface at fracture surface of a 30% CF/PA6 specimen. Light blue outline highlights good fibre-matrix interface and red outline highlights poor adhesion, voids, and/or sites of fibre pullout.

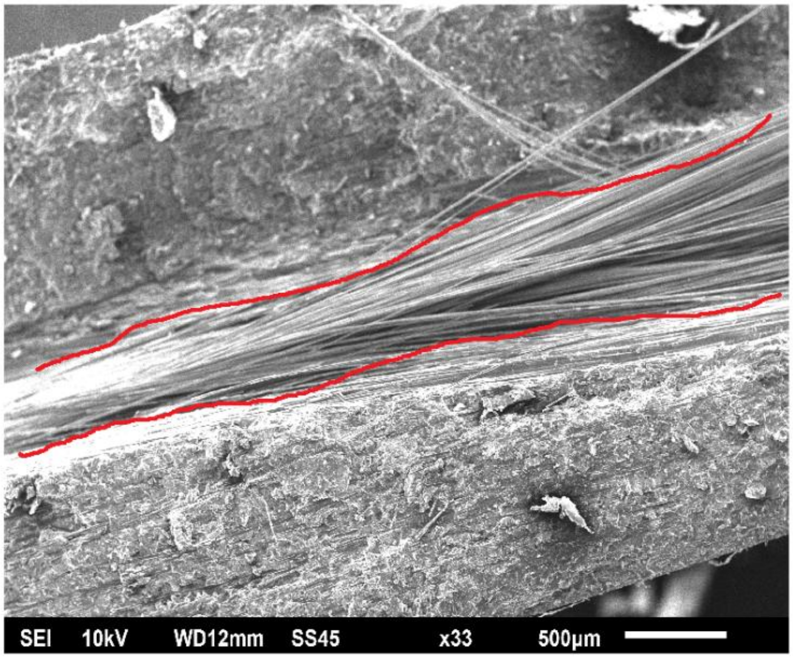

Figure 4.8: SEM micrograph of fibre-matrix interface at fracture surface of a 50% CF/PA6 specimen. Light blue outline highlights good fibre-matrix interface and red outline highlights poor adhesion, voids, and/or sites of fibre pullout.

The matrix material appears to sandwich the carbon fibre filler content in the case of the 50% carbon fibre loading, which results in a disproportionate concentration of the fibres within the central cross-sectional area of the composite. As a result, the wettability of fibres in the core of the plaque suffers, which in-turn, implies sub-par load transmittance from the matrix onto the filler content. The material properties of the composite, therefore, become more matrix-dependent as the filler content increases and the fibre wettability decreases.

The mass plateaus in fluid uptake for the PA6 composite dogbone test specimens immersed in various automotive fluids (shown in Table 4.2) generally correspond with the saturated mass uptake modelled by the PA6 composite films immersed in antifreeze, brake, and windshield washer fluid. The rate of solvent ingress for the tensile composite specimens is somewhat analogous to the PA6 composite films. For example, the peak mass uptake of 25% CF/PA6 composite specimens immersed in windshield washer and antifreeze is observed after 10 weeks of exposure. This is similar to the projected exposure time for the thicker dogbones as postulated by equation 6 using the diffusion coefficients obtained from the composite film study. In this case, it is apparent that the sample thickness is responsible for the longer time required to saturate the composite sample in the same automotive fluid. Furthermore, the peak solvent uptake and swelling generally appears to be constant with respect to the volume of PA6 present in the composite. Hence, the volume of fibre content does not appear to siginificantly influence the relative mass uptake of solvent, which implies a matrix-dominant sorption mechanism, despite the poor wettability noted for the higher carbon loadings.

Table 4.2. Maximum mass uptake relative to polymer mass fraction and swell thickness for PA6 composite specimens immersed in conventional automotive fluids for 20 weeks (3360 hours) at 23°C.

	Relative Max Mass Uptake (wt%)			***Max Thickness Swell (%)***		
Fluid	**25% CF**	**30% CF**	**50% CF**	**25% CF**	**30% CF**	**50% CF**
AF	5.2 ± 2.5	4.7 ± 0.7	2.4 ± 5.2	3.2 ± 1.9	3.4 ± 2.1	3.0 ± 1.4
BR	1.7 ± 2.8	1.4 ± 1.0	2.8 ± 2.2	3.0 ± 1.0	2.6 ± 0.2	3.2 ± 2.1
PW	3.3 ± 2.9	2.6 ± 1.6	3.4 ± 2.4	3.5 ± 1.4	3.0 ± 0.7	4.6 ± 1.5
MO	1.5 ± 6.5	2.9 ± 0.6	2.4 ± 5.4	2.6 ± 1.8	3.1 ± 1.0	3.3 ± 1.1
WW	7.9 ± 5.3	11.7 ± 0.9	8.6 ± 1.6	9.0 ± 3.0	10.5 ± 1.9	7.3 ± 2.3
GS	2.5 ± 6.4	8.4 ± 5.3	1.0 ± 2.4	4.2 ± 2.4	3.7 ± 1.6	4.0 ± 1.8

The only fluid that consistently promotes significant swelling is the windshield washer fluid, which is unsurprising considering the affinity of polyamides for small polar molecules like methanol. Oddly enough, the PA6 composite specimens do not appear to absorb significant volumes of the antifreeze and E-20 gasoline, despite both containing notable concentrations of other small polar molecules, like ethylene glycol and ethanol, which have a known sorption history with polyamides. In this case, the sample thickness is the limiting diffusion factor considering that the predictive diffusion curves are consistent with the data reported above. The diffusivity of the ethanol, like ethylene glycol, is ultimately constrained by the fact that it is considerably less polar and greater in size than a simple alcohol like methanol.

The color of the PA6 composite test specimens was assessed using 1931-CIE-xy chromaticity coordinates in order to detect any subtle shifts that would indicate ‘yellowing’ of the matrix material, which is a common ageing precursor for polyamides. The average chromaticity of untreated PA6 composite samples are [0.312, 0.324], [0.312, 0.324], and [0.312, 0.326] for 25%, 30%, and 50% carbon loadings respectively. The initial chromaticity readings of unaged composite specimens did not appear to be a significant function of the carbon loading. A yellow shift using this particular color space would involve tracing a gradual upward diagonal path towards the coordinates [0.400, 0.450] where the color yellow is transmitted. As an example, the color shift for 25% CF/PA6 test specimens immersed in windshield washer fluid is provided in Figure 4.9. It should be noted that the use of this 2D color space only considers chromaticity and neglects brightness, meaning that any potential subtle color fading may be unintentionally overlooked.

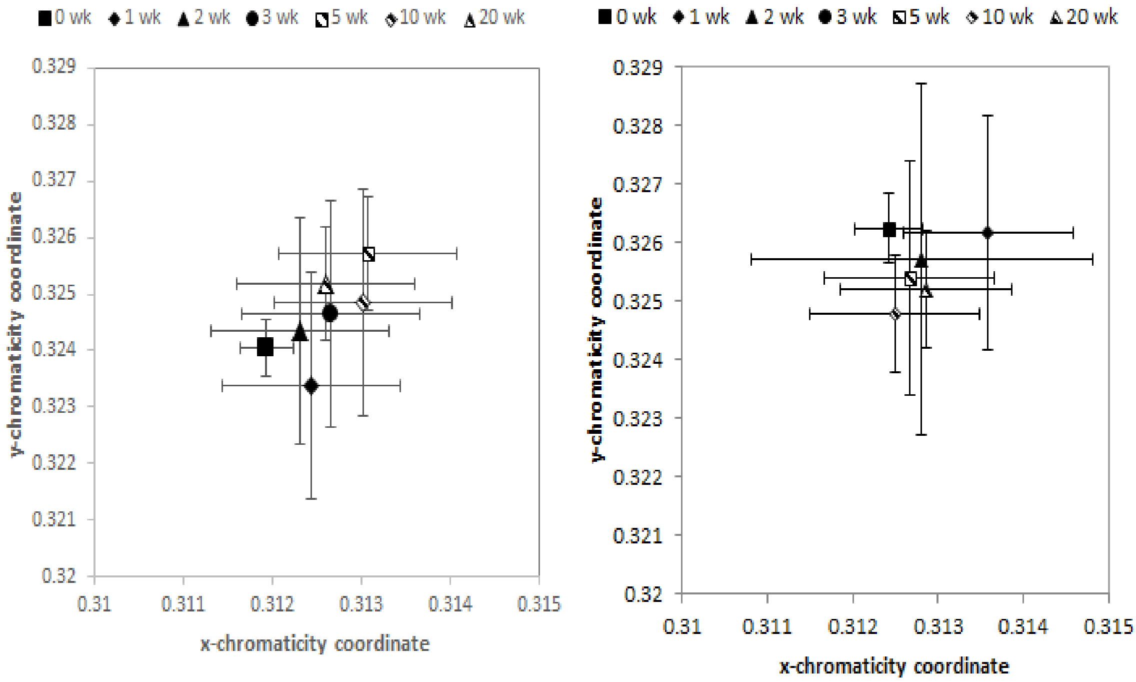

Figure 4.9. CIE xy chromaticity diagram for 25% CF/PA6 (left) and 50% CF/PA6 (right) composite test specimens immersed in windshield washer at 23°C.

Although a subtle diagonal trend appears to exist for the 25% CF/PA6 composite test specimens immersed in windshield washer fluid, the end color shift does not appear to be statistically significant enough to be able to claim that the fluid influenced the color regime of the composite surface. Indeed, the random color data clustering observed for the 50% CF/PA6 specimens also immersed in windshield washer supports that long term fluid exposure has a negligible effect on the color. Random data clustering, attributed to the heterogeneous color profiles of individual test specimens, is observed for all PA6 composite test specimens, regardless of fluid, immersion time, or carbon loading.

The effect of fluid exposure on the composite surface is not necessarily limited to the characteristic color profile, but could potentially extend to changes in surface texture as well. The surface topography of untreated 25% and 50% CF/PA6 are shown in Figure 4.10 for examples.

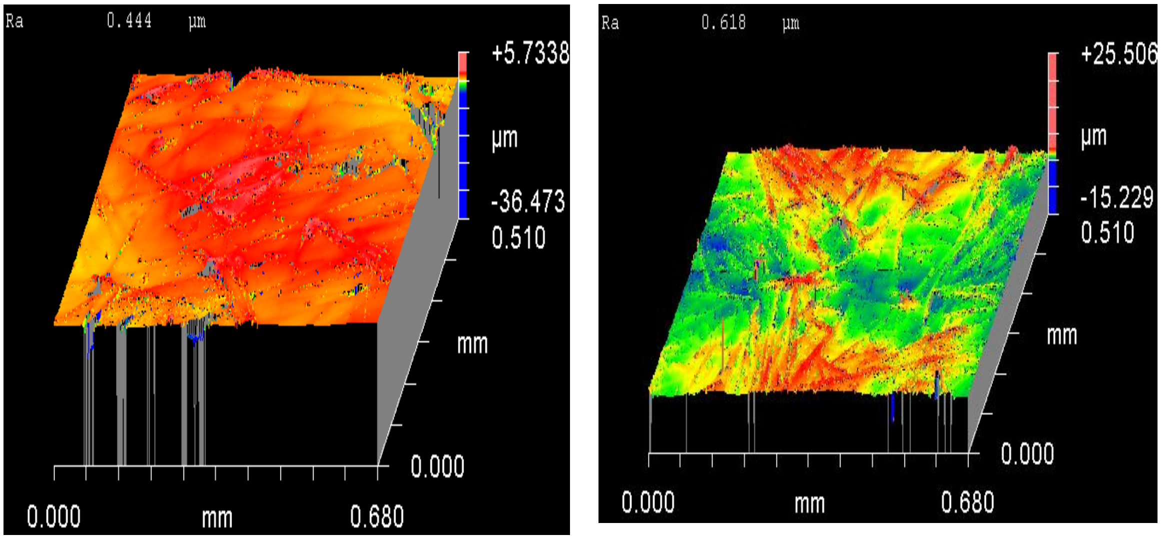

Figure 4.10. Surface topographies of 25% CF/PA6 (left) and 50% CF/PA6 (right) prior to immersion.

It is immediately evident from the texture profiles in Figure 4.10 that the original non-aged 50% CF/PA6 specimen had a significantly (~40%) rougher surface than compared to the lower 25% fibre loading. The increased surface roughness for higher carbon loadings is attributed to the increased frequency of carbon fibres embedded at the surface of the composite test specimen. Exposure to select automotive fluids at room temperature is shown in Figure 4.11 for 25% CF/PA6 composite test specimens.

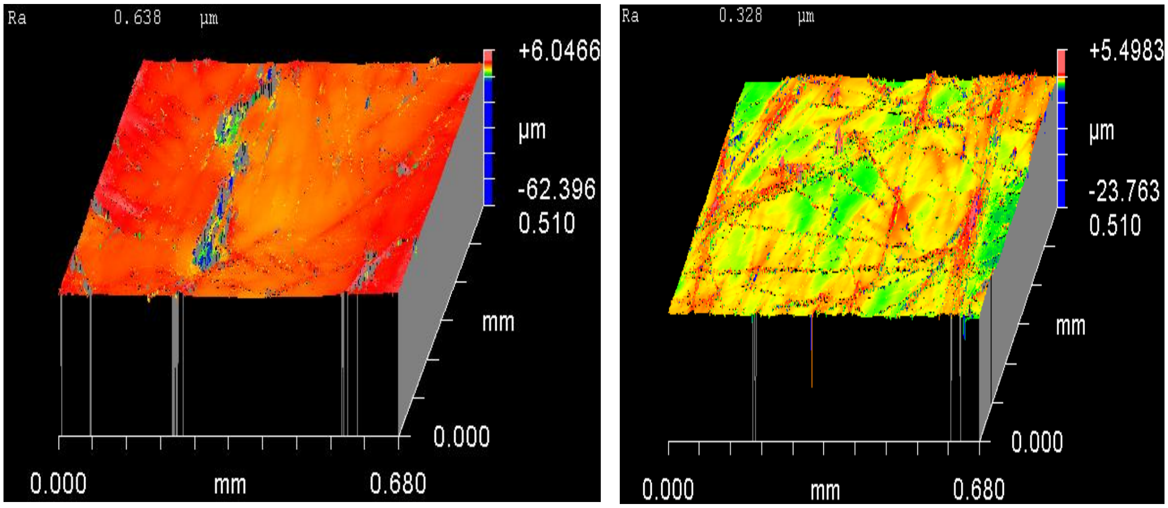

Figure 4.11. Surface topography of 25% CF/PA6 specimen after being immersed in E-20 gasoline for 20 weeks (left) and windshield washer fluid for 10 weeks (right) at 23°C.

The uniform height profile characteristic of the lower carbon loading is largely retained after long term exposure to E-20 gasoline. Likewise, the average surface roughness (Ra) does not appear to be significantly affected by exposure to windshield washer fluid. However, exposure to windshield washer fluid appears to have pushed some of the carbon fibres, denoted as ‘orange-red’ in the height plot, against the surface of the surrounding matrix as it swells. The lower ‘green’ cavities may infer the location of impermeable crystalline regions within the matrix while the higher ‘yellow’ regions may be the amorphous regions that are subject to swell once exposed to small polar molecules, like those found in windshield washer fluid. A quick area calculation of the purported crystalline regions of the 25% CF/PA6 specimen immersed in windshield washer suggests that the degree of crystallinity is approximately 25%. This estimated value aligns nicely with the average degree of crystallinity (26 ± 3%) reported for the analogous 25% CF/PA6 composite film specimen, reinforcing the belief that these regions were in fact crystallites.

The mechanical properties strongly depend on the carbon fibre length, concentration, orientation, and wettability. The theoretical transverse Young's modulus (E_T) and ultimate tensile strength (UTS) of the dogbone specimens may be estimated using the data from Table 3.1 and equation 4. The law of mixtures for a unidirectional composite material predicts that the transverse elastic moduli should be 3.25 GPa, 3.41 GPa, and 4.36 GPa for 25%, 30%, and 50%wt carbon loadings. Likewise, the tensile strength would be expected to increase from 90.4 MPa, 94.6 MPa, and 120.5 MPa for 25%, 30%, and 50%wt carbon loadings. In reality, the mechanical properties, as shown in Figure 4.12, do not adhere to an ideal composite framework. For instance, the ultimate tensile strength markedly decreases with higher fibre loadings, even prior to any form of long term fluid ageing. As such, it may be inferred that the surface contact between the dispersed fibre content and the bulk matrix is less thorough at higher fibre loadings considering that the load transmittance is subpar.

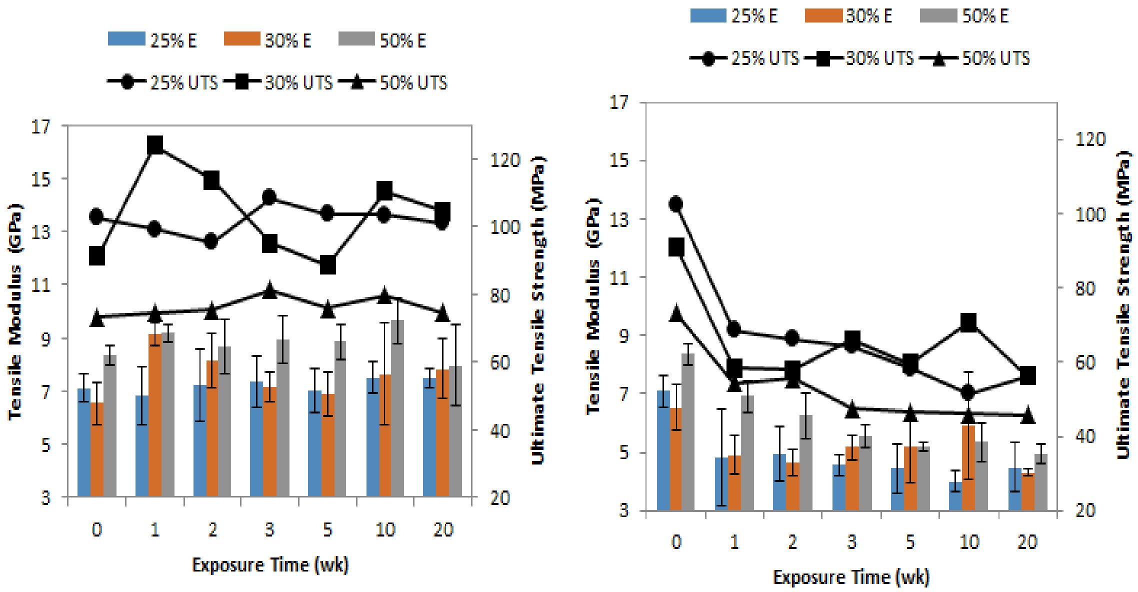

Figure 4.12. Tensile mechanical properties of transverse-oriented PA6 composite specimens for room temperature immersion in antifreeze (left) and windshield washer (right) over 20 weeks.

The transverse Young's modulus is markedly higher than the values predicted by equation 4, which may be attributed to uneven fibre distribution and orientation within the polyamide matrix. While the material stiffness agrees with the ideal model in that it increases with carbon loading, regardless of fluid exposure, the tensile strength appears to decrease with fibre weight loadings exceeding 25%. This later observation seems to correlate with the adverse fibre wetting noted for increased carbon loadings. The only fluid that appeared to strongly affect the mechanical properties of all three carbon loadings was the windshield washer fluid. Additionally, the elongation at break (ε_b) notably increased with exposure to windshield washer, suggesting plasticization of the matrix material. Exposure to E-20 gasoline appeared to weakly influence mechanical properties, with the greatest detrimental effects observed at the lowest carbon loading level. Significant variance is noted for the PA6 composite specimens exposed to brake fluid, which may be attributed to its relatively high alkalinity compared to the other five fluids. However, the apparent sorption rates, thermal properties, and mechanical properties of the exposed composite specimens do not support degradative ageing effects imposed by the brake fluid. A summary of the fluid effects, with respect to the untreated composite specimens, are provided in the table below.

Table 4.3. Effect on PA6 composite mechanical properties after 20 weeks exposure to room temperature automotive fluids.

	25% CF/PA6			***30% CF/PA6***			***50% CF/PA6***		
	E_T	**UTS**	**ε_b**	**E_T**	**UTS**	**ε_b**	**E_T**	**UTS**	**ε_b**
AF	N	N	N	N	N	N	N	N	W (-17%)
BR	M (+28%)	M (+28%)	W (-14%)	W (+12%)	M (+21%)	N	N	W (+18%)	N
PW	W (-15%)	W (-12%)	S (+38%)	W (+19%)	W (+15%)	N	N	M (+21%)	S (+33%)
MO	N	N	W (+12%)	W (-16%)	N	W (+14%)	M (-21%)	W (+12%)	M (+26%)
WW	S (-37%)	S (-44%)	S (+36%)	S (-41%)	S (-41%)	W (+18%)	S (-41%)	S (-36%)	W (+11%)
GS	M (-20%)	S (-32%)	W (-11%)	N	N	N	W (-19%)	N	W (-15%)

N = negligible effect ($\leq |10\%|$)

W = weak effect ($\leq |20\%|$)

M = moderate effect ($\leq |30\%|$)

S = strong effect ($> |30\%|$)

AF	Antifreeze
BR	Brake Fluid
PW	Powersteering Fluid
MO	SAE 5W-30 Motor Oil
WW	Windshield Washer Fluid
GS	E-20 Gasoline

The strong influence of the windshield washer fluid correlates with the significant solvent uptake and swelling reported in Table 4.2. Moreover, the mechanical properties of higher carbon loadings are less sensitive to automotive fluid exposure, particularly evident for exposure to E-20 gasoline at room temperature. This contradicts the previous expectation that the higher carbon loadings would be more sensitive to plasticizer content. Instead, this may be indicative of the fibre content behaving as an impenetrable barrier to advancing penetrant, ultimately limiting plasticization of the polymer matrix away from the composite surface.

While the degree of crystallinity, according to the composite film analysis, of the bulk polymer matrix appears to decrease with higher carbon loadings, it is possible that processing conditions of the higher carbon loadings are more susceptible to transcrystallization along the length of fibres. Indeed, the presence of most filler materials tends to promote preferential orientation of nucleation and crystal growth normal to the surface of filler content [59]. Moreover, Thomason and Van Rooyen [60] reported greater frequencies of transcrystallization along shorter carbon fibre lengths dispersed in polypropylene, with sporadic nucleation observed at the ends of fibres. According to Figure 3.1, the nominal fibre length decreases significantly for loadings exceeding 30% fibre content. This would suggest that fibre loadings exceeding 30% are more likely to promote transcrystallization. A crystalline boundary forming near the fibre-matrix interface would result in a less permeable membrane at the interface and contribute to greater tortuosity in the diffusion path through the amorphous regions of the matrix. As a result, the absorbed plasticizer content fails to effectively penetrate into the composite specimen and the subsequent plasticization of polymer chains found in the amorphous regions is supressed. The transcrystallization at the fibre-matrix interface may also promote a stiff percolating network, which is supported by the increasingly brittle fracture breaks (see Tables A.10-A.27) observed for higher fibre loadings.

4.1.3. Polyamide 6/6 Composite Case Study

Like the PA6 composite specimens, the long term physico-mechanical ageing effects were quantified by subjecting PA6/6 composite specimens to static room temperature immersion in automotive fluids over an extended period of time. The peak mass uptake and swell data are summarized in Table 4.4, which pertains to the longitudinal, flow-direction (F) samples of 35%, 40%, and 45% carbon loadings and transverse, cross-flow (CF) samples at the 40% carbon loading level; too few plaques were available to examine CF samples for the other loadings. Strangely, more fluid appears to be consistently absorbed for longitudinal cuts of the 40% CF/PA6/6 composite material over the same period of time. Gopu [61] observed that water molecules tended to diffuse faster along the length of fibres, since the moisture ingress pathway was characteristically convoluted moving across the fibres. Hence, the diffusion pathway for the transverse loading is likewise inhibitive to effective diffusion through the PA6/6 matrix.

Table 4.4. Peak mass uptake and thickness swelling relative to polymer mass fraction in PA6/6 composite specimens immersed in conventional automotive fluids for 10 weeks at 23°C.

	Relative Peak Mass Uptake (wt%)				***Peak Thickness Swell (%)***			
Carbon loading (wt%)	**35% (F)**	**40% (F)**	**40% (CF)**	**45% (F)**	**35% (F)**	**40% (F)**	**40% (CF)**	**45% (F)**
AF	X	8.2 ± 7.8	5.5 ± 1.8	X	X	2.9 ± 3.6	2.2 ± 1.3	X
BR	X	6.8 ± 3.8	1.8 ± 2.8	X	X	2.8 ± 1.9	3.7 ± 1.7	X
PW	X	5.8 ± 7.7	1.7 ± 3.8	X	X	2.9 ± 2.4	2.8 ± 3.4	X
MO	X	9.5 ± 2.7	3.7 ± 3.7	X	X	2.4 ± 1.2	4.0 ± 5.8	X
WW	11.5 ± 5.4	12.5 ± 5.5	13.7 ± 10.5	8.9 ± 2.7	5.4 ± 1.3	3.1 ± 2.9	6.0 ± 4.9	3.9 ± 4.4
GS	2.0 ± 0.2	7.5 ± 3.2	6.8 ± 2.5	1.8 ± 4.7	2.1 ± 2.5	4.4 ± 1.3	1.7 ± 1.0	0.8 ± 2.7

Interestingly, the mass uptake of the E-20 gasoline appears to increase with higher fibre loadings in PA6/6 composites. For a matrix dominant sorption mechanism, the relative plateau in solvent uptake would be expected to be constant with respect to the volume of polymer matrix. In Table 4.4, the apparent plateau solvent uptake for 40% CF/PA6/6 composite specimens is at least two times greater than the peak solvent uptake for a 35% fibre loading, despite the lower volume of polyamide matrix capable of interacting with the fluid. It is hypothesized that the significant surface delamination (see Figure 4.13) that occurred at higher carbon loadings of PA6/6 composite specimens may have contributed to the increased fluid sorption rates compared to the matrix-dominant diffusion mechanism noted for the PA6 composite specimens. In this context, delamination refers to the local separation of fibres from the bulk polymer matrix, which may be associated to debonding at the fibre-matrix interface. For instance, Pethrick et al [62] showed that selective fluid ingress into a carbon fibre reinforced plastic joint resulted in swelling and plasticization. In some cases, the effects of plasticization were reversible with drying, but irreversible change occurred when significant swelling created voids at the interface which could not be eliminated via drying cycle. Likewise, the purported swelling history induced by the windshield washer fluid makes it a viable candidate for promoting similar permanent interfacial damage and separation in the PA6/6 composite specimens, which may lend to further fluid ingress into the newly opened pores, voids, and cracks.

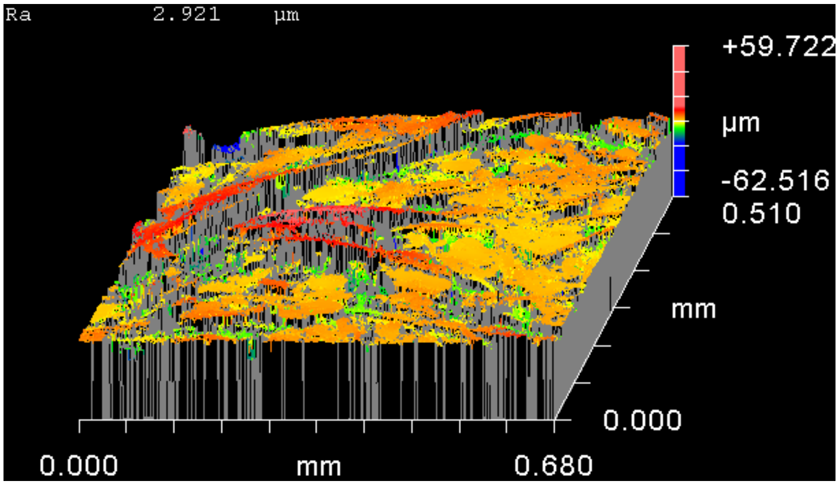

Figure 4.13. Surface topography of 45% CF/PA6/6 specimen after being immersed in windshield washer fluid for 10 weeks at 23°C.

In general, the overall solvent uptake is expected to decrease for matrix-dominant absorption mechanisms in PA6/6 composites given that the superior molecular alignment of PA6/6 polymer chains restricts effective fluid penetration and interaction. Therefore, the PA6/6 composite specimens are expected to better resist automotive fluid absorption compared to the PA6 composite specimens. However, it is seen by Table 4.2 versus Table 4.4 that the peak swelling and fluid intake of the transverse 40% CF/PA6/6 composite specimens are similar to transverse PA6 composite specimens immersed in the same automotive fluids.

The bulk of the deleterious changes to the PA6/6 composite mechanical properties occur after three weeks of exposure to the windshield washer fluid, regardless of fibre orientation, as shown in Figure 4.14. Similar losses for the PA6 composite materials occur much faster, after only one week of exposure. This observation can be attributed to the greater chemical resistance of the PA6/6 matrix.

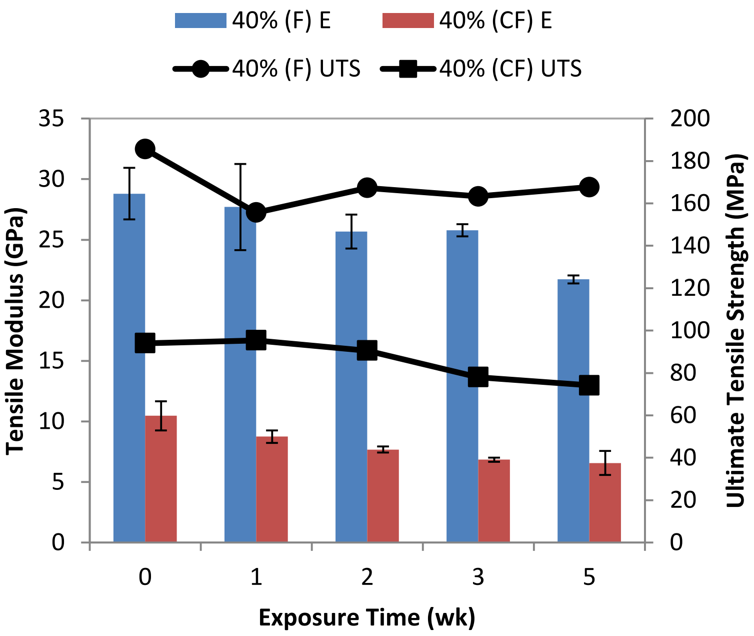

Figure 4.14. Tensile mechanical properties of longitudinal and transverse 40w% CF/PA6/6 composite specimens immersed in windshield washer fluid at 23°C.

The maximum drop in ultimate tensile strength, relative to the untreated samples, is proportionally greater for the transverse properties (21% loss) than the longitudinal (16% loss). This makes sense considering that the transverse properties are more sensitive to physico-mechanical changes in the matrix material, which is more likely to respond to fluid exposure than the carbon filler.

Almost all of the automotive fluids appear to significantly influence the material flexibility, as inferred from the elongation at break, values in Table 4.5. However, the results from elevated temperature exposure in the next section indicate that only the windshield washer consistently produces deleterious mechanical effects to the PA6/6 composite.

Table 4.5. Effect on longitudinal (F) PA6/6 composite mechanical properties after 10 weeks exposure to room temperature automotive fluids.

	35% (F)			***40% (F)***			***45% (F)***		
	E	**UTS**	**ε_b**	**E**	**UTS**	**ε_b**	**E**	**UTS**	**ε_b**
AF	X	X	X	W (-14%)	W (+12%)	S (+31%)	X	X	X
BR	X	X	X	W (-12%)	N	M (+20%)	X	X	X
PW	X	X	X	N	M (+24%)	S (+42%)	X	X	X
MO	X	X	X	N	N	S (+32%)	X	X	X
WW	M (-28%)	M (-21%)	W (+11%)	M (-23%)	W (-16%)	M (+26%)	S (-43%)	S (-32%)	S (+36%)
GS	N	M (+20%)	M (+22%)	N	N	N	N	N	N

N = negligible effect (≤$|10\%|$)

W = weak effect (≤$|20\%|$)

M = moderate effect (≤$|30\%|$)

S = strong effect (>$|30\%|$)

AF	Antifreeze
BR	Brake Fluid
PW	Powersteering Fluid
MO	SAE 5W-30 Motor Oil
WW	Windshield Washer Fluid
GS	E-20 Gasoline

The loss in mechanical properties after 10 weeks exposure to windshield washer fluid (see Table 4.5) appears to be more pronounced for higher carbon loadings. The solvent uptake was shown to increase with fibre loadings in Table 4.4, despite lower apparent volumes of polyamide matrix available to absorb the fluid. The significant surface delamination, especially evident after swelling in windshield washer fluid, of higher carbon loadings of the PA6/6 composite specimens likely contributes to further fluid uptake across the fibre-matrix interface. As a result, significant volumes of windshield washer fluid are allowed to effectively penetrate into the bulk PA6/6 matrix. Greater penetration ultimately implies more effective plasticization that occurs beyond the surface region of the composite material. While swelling in windshield washer fluid is also observed for the PA6 composite specimens, the surface topography does not imply the existence of a significant fluid transport pathway at sites of surface micro-cracking, unlike in Figure 4.13 for the PA6/6 composites. The extent of plasticization of the PA6/6 composite specimens is likewise reflected in the mechanical data in Table 4.5. These results also imply the existence of an interface-dominant absorption mechanism operative for the PA6/6 composite specimens, given the significant influence of fibre content presented so far

4.2. Elevated Temperature Immersion

The effect of elevated temperature is also assessed for the PA6 and PA6/6 composite specimens by static immersion. The PA6 composite test specimens were immersed in all six fluids at elevated temperatures (70 ± 5°C for antifreeze, brake, powersteering, motor oil, and windshield washer fluid; 50 ± 5°C for E-20 gasoline) for a period of six weeks. The 40% CF/PA6/6 composite test specimens were subjected to motor oil, windshield washer fluid, and E-20 gasoline at the same elevated temperatures.

No significant trends in discoloration are observed for the elevated temperature conditions in any of the test specimens. However, the peak mass uptake and thickness swelling, shown in Tables 4.6 and 4.7 for the PA6 and PA6/6 composite specimens, are clearly temperature dependent.

Table 4.6. Peak mass uptake and thickness swelling relative to polymer volume for PA6 composite specimens immersed in conventional automotive fluids over 6 weeks at elevated temperatures.

	Relative Peak Mass Uptake (wt%)			***Peak Thickness Swell (%)***		
Fluid	**25%**	**30%**	**50%**	**25%**	**30%**	**50%**
AF	10.3 ± 2.7	6.7 ± 2.7	4.2 ± 4.2	3.8 ± 1.5	2.4 ± 2.8	6.1 ± 3.4
BR	6.5 ± 0.5	5.9 ± 5.0	5.8 ± 4.4	1.9 ± 1.3	4.3 ± 4.5	3.9 ± 4.3
PW	3.9 ± 1.9	4.6 ± 6.6	2.4 ± 2.2	0.5 ± 2.8	4.8 ± 5.1	1.9 ± 4.3
MO	4.5 ± 4.1	2.7 ± 0.6	3.0 ± 8.2	1.4 ± 0.7	0.8 ± 1.5	1.0 ± 2.1
WW	13.5 ± 2.0	11.3 ± 7.6	14.0 ± 3.6	6.7 ± 1.1	8.4 ± 5.6	9.1 ± 3.0
GS	8.0 ± 0.5	6.3 ± 2.6	4.0 ± 6.0	8.2 ± 0.6	5.1 ± 0.9	2.9 ± 4.2

Table 4.7. Peak mass uptake and thickness swelling relative to polymer volume for 40% CF/PA6/6 composite specimens immersed in select conventional automotive fluids over 6 weeks at elevated temperatures.

	Relative Peak Mass Uptake (wt%)		***Peak Thickness Swell (%)***	
Fluid	**40% (F)**	**40% (CF)**	**40% (F)**	**40% (CF)**
MO	6.3 ± 3.7	6.7 ± 3.7	2.8 ± 2.3	3.2 ± 1.3
WW	14.3 ± 7.3	11.8 ± 6.2	6.7 ± 4.0	10.8 ± 8.5
GS	9.3 ± 9.3	6.5 ± 3.5	2.4 ± 4.0	2.6 ± 1.7

With regards to the PA6 composite specimens, the peak swelling and mass uptake of antifreeze and E-20 gasoline is nearly 2-3 times greater than compared to the equivalent static room temperature immersion test. Additionally, the apparent plateau absorption values for all fluids are more uniform across the variable carbon loadings at higher temperatures. This implies that the relative plateau in absorption capacity increases with higher carbon loadings, since the volume of available polyamide matrix decreases. The increased fluid uptake is likely a response to the deteriorating wettability between the fibre and matrix at higher carbon loadings. The elevated temperature conditions would appear to expedite fluid transport across the matrix such that the flow impedance induced by high filler contents near the surface is relatively negligible over long term exposure periods. Moreover, the temperature of the fluid that diffuses into the PA6 composite enters at a temperature exceeding the glass transition temperature of the bulk matrix material. Therefore, amorphous regions in contact with the heated absorbed fluid will allow for more effective diffusion as the polymer chains become more flexible at temperatures above the glass transition temperature.

While elevated temperatures appears to accelerate fluid uptake for the PA6 and PA6/6 composites, the end loss of mechanical properties are generally similar to room temperature ageing after a longer period in windshield washer fluid. This implies that the influence of elevated temperature is constrained to enhanced fluid sorption, rather than thermal degradation. The insignificant post-exposure discoloration of the composite specimens is in agreement with the idea that limited chemical reaction and chain scission has been initiated by the operative elevated temperature conditioning.

Exposure to antifreeze and E-20 gasoline at elevated temperatures resulted in significant losses in material stiffness and tensile strength (see Table 4.8) of the PA6 composite specimens. This result would suggest that the small polar molecules, presumably ethylene glycol and ethanol, more effectively diffuse into the composite matrix at elevated temperatures above the glass transition temperature. The increasing elongation at break accompanying loss in mechanical properties suggests that the fluids induce some degree of plasticization on the respective polyamide matrix. The PA6/6 composite specimens, however, did not appear to respond differently to the E-20 gasoline at 50°C, as shown in Table 4.8.

Table 4.8. Effect on PA6 composite mechanical properties after 6 weeks exposure to elevated temperature automotive fluids.

	25%			***30%***			***50%***		
	E	**UTS**	**ε_b**	**E**	**UTS**	**ε_b**	**E**	**UTS**	**ε_b**
AF	S (-40%)	S (-44%)	M (+24%)	M (-30%)	S (-48%)	N	W (-19%)	M (-26%)	W (+17%)
BR	N	N	W (-15%)	N	N	W (-19%)	N	W (-16%)	N
PW	N	N	W (-14%)	M (+21%)	M (+25%)	N	M (+23%)	M (+23%)	N
MO	N	N	N	W (+13%)	N	S (-31%)	M (+25%)	W (+14%)	W (-17%)
WW	S (-42%)	S (-49%)	M (+24%)	S (-31%)	S (-35%)	M (+22%)	S (-37%)	S (-31%)	S (+72%)
GS	M (-30%)	M (-22%)	M (+24%)	M (-28%)	S (-37%)	W (+18%)	W (-12%)	W (-15%)	S (+53%)

N = negligible effect (≤ $|10\%|$)

W = weak effect (≤ $|20\%|$)

M = moderate effect (≤ $|30\%|$)

S = strong effect (> $|30\%|$)

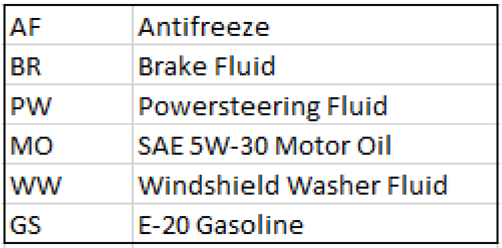

AF	Antifreeze
BR	Brake Fluid
PW	Powersteering Fluid
MO	SAE 5W-30 Motor Oil
WW	Windshield Washer Fluid
GS	E-20 Gasoline

Table 4.9. Effect on 40% CF/PA6/6 composite mechanical properties after 6 weeks exposure to elevated temperature automotive fluids.

	40% (F)			***40% (CF)***		
	E	**UTS**	**ε_b**	**E**	**UTS**	**ε_b**
MO	N	N	N	N	N	N
WW	S (-42%)	S (-30%)	W (+17%)	S (-44%)	S (-44%)	M (+26%)
GS	N	W (+16%)	N	N	W (+19%)	M (+21%)

N = negligible effect (≤$|10\%|$)

W = weak effect (≤$|20\%|$)

M = moderate effect (≤$|30\%|$)

S = strong effect (>$|30\%|$)

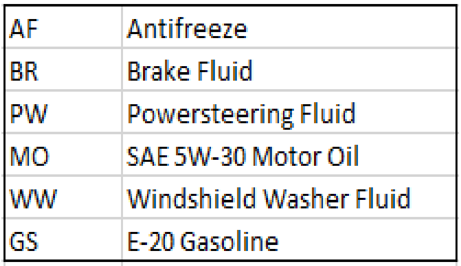

AF	Antifreeze
BR	Brake Fluid
PW	Powersteering Fluid
MO	SAE 5W-30 Motor Oil
WW	Windshield Washer Fluid
GS	E-20 Gasoline

The effect of the antifreeze, windshield washer and E-20 gasoline on the mechanical properties of the PA6 composite specimens is most significant at the lower carbon loadings, similar to the room temperature immersion conditions. According to Table 4.6, the relative solvent uptake at elevated temperatures increases with carbon fibre loadings, despite the lower PA6 volume available to absorb the fluids. Therefore, it is likely that some of the absorbed fluid sits along the fibre-matrix interface given the deteriorating state of fibre wettability attributed to higher fibre loadings. Fluid transfer is known to be inhibitive moving across the width of fibres, so it appears that the higher carbon loadings oriented in the transverse direction behave as an increasingly impenetrable barrier to a straight diffusive pathway further into the composite specimen.

It is also conceivable for pre-existing sites of transcrystallization, which are more likely for higher carbon fibre loadings and inferred by the shorter fibre distribution, to impede fluid transfer along the fibre-matrix interface. In that case, the absorbed fluid at the fibre-matrix interface would be trapped between two impermeable surfaces, including the carbon fibre and the enveloping crystalline phase that traces the length of the fibre. In either case, the extent of plasticization observed by the composite material is dictated by the ability of the solvent to diffuse through the specimen thickness. As such, the lower carbon fibre loading offers the least tortuous pathway for diffusion into the composite core and subsequently observes the highest extent of deleterious effects on the mechanical properties via plasticization of the amorphous regions.

Chapter 5 SHORT TERM ENVIRONMENTAL STRESS CRACKING

5.1. Physico-Mechanical Characterization of Surface Damage

The experimental design for testing environmental stress cracking (ESC) of the PA6 composite tensile dogbone samples aimed to accelerate physical ageing by 1) exploiting the established high rates of water absorption and subsequent plasticization into the polyamide matrix and 2) applying significant but constant strain approaching the yield stress limit of the respective material. Acoustic emission testing can indicate internal material damage from the ESC conditioning without having to utilize more destructive means of characterization.

The surface of the deflected PA6 composite specimens were scanned for any evidence of matrix cracking using a reflected light microscope, usually at the site of the uppermost deflection as shown in Figure 5.1. Samples that cracked as they were mounted to the three-point deflection apparatus, prior to ESC conditioning, were discarded as the matrix cracking could not be attributed to the accelerated ageing techniques employed in the study.

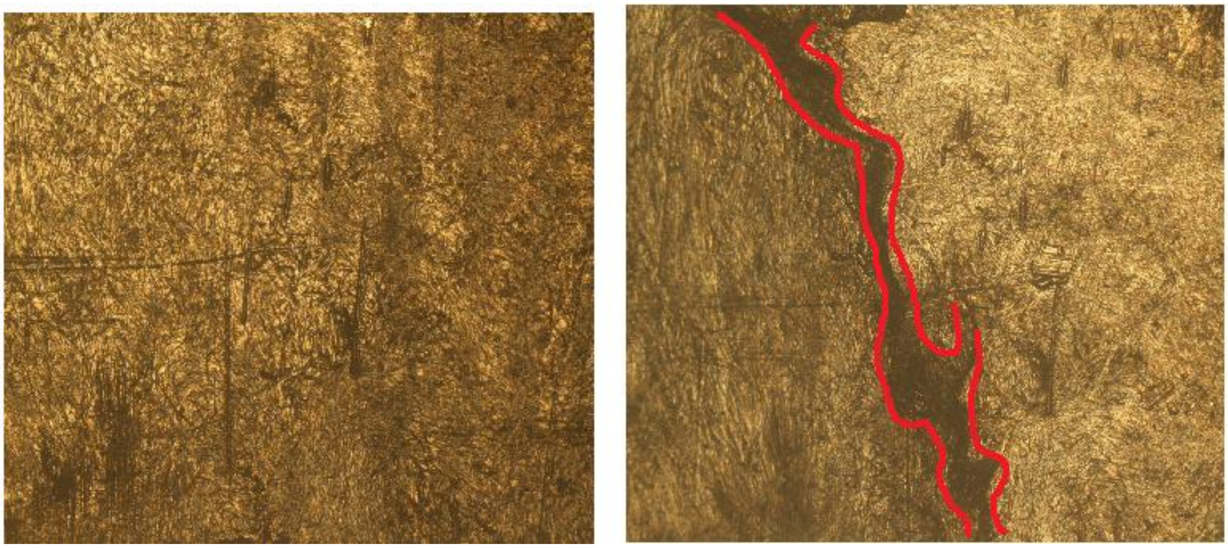

Figure 5.1. Micrograph of uppermost deflected surface of 50% CF/PA6 tensile dogbone specimen before (left) and after (right) one hour exposure at 70°C and 25% relative humidity.

Each occurrence of matrix surface cracking was recorded in order to detect any trend pertaining to increasing temperature and humidity and premature material failure. However, the summary of matrix crack events, provided in Table 5.1, only suggests that the frequency of matrix cracking increases with carbon fibre loading for the PA6 composite specimens under stress.

Table 5.1. Frequency of matrix surface cracking after ESC conditioning in various temperature and humidity environments for CF/PA6 composite specimens.

Temperature (°C)	***Relative Humidity (%RH)***	***Carbon Fibre Loading (%wt)***			
		25	**30**	**40**	**50**
50	*5*	0/5	0/5	1/5	4/5
50	*25*	0/5	0/5	0/5	0/5
50	*50*	0/5	1/3	0/5	0/3
60	*5*	1/5	0/4	0/4	0/4
60	*25*	1/5	0/5	0/3	1/5
60	*50*	0/5	1/5	1/3	0/5
70	*5*	0/5	0/5	1/5	0/4
70	*25*	0/5	0/4	0/4	2/4
70	*50*	0/5	0/4	0/4	1/5
Total Failure Rate (%)		< 5%	5%	< 8%	20%

The total failure rates would also appear to be consistent with the standard deviation of the tensile strength of the untreated material properties. For instance, the standard deviation for the untreated 25%, 30%, 40%, and 50% CF/PA6 composite tensile strength is 7, 7, 9, and 12% respectively. There is no discernible trend between temperature and humidity on the magnitude of the tensile strength (see Figure 5.2). However, the tensile strength of higher carbon loadings tended to decline after ESC treatment, which reflects the higher occurrence rate of matrix cracking on the surface. The tensile strength variances noted in Figure 5.2 are not especially abnormal for the low fibre content PA6 composite specimens, given the inherent heterogeneous nature of composite material. However, there is significant variance for some of the higher carbon fibre content PA6 composite test specimens. However, the variance is too sporadic to reliably assess the effect of short term temperature and humidity exposure.

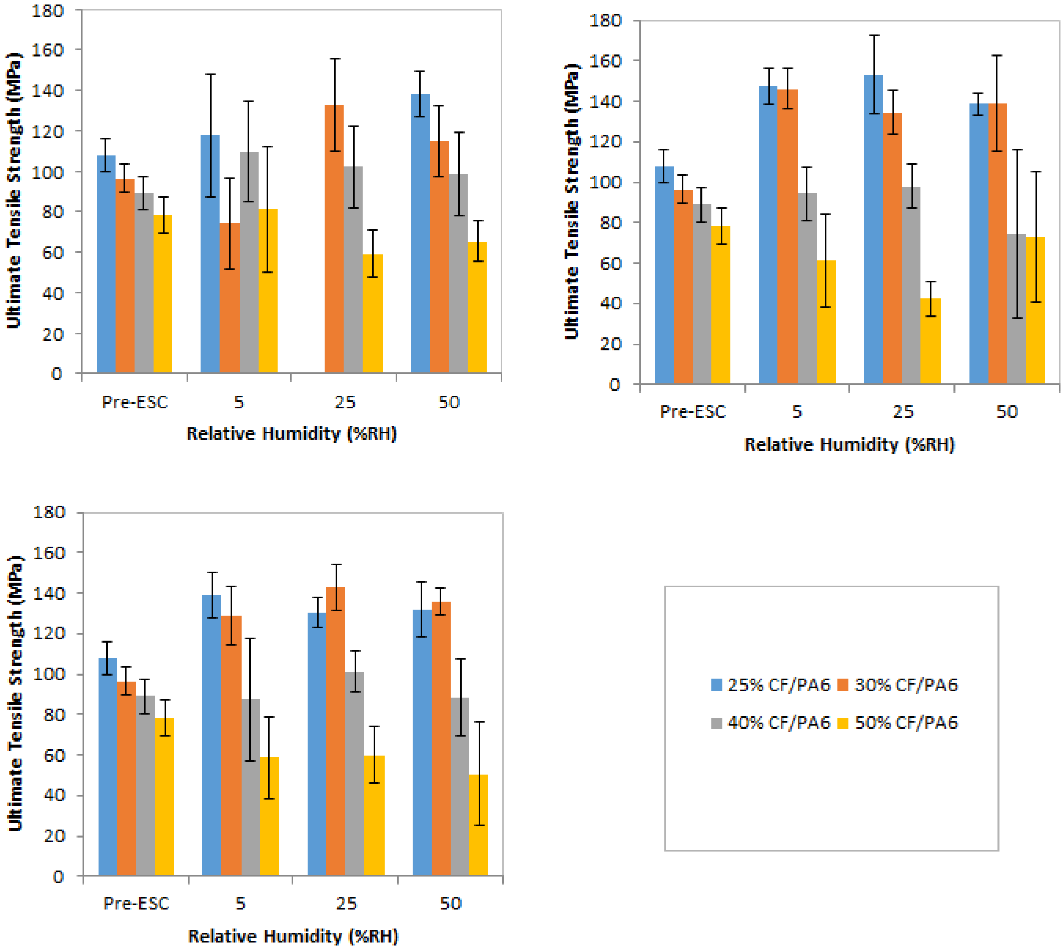

Figure 5.2. Ultimate tensile strength of stressed PA6 composite specimens after 1 hour steady state exposure to variable humidity levels at 50°C (upper-left), 60°C (upper-right), and 70°C (bottom-left).

5.2. Ultrasonic Emission Characterization of Internal Damage

Even though some composite samples may not exhibit obvious signs of material failure, such as matrix cracking at the surface, the application of ESC conditioning could still theoretically initiate the formation of internal microcracks and fibre fracture to relieve stress experienced by the bulk matrix. To quantify any potential internal damage to the composite material, the peak amplitude variance of the output time-domain signal from a 500 kHz input pulse, as shown in Figure 5.3, is compared before and after ESC conditioning.

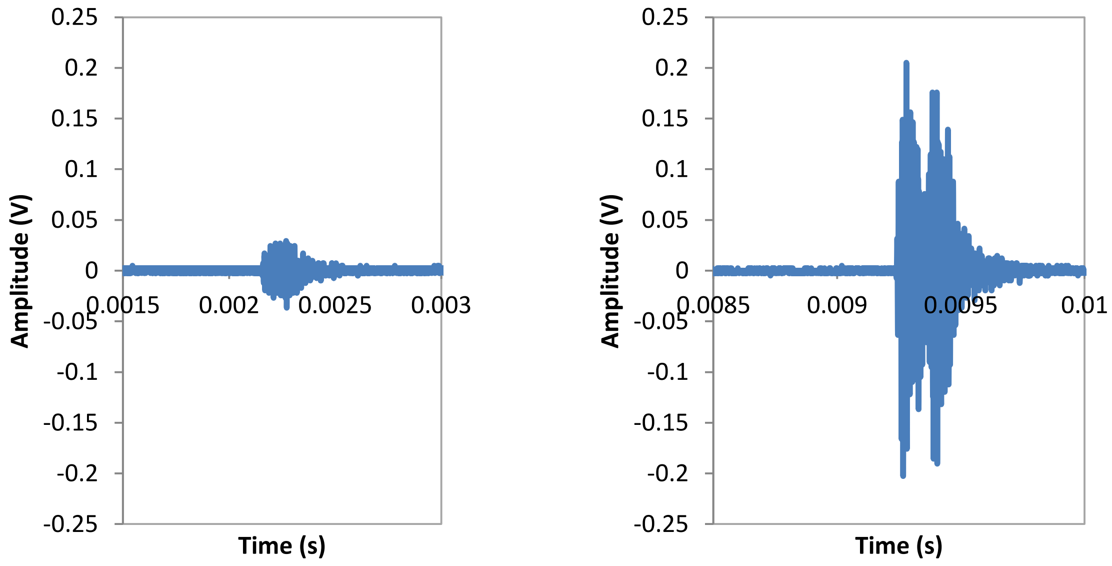

Figure 5.3. Example of filtered acoustic emission (AE) event signal from 500 kHz burst signal for a deflected 25% CF/PA6 (left) and 50% CF/PA6 specimen (right) post-exposure to 70°C and 25%RH.

Generally, the signal duration and peak amplitude were greater in magnitude for specimens with a higher fibre loading. El-Sabbagh et al [63] noted that higher natural fibre content dispersed in polypropylene yielded more effective sound wave propagation, where the sound pulse speed would increase

1% for every 8.3% increase in fibre volume content. However, El-Sabbagh et al [63] also noted that poor adhesion quality between the fibre-matrix interface would result in the formation of voids and subsequently greater resistance to wave propagation. The quality of the fibre-matrix interface, concerning wettability and fibre dispersion, for the PA6 composites is comparatively subpar at the higher fibre loading levels based on the microscopic and mechanical analyses shown in section 4.1.2. Consequently, the output signal duration may be longer as the initial ultrasonic pulse is impeded by the increasingly heterogeneous media, namely voids and defects due to poor wettability, imparted by increasing the fibre filler content.

According to Valentin et al [64], higher peak amplitudes are expected to correlate with matrix cracking parallel to the fibre content while low amplitude signals are marginally indicative of fibre breaks. Ideally, the normalized variance of peak amplitude equal to one or less suggests that no new significant acoustic emission (AE) events have been detected following ESC conditioning. Normalized variances that are significantly greater than one are expected to be related to matrix cracking while the low amplitude signals produced by fibre fracture may be ultimately indistinguishable from the inherent material variance using this simple approach. Figure 5.4 shows the normalized peak amplitude variance obtained for the four carbon loadings under stress while exposed to increasing temperature and humidity levels.

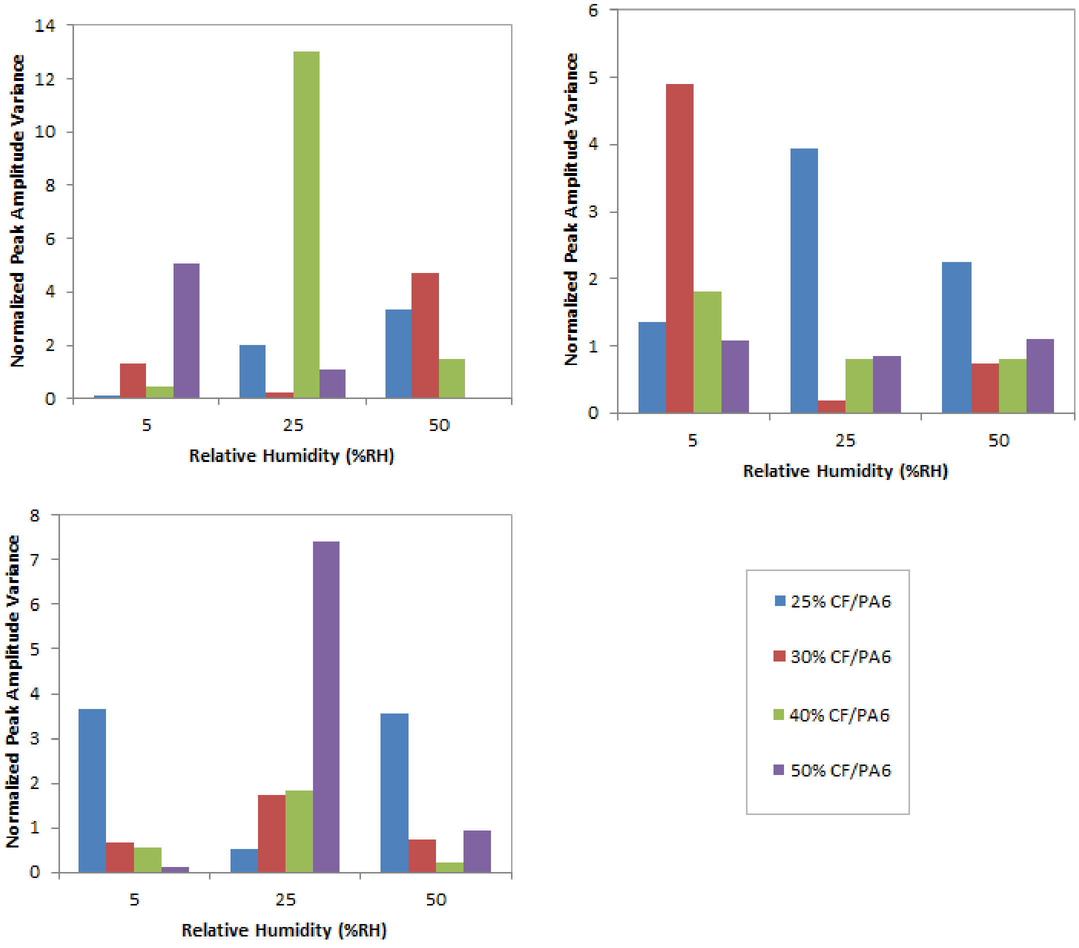

Figure 5.4. Normalized peak amplitude variance of stressed PA6 composite specimens after 1 hour steady state exposure to variable humidity levels at 50°C (upper-left), 60°C (upper-right), and 70°C (bottom-left).

Based on observations from Figure 5.4, the peak amplitude variance does not appear to correlate with the observed matrix cracking incidents. For example, the highest peak amplitude variance after low temperature ESC conditioning was for the 40% CF/PA6 deflected specimens at medium humidity settings, despite the fact that no matrix cracking incidents were observed. Presumably, the deflected 50% CF/PA6 specimens at low humidity levels should have produced the largest peak amplitude variance for the low temperature setting considering that it had the highest incident rate of surface matrix cracking. At first, there does not appear to be any discernible trend pertaining to the temperature or humidity exposure for most of the carbon loadings given the somewhat random distribution of peak variability. Recall, however, that the peak amplitude of the output signal itself would increase, along with the signal duration, with increasing fibre loadings. Therefore, it may be difficult to detect low amplitude fibre fractures within the higher fibre loadings which already produce relatively high peak amplitude signals. The purported increased sensitivity to fibre fracture, or other low amplitude events, at lower carbon loadings may explain the notable amplitude variance observed for the deflected 25% CF/PA6 specimens after most ESC treatments, despite having the lowest matrix crack incidents. Increased temperature conditioning generally shows that the peak amplitude variance decreases with higher carbon loadings.

Chapter 6 CONCLUSIONS AND FUTURE WORK

6.1. Conclusions

The ageing characterization of carbon fibre-reinforced polyamide composites in this work assesses the relative retention of physico-mechanical properties with exposure to various chemical, temperature, moisture, and stress environments. The quality of the fibre-matrix interface perceivably declines with higher fibre loadings dispersed in the PA6 matrix. The subsequent void space in the interfacial region at higher loadings is more susceptible to hold and transport fluid along the surface of the fibres.

At elevated temperatures, the relative plateau in mass uptake of solvents containing small polar molecules tended to increase with higher carbon loadings, despite the lower apparent volume of polyamide matrix capable of absorbing and swelling in the presence of the fluid. This suggests that some of the absorbed fluid occupies the void space in the interface region instead of being dispersed within the limited polyamide matrix.

The IR spectra of exposed 50% CF/PA6 composite films produced characteristic peaks reminiscent of the absorbed fluid, which may suggest the presence of absorbed fluid sitting along isolated pockets along the fibre-matrix interface. Moreover, the impermeable core fibre content inhibits progressive fluid diffusion deeper into the composite material, especially for higher carbon loadings. Indeed, the deleterious effects to the mechanical properties are most significant for the lower carbon fibre loadings for the PA6 composites, which reflect the purported inhibitive nature to diffusion pathways induced by the increased fibre loadings.

Likewise, the interface-dominant sorption mechanism across the fibre pathway is reflected in the PA6/6 composite specimens, where the mechanical properties of the composite material were generally more sensitive to fluid exposure at the higher carbon loadings. The interface-dominant sorption mechanism is attributed to the significant surface delamination observed after swelling in windshield washer, which subsequently grants the absorbing fluid an additional pathway via surface microcracks into the composite. The delamination is less severe for lower carbon fibre loadings, so the fluid is less likely to effectively penetrate into the core composite material.

Consequently, the deleterious effects to mechanical properties are most prominent at the higher carbon loadings for the PA6/6 composite. The PA6 and PA6/6 composites both experienced some degree of deleterious effects to mechanical properties after long term exposure to antifreeze, windshield washer fluid, and E-20 gasoline, However, the deleterious effects, attributed to the effective plasticization of small polar molecules found in the respective fluid composition, is more significant for the PA6 composite. This is attributed to superior molecular alignment of the PA6/6 polymer chains, which subsequently inhibits polar molecules from inserting themselves within the free volume space between the chains and initiating a plasticizing effect. Moreover, elevated temperatures exceeding the glass transition temperature of the polymer matrix expedited fluid transport of the larger polar molecules found in antifreeze and E-20 gasoline, leading to increased sorption and extent of plasticization in the bulk polymer.

6.2. Recommendations

Based on the work conducted thus far, a need still exists to reliably correlate and quantify internal damage within the composite frame. Short term ESC conditioning proved insufficient to produce significant ageing effects. Instead, a cyclic ESC conditioning strategy should be considered for effective crack initiation and propagation to occur. Composite specimens immersed in fluids at temperatures exceeding 70°C would also be an interesting area of future work in order to assess the susceptibility to direct chemical attack. The apparent interface-dominant sorption mechanism of the PA6/6 composite material warrants further examination, especially pertaining to the fluid penetration pathway into the matrix.

REFERENCES

[1] R. Heuss, N. Müler, W. van Sintern, A. Starke and A. Tschiesner, "Lightweight, heavy impact. How carbon fiber and other lightweight materials will develop across industries and specifically automotive," McKinsey & Company, 2012.

[2] L. W. McKeen, "Polyamides," in *The Effects of Temperature and other Factors on Plastics and Elastomers*, Kidlington, Oxfordshire: Elsevier Inc., 2014, pp. 139-157.

[3] A. A. Collyer, A Practical Guide to the Selection of High Temperature Engineering Thermoplastics, Oxford: Elsevier Science Publishers Ltd, 1990.

[4] M. Alger, Polymer Science Dictionary, Springer Science & Business Media, 1996.

[5] Y. Meng and S. Tjong, "Rheology and morphology of compatibilized polyamide 6 blends containing liquid crystalline copolyesters," *Polymer,* vol. 39, no. 1, pp. 99-107, 1998.

[6] M. L. Clingerman, J. P. Konell, E. H. Weber, J. A. King and K. H. Schulz, "Comparisons of electrical, thermal, and mechanical properties of carbon filled resins," in *SPE/ANTEC 2001 Proceedings*, Dallas, 2001.

[7] G. H. Motlagh, "Carbon Fibre-Carbon Black Interactions and Fibre Orientation in Electrically Conductive Amorphous Thermoplastic Composites: Ph.D. dissertation," McMaster University, Hamilton, 2007.

[8] Z. Behdouj, M. Jamshid, M. Latifi and M. Halvaei, "Study on the effect of fiber cross section shape of polypropylene fibers on mechanical properties of cement composites," in *4th International Conference on Concrete & Development*, Tehran, 2013.

[9] W. Steinmann and A.-K. Saelhoff, "Essential Properties of Fibres for Composite Applications," in *Fibrous and Textile Materials for Composite Applications*, 1 ed., S. Rana and R. Fangueiro, Eds., Springer Singapore, 2016, pp. 39-73.

[10] B. Salar, "Fibre Reinforced Polyester Composites," in *Polyester*, H. E. M. Saleh, Ed., InTech Open Access, 2012, pp. 135-166.

[11] W. D. Callister, "Composites," in *Materials Science and Engineering: An Introduction*, 7th ed., John Wiley & Sons, Inc., 2007, pp. 577-620.

[12] M. Elices and J. Llorca, Fiber Fracture, Kidlington: Elsevier Science, Ltd., 2002.

[13] L. C. Pardini and L. G. B. Manhani, "Influence of the Testing Gage Length on the Strength, Young's Modulus and Weibull Modulus of Carbon Fibres and Glass Fibres," *Materials Research,* vol. 5, no. 4, pp. 411-420, 2002.

[14] B. D. Agarwal and L. J. Broutman, Analysis and Performance of Fibre Composites, 2nd ed., New York: John Wiley & Sons, Inc., 1990, pp. 59-72.

[15] B. Bakir and H. Hashem, "Effect of fibre orientation for fibre glass on reinforced composite material on mechanical properties," *International Journal of Mining, Metallurgy & Mechanical Engineering,* vol. 1, no. 5, pp. 341-345, 2013.

[16] F. K. Alves de Sousa, I. Ujike and A. Kadota, "Effect of different fibre angles for composite material with fibreglass reinforced on mechanical properties," *International Journal of Mining, Metallurgy & Mechanical Engineering ,* vol. 4, no. 1, pp. 1-6, 2016.

[17] P. W. Jackson and D. Cratchley, "The effect of fibre orientation on the tensile strength of fibre-reinforced metals," *Journal of the Mechanics and Physics of Solids,* vol. 14, no. 1, pp. 49-64, 1966.

[18] R. H. Knibbs and J. B. Morris, "The effects of fibre orientation on physical properties of composites," *Composites,* vol. 5, no. 5, pp. 209-218, 1974.

[19] L. C. Sawyer, D. T. Grubb and G. F. Meyers, "Composites," in *Polymer Microscopy*, 3rd ed., New York, Springer New York, 2008, pp. 354-380.

[20] S. Lampman, "Environmental and Chemical Effects," in *Characterization and Failure of Plastics*, ASM International, 2003, pp. 146-152.

[21] J. E. Mark, Polymer Data Handbook, Oxford University Press, Inc. , 1999.

[22] R. C. Wyatt and K. Ashbee, "Debonding in carbon fibre/polyester resin composites exposed to water: Comparison with 'E' glass fibre composites," *Fibre Science and Technology,* vol. 2, no. 1, pp. 29-40, 1969.

[23] A. S. Maxwell, W. R. Broughton, G. Dean and G. D. Sims, Review of accelerated ageing methods and lifetime prediction techniques for polymeric materials, Teddington: National Physical Laboratory, 2005.

[24] L. T. Drzal, M. J. Rich, M. F. Koenig and P. F. Lloyd, "Adhesion of Graphite Fibres to Epoxy Matrices: II. The Effect of Fibre Finish," *The Journal of Adhesion,* vol. 16, no. 2, pp. 133-152, 1983.

[25] A. Rios de Anda, "Influence of the solvent sorption, additivation, and chemical modification on the molecular mobility of Polyamide 6,6 amorphous phase and its consequences on the tensile and impact strength properties of this polymer: Ph.D. dissertation," Claude Bernard University Lyon 1, Lyon, 2012.

[26] C. Reichardt, Solvents and Solvent Effects in Organic Chemistry, 3rd ed., Wiley-VCH Publishers, 2003.

[27] R. Puffr and J. Šebenda, "On the Structure and Properties of Polyamides. XXVII. The Mechanism of Water Sorption in Polyamides.," *Journal of Polymer Science: Part C,* vol. 16, no. 1, pp. 79-93, 1967.

[28] L. -A. Fillot, S. Ghiringhelli, C. Prebet and S. Rossi, "Biofuels Barrier Properties of Polyamide 6 and High Density Polyethylene," *Oil & Gas Science and Technology,* vol. 70, no. 2, pp. 335-351, 2015.

[29] G. S. Springer and C.-H. Shen, "Moisture Absorption and Desorption of Composite Materials," *Journal of Composite Materials,* vol. 10, no. 1, pp. 2-20, 1976.

[30] M. Sabard, "Effet des conditions de procédé et des nanocharges sur la morphologie et les propriétés de sorption à l'eau et à l'ethanol: Ph.D. dissertation," Claude Bernard University Lyon 1, Lyon, 2011.

[31] D. Benavente, P. Lock, M. Ángeles García Del Cura and S. Ordóñez, "Predicting the capillary imbibition of porous rocks from microstructure," *Transport in Porous Media,* vol. 49, no. 1, pp. 56-76, 2002.

[32] S. Paulidou and C. D. Papaspyrides, "The effect of hygrothermal history on water sorption and interlaminar shear strength of glass/polyester composites with different interfacial strength," *Composites: Part A,* vol. 34, pp. 1117-1124, 2003.

[33] B. Zhang, L. Liu, Z. Wu and D. Wang, "Experimental investigation of porosity in carbon/epoxy composite laminates," in *Proceedings of the 4th Asian-Australian Conference on Composite Material*, Sydney, 2004.

[34] P. A. Kumar, K. Varughese and S. Thomas, "Transport behavior of high density polyethylene/ethylene propylene diene terpolymer rubber blends," in *MACRO 2000: 6th*

Conference, Kanpur, 2000.

[35] M. R. Thompson, B. Mu, C. M. Ewaschuk, Y. Cai, K. J. Oxby and J. Vlachopoulos, "Long term storage of biodiesel/petrol diesel blends in polyethylene fuel tanks," *Fuel,* vol. 108, pp. 771-779, 2013.

[36] L. J. Broutman and R. H. Krock, Composite Materials: Interfaces in Polymer Matrix Composites, vol. 6, E. P. Plueddemann, Ed., New York City: Academic Press, 1974.

[37] A. Agster, "Die Einwirkung höherer Temperaturen auf natürliche und synthetische Faserstoffe," *Melliand Textilberichte,* vol. 37, no. 11, pp. 1338-1344, 1956.

[38] S. Ramazani, M. Morshed and M. Ghane, "Effects of service temperature on structure and mechanical properties of polyamide 6 and 66 tyre cords," *Journal of Polymer Research,* vol. 18, no. 4, pp. 781-792, 2011.

[39] T. Karstens and V. Rossbach, "Thermo-oxidative degradation of polyamide 6 and 6,6. Kinetics of the formation and inhibition of UV/VIS-active chromophores," *Die Makromolekulare Chemie,* vol. 190 , no. 12, pp. 3033-3053, 1989.

[40] V. G. Valk, H. Krüssmann and P. Diehl, "Über den Licht- und Hitzeabbau Faseraufbauender Hochpolymerer," *Die Makromolekulare Chemie,* vol. 107, no. 1, pp. 158-169, 1967.

[41] T. S. Gates and M. A. Grayson, "On the Use of Accelerated Aging Methods for Screening High Temperature Polymeric Composite Materials," in *40th Structures, Structural, Dynamics, and Materials Conference and Exhibit*, St Louis, 1999.

[42] J. Reis, T. de Sanťanna, P. P. Coutinho, A. H. Monteiro, S. Teixeira, E. G. Chaves and H. S. da Costa Mattos, "Coupled effect of ageing and temperature in the mechanical behaviour of a polyamide," *Polymer Testing,* vol. 53, pp. 267-275, 2016.

[43] B. Singh and N. Sharma, "Mechanistic Implications of Plastics Degradation," *Polymer Degradation and Stability,* vol. 93, no. 3, pp. 561-584, 2008.

[44] S. Pillay, U. K. Vaidya and G. M. Janowski, "Effects of moisture and UV exposure on liquid molded carbon fabric reinforced nylon 6 composite laminates," *Composites Science and Technology,* vol. 69, no. 6, pp. 839-846, 2009.

[45] *Ultramid 8202 HS Polyamide 6,* BASF (technical datasheet), 2016.

[46] *Ultramid A3W PA66,* BASF (technical datasheet), 2016.

[47] *Zoltek PX35 Commercial Carbon Fibre,* Zoltek (technical datasheet), 2016.

[48] "Pennzoil Platinum SAE 5W-30 Full Synthetic Motor Oil, SDS No. 800001003703," Shell Canada Products, Calgary, 2016.

[49] "Prestone Extended Life 5/150 Antifreeze/Coolant, MSDS No. 410," FRAM Group (Canada), Inc., Mississauga, 2011.

[50] "Brake Fluid DOT 3, SDS No. 1515," Recochem Inc. , Montreal, 2015.

[51] "Prestone Power Steering Fluid, MSDS No. 589," FRAM Group (Canada), Inc., Mississauga, 2011.

[52] S. Abbasi, "Rheology, Properties and Microstructure Development of Polymer/Carbon Nanotube Composites in Microinjection Molding Process: Ph.D dissertation," Université de Montréal, Montreal, 2009.

[53] E. C. Bothelo, Ł. Figiel, M. C. Rezende and B. Lauke, "Mechanical behavior of carbon fiber reinforced polyamide composites," *Composites Science and Technology,* vol. 63, no. 13, pp. 1843-1855, 2003.

[54] K. Krishnan and R. S. Krishnan, "Raman and Infrared Spectra of Ethylene Glycol," *Proceedings of the Indian Academy of Sciences - Section A,* vol. 64, no. 2, pp. 111-122, 1996.

[55] E. K. Plyler, "Infrared Spectra of Methanol, Ethanol, and n-Propanol," *Journal of Research of the National Bureau of Standards,* vol. 48, no. 4, pp. 281-286, 1952.

[56] L. Pandiscia, "Analysis of Automotive Fluids Using with FTIR," JASCO, Inc., [Online]. Available: www.jascoinc.com/ftir/analysis-of-automotive-fluids-using-with-ftir.

[57] K. Wapner and G. Grundmeier, "Spatially resolved measurements of the diffusion of water in a model adhesive/silicon lap joint using FTIR-transmission microscopy," *International Journal of Adhesion & Adhesives,* vol. 24, no. 3, pp. 193-200, 2004.

[58] L. Rebenfeld, G. P. Desio and J. C. Wu, "Effects of Fibers on the Glass Transition Temperature of Polyethylene Sulfide Composites," *Journal of Applied Polymer Science,* vol. 42, no. 3, pp. 801-805, 1991.

[59] D. Frihi, A. Layachi, S. Gherib, S. Stoclet, K. Masenelli-Varlot and H. Satha, "Crystallization of glass-fiber-reinforced polyamide 66 composites: Influence of glass-fiber content and cooling rate," *Composites Science and Technology,* vol. 130, pp. 70-77, 2016.

[60] J. L. Thomason and A. A. Van Rooyen, "Transcrystallized interface in thermoplastic composites: Part II. Influence of interfacial stress, cooling rate, fibre properties and polymer molecular weight," *Journal of Materials Science,* vol. 27, no. 4, pp. 897-907, 1992.

[61] J. Gopu, "A Review of Mechanisms and Fracture Mechanics of Moisture Ingress in Composite Systems: Master's thesis," Ryerson University, Toronto, 2012.

[62] R. A. Pethrick, G. S. Armstrong, W. M. Banks, R. L. Crane and D. Hayward, "Dielectric and mechanical studies of the durability of adhesively bonded aluminum structures subjected to temperature cycling. Part 1. Examination of moisture absorption.," *Proceedings of the Institution of Mechanical Engineers, Part L: Journal of Materials: Design and Applications,* vol. 218, no. 3, pp. 169-182, 2004.

[63] A. El-Sabbagh, L. Steuernagel and G. Ziegmann, "Ultrasonic testing of natural fibre polymer composites: effect of fibre content, humidity, stress on sound speed and comparison to glass fibre polymer composites," *Polymer Bulletin,* vol. 70, no. 2, pp. 371-390, 2013.

[64] D. Valentin, P. Bonniau and A. R. Bunsell, "Failure mechanism discrimination in carbon fibre-reinforced epoxy composites," *Composites,* vol. 14, no. 4, pp. 345-351, 1983.

[65] B. Duncan, J. Urquhart and S. Roberts, "Review of Measurment and Modelling of Permeation and Diffusion in Polymers," National Physical Laboratory, Teddington, 2005.

APPENDIX

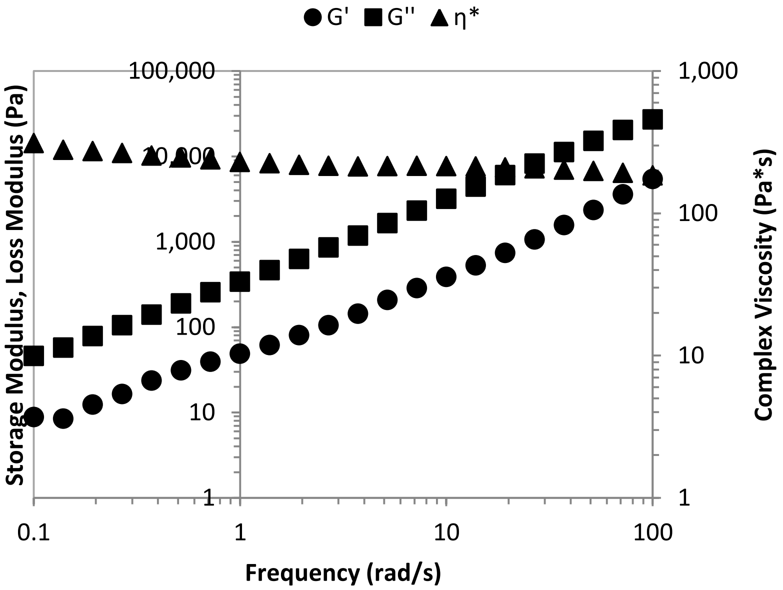

Figure A.1. Rheological properties of unfilled PA6 composite specimens at 240°C.

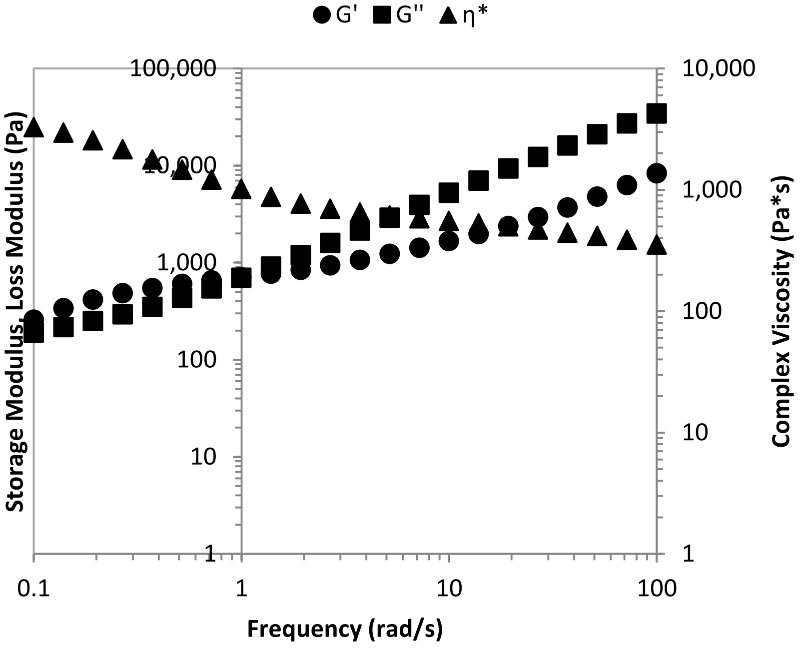

Figure A.2. Rheological properties of 25% CF/PA6 composite specimens at 240°C.

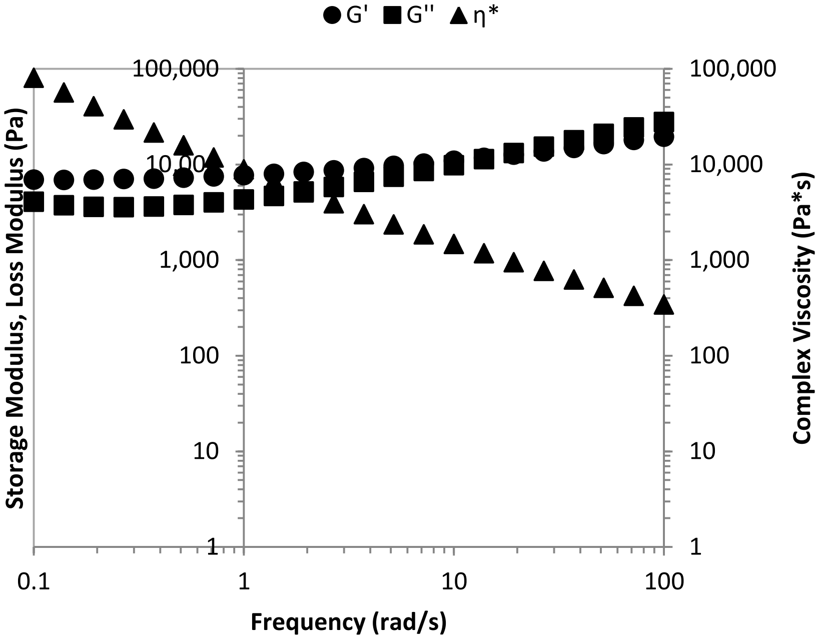

Figure A.3. Rheological properties of 50% CF/PA6 composite specimens at 240°C.

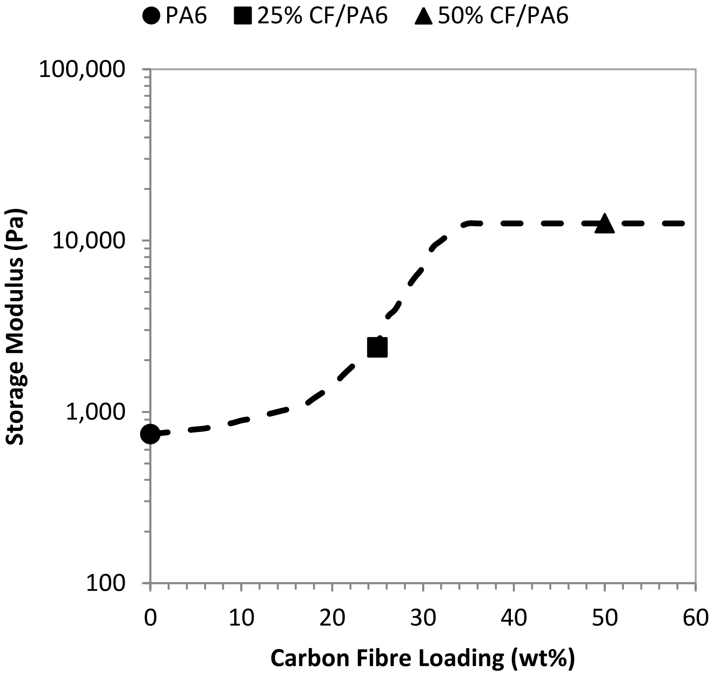

Figure A.4. Storage modulus of CF/PA6 composite as a function of fibre loading at 240°C (20 rad/s). Dotted line corresponds to conceptual fitted curve to interpolate approximate percolation threshold.

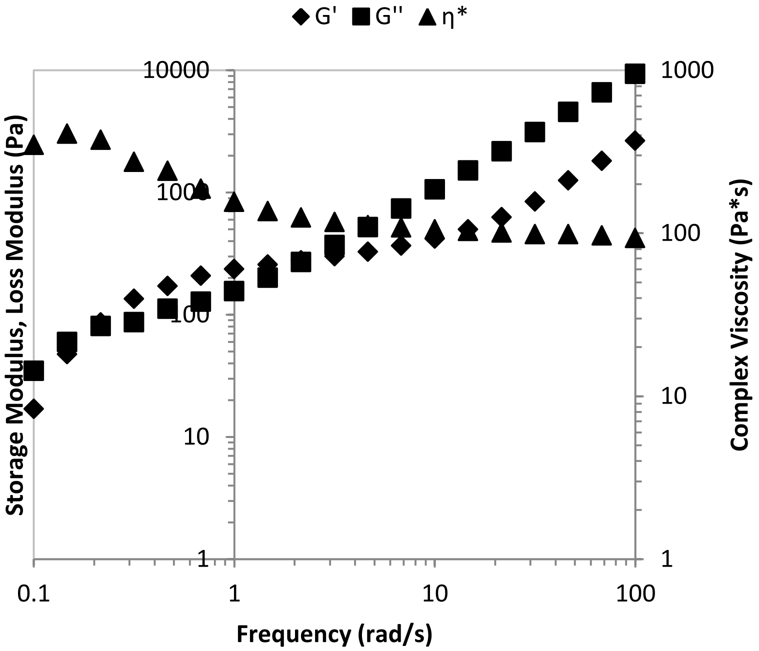

Figure A.5. Rheological properties of unfilled PA6/6 composite specimens at 275°C.

The fluid ingress modelling techniques applied to the PA6 composite films in Figure 4.5 have also been implemented for the analogous CF/PA6 composite dogbone specimens used in the primary immersion study. The diffusion coefficients for the unfilled PA6 films in various automotive fluids, shown in Table 4.1, are assumed to be equally applicable for the dogbone specimens. The Fickian mass transfer component is corrected for sample thickness and the capillary-absorption coefficient is approximated by finding the best fit to the fluid sorption data. The absorption coefficients are summarized in Table A.1.

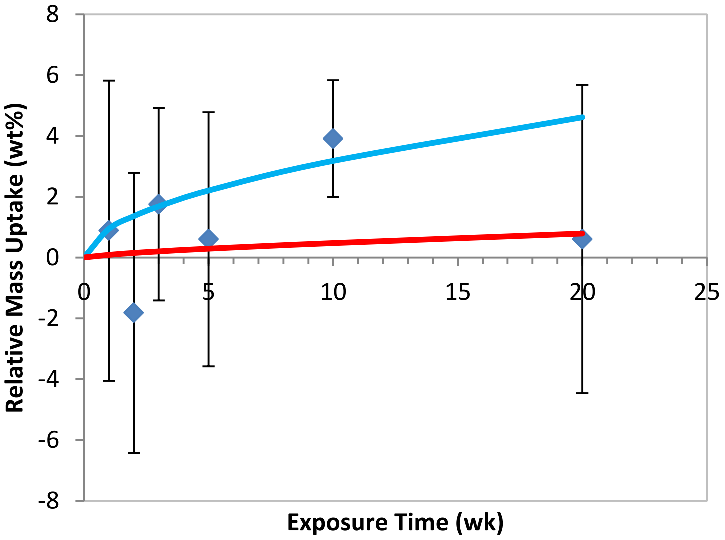

Figure A.6. Antifreeze absorption into transverse 25% CF/PA6 dogbone specimens after room temperature static immersion. Red line corresponds to Fickian model and cyan line corresponds to dual-stage model that considers simultaneous Fickian diffusion and capillary-based convective fluid transport.

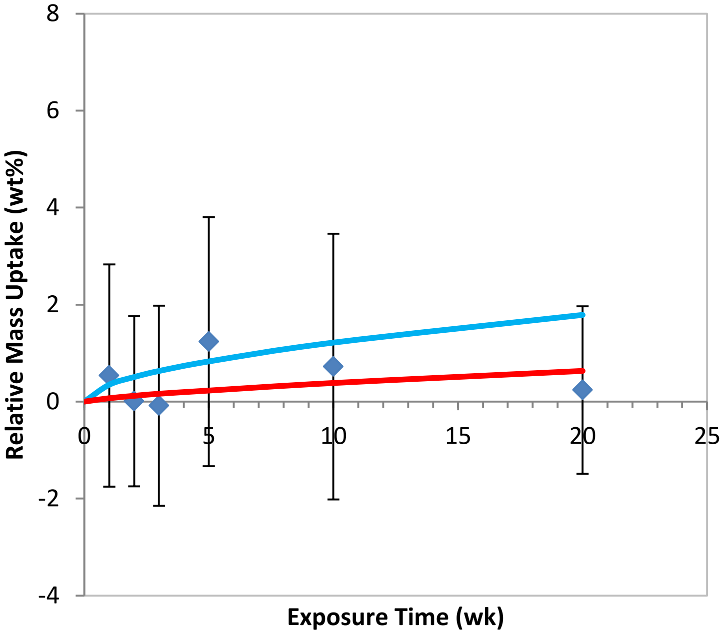

Figure A.7. Antifreeze absorption into transverse 50% CF/PA6 dogbone specimens after room temperature static immersion. Red line corresponds to Fickian model and cyan line corresponds to dual-stage model that considers simultaneous Fickian diffusion and capillary-based convective fluid transport.

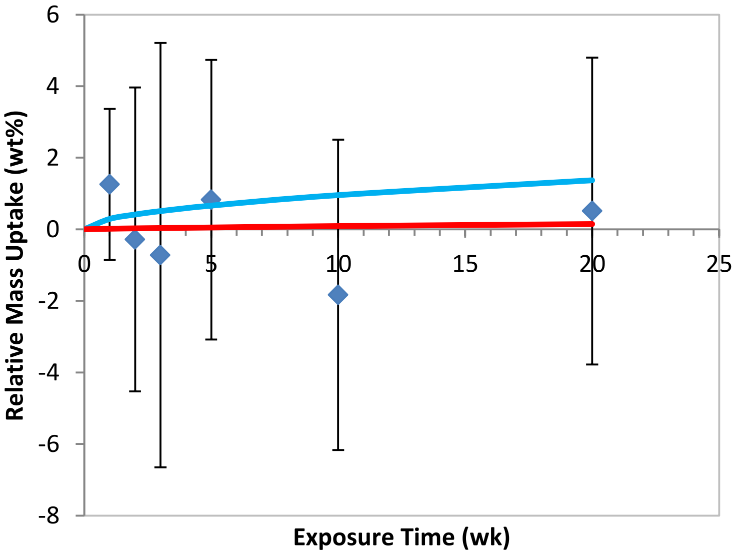

Figure A.8. Brake fluid absorption into transverse 25% CF/PA6 dogbone specimens after room temperature static immersion. Red line corresponds to Fickian model and cyan line corresponds to dual-stage model that considers simultaneous Fickian diffusion and capillary-based convective fluid transport.

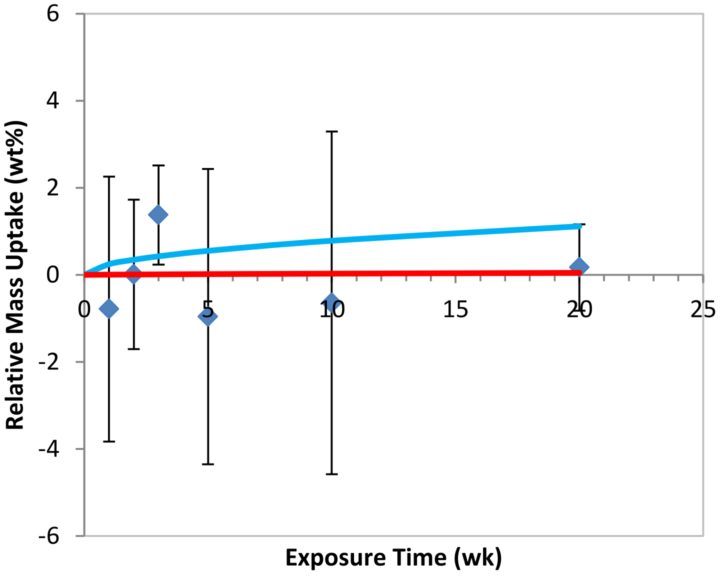

Figure A.9. Brake fluid absorption into transverse 50% CF/PA6 dogbone specimens after room temperature static immersion. Red line corresponds to Fickian model and cyan line corresponds to dual-stage model that considers simultaneous Fickian diffusion and capillary-based convective fluid transport.

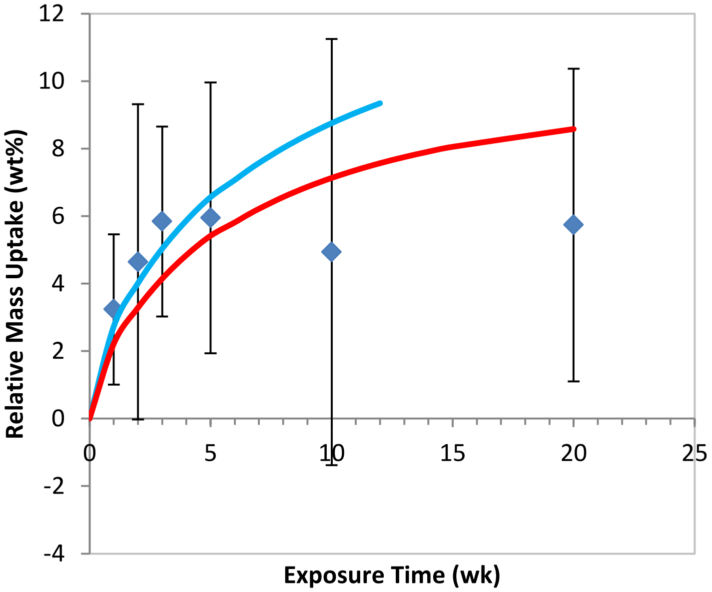

Figure A.10. Windshield washer fluid absorption into transverse 50% CF/PA6 dogbone specimens after room temperature static immersion. Red line corresponds to Fickian model and cyan line corresponds to dual-stage model that considers simultaneous Fickian diffusion and capillary-based convective fluid transport.

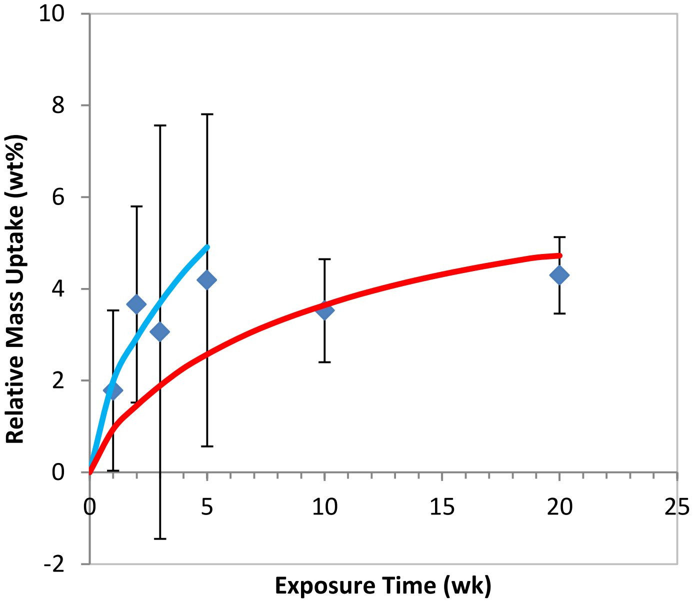

Figure A.11. Windshield washer fluid absorption into transverse 50% CF/PA6 dogbone specimens after room temperature static immersion. Red line corresponds to Fickian model and cyan line corresponds to dual-stage model that considers simultaneous Fickian diffusion and capillary-based convective fluid transport.

Table A.1. Capillary-absorption constant summary for fitted hybrid fluid ingress model for PA6 composite tensile specimens immersed in antifreeze, brake, and windshield washer fluid for 20 weeks (3360 hours) at room temperature.

	Carbon Fibre Loading (wt%)		
Fluid	**25**	**30**	**50**
Antifreeze	0.0025 g·h$^{-1/2}$	0.0022 g·h$^{-1/2}$	0.0010 g·h$^{-1/2}$
Brake	0.0008 g·h$^{-1/2}$	0.0010 g·h$^{-1/2}$	0.0008 g·h$^{-1/2}$
Windshield Washer	0.0015 g·h$^{-1/2}$	0.0050 g·h$^{-1/2}$	0.0035 g·h$^{-1/2}$

The influence of capillary action is immediately apparent from Table A.1, which notes a significant increase in the capillary-absorption constant for higher carbon loadings immersed in windshield washer fluid. However, a degree of scepticism is recommended, considering that the Fickian diffusion model is technically sufficient to describe the fluid ingress into the PA6 dogbone composite specimens according to Figures A.10 and A.11. Indeed, the overall reliance on capillary action would be expected to be suppressed for fluids with higher rates of diffusion into the composite specimen. Curiously, the samples immersed in antifreeze and brake fluid suggests that the inferred capillary action is generally constant regardless of filler content. This may suggest the fibre-matrix interface generally maintains the same degree of wettability for the PA6 composite material, since the void space available to hold fluid does not appear to change relative to the fibre loading volume. Otherwise, the capillary-absorption coefficients would have been expected to increase with respect to the fibre loading.

Table A.2. Thermal properties of unfilled PA6 films immersed in antifreeze fluid at 23°C.

Exposure Time (wk)	T_m (°C)	Degree of Crystallinity (%)	T_g (°C)
0	223.05	30.36	51.82
1	220.95	38.87	40.93
3	221.46	23.19	46.42
5	222.52	21.73	41.69
10	222.10	18.68	46.49

Table A.3. Thermal properties of unfilled PA6 films immersed in brake fluid at 23°C.

Exposure Time (wk)	T_m (°C)	Degree of Crystallinity (%)	T_g (°C)
0	223.05	30.36	51.82
1	221.39	25.73	49.90
3	222.06	28.19	46.01
5	222.35	27.50	42.01
10	222.40	21.51	46.08

Table A.4. Thermal properties of unfilled PA6 films immersed in windshield washer fluid at 23°C.

Exposure Time (wk)	T_m (°C)	Degree of Crystallinity (%)	T_g (°C)
0	223.05	30.36	51.82
1	220.86	34.10	48.63
3	223.12	28.79	52.01
5	222.81	21.59	41.59
10	222.90	23.61	29.45

Table A.5. Thermal properties of 25% CF/PA6 films immersed in antifreeze fluid at 23°C.

Exposure Time (wk)	T_m (°C)	Degree of Crystallinity (%)	T_g (°C)
0	221.58	23.54	53.45
1	221.04	28.63	45.65
3	221.21	23.90	38.66
5	221.92	22.15	34.99
10	221.40	21.47	32.62

Table A.6. Thermal properties of 25% CF/PA6 films immersed in brake fluid at 23°C.

Exposure Time (wk)	T_m (°C)	Degree of Crystallinity (%)	T_g (°C)
0	221.58	23.54	53.45
1	221.09	23.54	41.36
3	221.03	28.47	46.04
5	222.38	27.80	39.29
10	220.88	30.81	43.55

Table A.7. Thermal properties of 25% CF/PA6 films immersed in windshield washer fluid at 23°C.

Exposure Time (wk)	T_m (°C)	Degree of Crystallinity (%)	T_g (°C)
0	221.58	23.54	53.45
1	220.30	27.22	52.58
3	221.77	26.72	52.93
5	220.99	25.35	57.07
10	221.28	21.47	38.84

Table A.8. Thermal properties of 25% CF/PA6 films immersed in antifreeze fluid at 23°C.

Exposure Time (wk)	T_m (°C)	Degree of Crystallinity (%)	T_g (°C)
0	219.62	21.35	60.61
1	219.30	16.82	40.79
3	218.72	20.93	45.52
5	216.45	20.23	38.55
10	217.56	16.75	37.57

Table A.9. Thermal properties of 50% CF/PA6 films immersed in brake fluid at 23°C.

Exposure Time (wk)	T_m (°C)	Degree of Crystallinity (%)	T_g (°C)
0	219.62	21.35	60.61
1	218.08	19.26	42.40
3	218.28	17.45	47.29
5	217.48	18.78	42.33
10	218.57	19.37	46.47

Table A.10. Thermal properties of 50% CF/PA6 films immersed in windshield washer fluid at 23°C.

Exposure Time (wk)	T_m (°C)	Degree of Crystallinity (%)	T_g (°C)
0	219.62	21.35	60.61
1	218.92	21.87	43.32
3	218.13	20.17	50.84
5	219.66	21.52	36.62
10	219.85	17.44	27.22

Table A.11. Mechanical properties of transverse 25% CF/PA6 composite specimens over 20 weeks of room temperature immersion in antifreeze.

t (wk)	E (GPa)	UTS (MPa)	ε_b (%)
0	7.11 ± 0.55	108.0 ± 8.0	2.29 ± 0.23
1	6.79 ± 1.09	104.8 ± 18.7	2.31 ± 0.49
2	7.22 ± 1.35	100.8 ± 21.3	2.16 ±0.40
3	7.35 ± 0.96	113.9 ± 15.4	2.08 ± 0.18

5	7.01 ± 0.83	109.2 ± 11.4	2.27 ± 0.22
10	7.50 ± 0.60	109.0 ± 12.5	2.04 ± 0.48
20	7.49 ± 0.33	106.5 ± 11.8	2.17 ± 0.27

Table A.12. Mechanical properties of transverse 25% CF/PA6 composite specimens over 20 weeks of room temperature immersion in brake fluid.

t (wk)	E (GPa)	UTS (MPa)	ε_b (%)
0	7.11 ± 0.55	108.0 ± 8.0	2.29 ± 0.23
1	8.07 ± 0.71	128.1 ± 7.2	2.29 ± 0.50
2	8.44 ± 0.52	120.3 ± 12.4	1.98 ± 0.07
3	8.29 ± 1.43	116.5 ± 35.7	1.85 ± 0.33
5	7.47 ± 1.16	117.6 ± 13.3	2.10 ± 0.29
10	8.09 ± 0.82	119.2 ± 26.8	1.91 ± 0.56
20	9.11 ± 1.58	129.1 ± 29.7	1.96 ± 0.39

Table A.13. Mechanical properties of transverse 25% CF/PA6 composite specimens over 20 weeks of room temperature immersion in powersteering fluid.

t (wk)	E (GPa)	UTS (MPa)	ε_b (%)
0	7.11 ± 0.55	108.0 ± 8.0	2.29 ± 0.23
1	6.63 ± 0.22	98.4 ± 15.1	2.36 ± 0.57
2	7.85 ± 0.79	105.8 ± 22.3	2.08 ± 0.53
3	6.31 ± 0.29	103.1 ± 1.5	2.72 ± 0.36
5	5.65 ± 0.68	89.8 ± 10.1	3.13 ± 0.09
10	6.88 ± 1.03	108.9 ± 9.8	2.61 ± 0.32
20	6.02 ± 0.86	95.0 ± 7.0	3.16 ± 0.39

Table A.14. Mechanical properties of transverse 25% CF/PA6 composite specimens over 20 weeks of room temperature immersion in SAE 5W-30 motor oil.

t (wk)	E (GPa)	UTS (MPa)	ε_b (%)

0	7.11 ± 0.55	108.0 ± 8.0	2.29 ± 0.23
1	7.84 ± 0.37	113.5 ± 8.7	2.11 ± 0.68
2	7.57 ± 1.87	116.3 ± 25.1	2.39 ± 0.89
3	7.57 ± 0.67	111.3 ± 15.6	1.99 ± 0.25
5	6.16 ± 1.64	94.3 ± 30.4	2.61 ± 0.46
10	7.00 ± 1.38	106.9 ± 15.0	2.63 ± 0.45
20	7.44 ± 1.13	105.8 ± 4.5	2.58 ± 0.64

Table A.15. Mechanical properties of transverse 25% CF/PA6 composite specimens over 20 weeks of room temperature immersion in windshield washer fluid.

t (wk)	E (GPa)	UTS (MPa)	ε_b (%)
0	7.11 ± 0.55	108.0 ± 8.0	2.29 ± 0.23
1	4.84 ± 1.67	73.6 ± 23.5	3.03 ± 0.58
2	4.92 ± 0.93	71.0 ± 13.6	2.65 ± 0.05
3	4.57 ± 0.37	69.2 ± 16.0	3.03 ± 0.13
5	4.45 ± 0.83	63.1 ± 8.1	2.85 ± 0.25
10	4.01 ± 0.37	56.1 ± 2.1	3.11 ± 0.39
20	4.49 ± 0.85	60.8 ± 9.7	2.91 ± 0.08

Table A.16. Mechanical properties of transverse 25% CF/PA6 composite specimens over 20 weeks of room temperature immersion in E-20 gasoline.

t (wk)	E (GPa)	UTS (MPa)	ε_b (%)
0	7.11 ± 0.55	108.0 ± 8.0	2.29 ± 0.23
1	7.73 ± 1.74	113.5 ± 30.0	2.44 ± 0.45
2	7.14 ± 1.03	108.2 ± 8.5	2.22 ± 0.61
3	6.42 ± 0.22	96.1 ± 9.0	2.44 ± 0.35
5	6.52 ± 0.69	97.3 ± 9.8	2.34 ± 0.25

10	5.94 ± 0.45	87.6 ± 4.1	2.42 ± 0.34
20	5.66 ± 0.40	73.6 ± 7.9	2.03 ± 0.50

Table A.17. Mechanical properties of transverse 30% CF/PA6 composite specimens over 20 weeks of room temperature immersion in antifreeze.

t (wk)	E (GPa)	UTS (MPa)	ε_b (%)
0	6.53 ± 0.80	96.4 ± 7.0	2.03 ± 0.27
1	9.11 ± 0.44	129.7 ± 14.9	1.90 ± 0.42
2	8.15 ± 1.01	119.5 ± 17.6	1.82 ± 0.36
3	7.17 ± 0.57	100.4 ± 15.0	1.75 ± 0.42
5	6.88 ± 0.82	93.7 ± 19.1	1.73 ± 0.48
10	7.62 ± 1.91	116.1 ± 19.1	1.95 ± 0.13
20	7.84 ± 1.10	110.0 ± 28.3	1.86 ± 0.54

Table A.18. Mechanical properties of transverse 30% CF/PA6 composite specimens over 20 weeks of room temperature immersion in brake fluid.

t (wk)	E (GPa)	UTS (MPa)	ε_b (%)
0	6.53 ± 0.80	96.4 ± 7.0	2.03 ± 0.27
1	7.27 ± 1.29	112.0 ± 16.4	2.38 ± 0.72
2	8.81 ± 1.54	127.8 ± 32.1	1.84 ± 0.44
3	8.03 ± 1.52	125.1 ± 20.2	1.94 ± 0.13
5	7.98 ± 1.16	109.5 ± 33.4	1.55 ± 0.36
10	8.98 ± 0.88	124.7 ± 11.8	1.66 ± 0.07
20	8.23 ± 0.94	125.6 ± 2.1	1.95 ± 0.27

Table A.19. Mechanical properties of transverse 30% CF/PA6 composite specimens over 20 weeks of room temperature immersion in powersteering fluid.

t (wk)	E (GPa)	UTS (MPa)	ε_b (%)
0	6.53 ± 0.80	96.4 ± 7.0	2.03 ± 0.27

1	7.28 ± 1.70	105.2 ± 2.8	1.86 ± 0.68
2	8.56 ± 0.94	125.0 ± 11.6	1.89 ± 0.26
3	7.69 ± 1.13	110.2 ± 28.8	1.82 ± 0.35
5	8.05 ± 0.85	120.0 ± 10.0	2.06 ± 0.23
10	7.70 ± 1.74	114.1 ± 13.7	2.40 ± 0.34
20	8.73 ± 0.87	118.9 ± 8.1	2.01 ± 0.23

Table A.20. Mechanical properties of transverse 30% CF/PA6 composite specimens over 20 weeks of room temperature immersion in SAE 5W-30 motor oil.

t (wk)	E (GPa)	UTS (MPa)	ε_b (%)
0	6.53 ± 0.80	96.4 ± 7.0	2.03 ± 0.27
1	8.09 ± 2.72	142.4 ± 50.1	2.35 ± 0.73
2	8.01 ± 0.99	110.0 ± 15.8	2.05 ± 0.46
3	7.80 ± 1.32	112.4 ± 26.4	2.13 ± 0.10
5	7.28 ± 1.11	99.3 ± 29.4	1.76 ± 0.73
10	8.11 ± 1.37	109.2 ± 14.4	2.05 ± 0.06
20	6.13 ± 0.04	103.9 ± 3.2	2.35 ± 0.02

Table A.21. Mechanical properties of transverse 30% CF/PA6 composite specimens over 20 weeks of room temperature immersion in windshield washer fluid.

t (wk)	E (GPa)	UTS (MPa)	ε_b (%)
0	6.53 ± 0.80	96.4 ± 7.0	2.03 ± 0.27
1	4.91 ± 0.65	63.1 ± 5.3	1.95 ± 0.36
2	4.64 ± 0.45	62.6 ± 13.2	2.37 ± 0.39
3	5.17 ± 0.44	70.8 ± 4.2	2.22 ± 0.11
5	5.16 ± 1.20	64.2 ± 9.0	2.19 ± 0.23
10	5.91 ± 1.84	75.7 ± 18.4	2.31 ± 0.68

20	4.29 ± 0.12	61.0 ± 6.5	2.40 ± 0.14

Table A.22. Mechanical properties of transverse 30% CF/PA6 composite specimens over 20 weeks of room temperature immersion in E-20 gasoline.

t (wk)	E (GPa)	UTS (MPa)	ε_b (%)
0	6.53 ± 0.80	96.4 ± 7.0	2.03 ± 0.27
1	6.25 ± 1.53	94.8 ± 17.1	1.99 ± 0.30
2	6.81 ± 0.36	95.1 ± 12.2	2.44 ± 0.65
3	7.41 ± 0.75	109.2 ± 23.0	2.06 ± 0.34
5	7.95 ± 1.32	108.7 ± 1.1	1.91 ± 0.26
10	7.66 ± 1.47	106.7 ± 17.6	2.01 ± 0.55
20	6.97 ± 0.85	100.0 ± 8.4	2.04 ± 0.52

Table A.23. Mechanical properties of transverse 50% CF/PA6 composite specimens over 20 weeks of room temperature immersion in antifreeze.

t (wk)	E (GPa)	UTS (MPa)	ε_b (%)
0	8.36 ± 0.32	78.3 ± 9.2	1.27 ± 0.10
1	9.18 ± 0.35	79.6 ± 1.9	0.80 ± 0.10
2	8.67 ± 1.01	80.4 ± 3.2	0.92 ± 0.20
3	8.93 ± 0.87	86.5 ± 6.5	0.95 ± 0.12
5	8.85 ± 0.66	81.0 ± 12.5	0.85 ± 0.17
10	9.65 ± 0.85	84.9 ± 10.5	0.82 ± 0.11
20	7.97 ± 1.50	79.5 ± 11.5	1.05 ± 0.25

Table A.24. Mechanical properties of transverse 50% CF/PA6 composite specimens over 20 weeks of room temperature immersion in brake fluid.

t (wk)	E (GPa)	UTS (MPa)	ε_b (%)
0	8.36 ± 0.32	78.3 ± 9.2	1.27 ± 0.10

1	8.96 ± 1.44	67.8 ± 10.2	0.70 ± 0.17
2	9.38 ± 0.97	93.8 ± 3.8	1.04 ± 0.15
3	9.89 ± 0.83	83.5 ± 17.6	0.84 ± 0.27
5	9.48 ± 1.30	72.0 ± 19.9	0.73 ± 0.34
10	9.38 ± 0.38	83.4 ± 14.0	0.80 ± 0.19
20	8.06 ± 1.62	92.7 ± 11.6	1.23 ± 0.32

Table A.25. Mechanical properties of transverse 50% CF/PA6 composite specimens over 20 weeks of room temperature immersion in powersteering fluid.

t (wk)	E (GPa)	UTS (MPa)	ε_b (%)
0	8.36 ± 0.32	78.3 ± 9.2	1.27 ± 0.10
1	8.59 ± 0.86	68.3 ± 2.0	0.72 ± 0.12
2	8.71 ± 0.77	84.5 ± 14.3	0.92 ± 0.16
3	9.20 ± 0.87	79.5 ± 8.5	0.86 ± 0.02
5	7.95 ± 1.56	73.9 ± 22.5	0.91 ± 0.12
10	8.72 ± 1.21	74.6 ± 21.0	0.99 ±0.43
20	7.51 ± 1.17	94.9 ± 5.35	1.69 ± 0.27

Table A.26. Mechanical properties of transverse 50% CF/PA6 composite specimens over 20 weeks of room temperature immersion in SAE 5W-30 motor oil.

t (wk)	E (GPa)	UTS (MPa)	ε_b (%)
0	8.36 ± 0.32	78.3 ± 9.2	1.27 ± 0.10
1	8.85 ± 1.00	63.7 ± 16.7	0.65 ± 0.16
2	9.30 ± 0.48	86.3 ± 8.1	0.92 ± 0.12
3	8.67 ± 0.77	88.0 ± 11.5	1.08 ± 0.43
5	8.34 ± 1.10	63.0 ± 28.4	0.77 ± 0.45
10	8.68 ± 0.90	92.5 ± 0.7	1.18 ± 0.21

20	6.62 ± 0.89	88.0 ± 6.7	1.60 ± 0.26

Table A.27. Mechanical properties of transverse 50% CF/PA6 composite specimens over 20 weeks of room temperature immersion in windshield washer fluid.

t (wk)	E (GPa)	UTS (MPa)	ε_b (%)
0	8.36 ± 0.32	78.3 ± 9.2	1.27 ± 0.10
1	6.91 ± 0.54	59.1 ± 9.6	0.86 ± 0.10
2	6.27 ± 0.78	60.3 ± 2.0	1.14 ± 0.21
3	5.55 ± 0.36	52.0 ± 9.5	1.15 ± 0.13
5	5.19 ± 0.14	51.1 ± 3.6	1.22 ± 0.01
10	5.35 ± 0.68	50.4 ± 9.9	1.10 ± 0.02
20	4.94 ± 0.34	50.2 ± 5.2	1.42 ± 0.24

Table A.28. Mechanical properties of transverse 50% CF/PA6 composite specimens over 20 weeks of room temperature immersion in E-20 gasoline.

t (wk)	E (GPa)	UTS (MPa)	ε_b (%)
0	8.36 ± 0.32	78.3 ± 9.2	1.27 ± 0.10
1	8.22 ± 0.80	83.8 ± 11.8	1.02 ± 0.05
2	9.06 ± 0.41	84.7 ± 5.7	0.91 ± 0.18
3	9.13 ± 0.96	77.0 ± 12.4	0.80 ± 0.25
5	9.35 ± 1.23	79.9 ± 6.1	0.80 ± 0.17
10	7.18 ± 1.09	75.2 ± 11.4	1.04 ± 0.17
20	6.73 ± 1.21	78.0 ± 7.0	1.08 ± 0.29

Table A.29. Mechanical properties of transverse 25% CF/PA6 composite specimens over 6 weeks of immersion in antifreeze at 70°C.

t (wk)	E (GPa)	UTS (MPa)	ε_b (%)
0	7.11 ± 0.55	108.0 ± 8.0	2.29 ± 0.23

1	5.86 ± 0.62	90.7 ± 7.6	2.53 ± 0.16
2	5.99 ± 1.34	91.7 ± 15.5	2.45 ± 0.64
3	6.46 ± 0.66	92.8 ± 15.6	2.23 ± 0.36
4	7.11 ± 2.36	107.3 ± 29.3	2.40 ± 0.19
5	4.43 ± 0.28	72.5 ± 3.3	2.84 ± 0.31
6	4.58 ± 0.55	64.7 ± 12.4	2.51 ± 0.42

Table A.30. Mechanical properties of transverse 25% CF/PA6 composite specimens over 6 weeks of immersion in brake fluid at 70°C.

t (wk)	E (GPa)	UTS (MPa)	ε_b (%)
0	7.11 ± 0.55	108.0 ± 8.0	2.29 ± 0.23
1	6.81 ± 0.43	104.7 ± 14.4	2.44 ± 0.24
2	6.74 ± 0.33	106.5 ± 2.6	2.37 ± 0.11
3	7.69 ± 1.11	116.3 ± 19.1	1.98 ± 0.06
4	8.64 ± 2.03	140.1 ± 34.9	2.19 ± 0.20
5	7.47 ± 2.31	120.0 ± 34.8	2.26 ± 0.27
6	7.84 ± 0.76	114.8 ± 2.5	1.95 ± 0.29

Table A.31. Mechanical properties of transverse 25% CF/PA6 composite specimens over 6 weeks of immersion in powersteering fluid at 70°C.

t (wk)	E (GPa)	UTS (MPa)	ε_b (%)
0	7.11 ± 0.55	108.0 ± 8.0	2.29 ± 0.23
1	6.67 ± 0.42	117.2 ± 4.4	2.84 ± 0.22
2	7.22 ± 0.51	119.3 ± 3.3	2.66 ± 0.12
3	7.18 ± 0.16	114.7 ± 4.5	2.15 ± 0.18
4	8.38 ± 0.53	124.6 ± 3.0	1.91 ± 0.16
5	7.64 ± 0.46	117.0 ± 8.7	1.96 ± 0.09

6	8.38 ± 1.68	127.2 ± 19.8	1.98 ± 0.19

Table A.32. Mechanical properties of transverse 25% CF/PA6 composite specimens over 6 weeks of immersion in SAE 5W-30 motor oil at 70°C.

t (wk)	E (GPa)	UTS (MPa)	ε_b (%)
0	7.11 ± 0.55	108.0 ± 8.0	2.29 ± 0.23
1	7.91 ± 0.40	120.7 ± 9.3	2.13 ± 0.07
2	8.56 ± 0.78	121.8 ± 17.8	1.94 ± 0.28
3	8.10 ± 1.05	120.1 ± 14.3	2.01 ± 0.09
4	7.97 ± 1.37	120.0 ± 17.0	2.18 ± 0.33
5	7.95 ± 0.48	123.9 ± 6.7	2.13 ± 0.07
6	9.15 ± 1.03	138.5 ± 14.1	2.02 ± 0.11

Table A.33. Mechanical properties of transverse 25% CF/PA6 composite specimens over 6 weeks of immersion in windshield washer fluid at 70°C.

t (wk)	E (GPa)	UTS (MPa)	ε_b (%)
0	7.11 ± 0.55	108.0 ± 8.0	2.29 ± 0.23
1	2.74 ± 0.48	56.2 ± 10.0	4.00 ± 0.81
2	3.35 ± 0.20	55.7 ± 7.9	3.89 ± 0.66
3	4.34 ± 0.74	65.3 ± 11.9	2.84 ± 0.39
4	3.42 ± 0.24	52.0 ± 11.5	2.91 ± 0.87
5	3.64 ± 0.29	55.6 ± 2.7	2.84 ± 0.22
6	4.11 ± 0.41	59.5 ± 6.9	2.62 ± 0.48

Table A.34. Mechanical properties of transverse 25% CF/PA6 composite specimens over 6 weeks of immersion in E-20 gasoline at 50°C.

t (wk)	E (GPa)	UTS (MPa)	ε_b (%)
0	7.11 ± 0.55	108.0 ± 8.0	2.29 ± 0.23

1	7.16 ± 1.16	105.1 ± 18.5	2.27 ± 0.14
2	6.82 ± 0.67	96.8 ± 9.6	1.99 ± 0.24
3	6.46 ± 0.60	97.2 ± 8.2	2.46 ± 0.28
4	6.94 ± 0.27	102.0 ± 5.0	2.21 ± 0.16
5	5.24 ± 0.82	83.0 ± 9.3	2.54 ± 0.37
6	5.39 ± 0.83	90.8 ± 10.3	2.85 ± 0.18

Table A.35. Mechanical properties of transverse 30% CF/PA6 composite specimens over 6 weeks of immersion in antifreeze at 70°C.

t (wk)	E (GPa)	UTS (MPa)	ε_b (%)
0	6.53 ± 0.80	96.4 ± 7.0	2.03 ± 0.27
1	6.89 ± 1.43	103.0 ± 32.8	2.28 ± 0.10
2	7.47 ± 1.18	96.5 ± 31.8	1.73 ± 0.50
3	5.96 ± 0.76	78.8 ± 7.1	1.91 ± 0.12
4	5.60 ± 0.69	72.9 ± 18.1	1.86 ± 0.24
5	5.16 ± 0.79	82.5 ± 19.7	1.98 ± 0.26
6	5.10 ± 0.83	53.3 ± 27.3	1.88 ± 0.31

Table A.36. Mechanical properties of transverse 30% CF/PA6 composite specimens over 6 weeks of immersion in brake fluid at 70°C.

t (wk)	E (GPa)	UTS (MPa)	ε_b (%)
0	6.53 ± 0.80	96.4 ± 7.0	2.03 ± 0.27
1	8.21 ±3.20	137.1 ± 77.6	2.52 ± 0.60
2	7.71 ± 0.80	107.7 ± 14.4	2.04 ± 0.06
3	9.48 ± 1.78	136.9 ± 51.1	1.79 ± 0.39
4	8.41 ± 1.34	113.9 ± 22.0	1.77 ± 0.13
5	8.72 ± 0.52	122.1 ± 5.0	1.78 ± 0.06

6	8.09 ± 0.35	97.4 ± 21.3	1.65 ± 0.21

Table A.37. Mechanical properties of transverse 30% CF/PA6 composite specimens over 6 weeks of immersion in powersteering fluid at 70°C.

t (wk)	E (GPa)	UTS (MPa)	ε_b (%)
0	6.53 ± 0.80	96.4 ± 7.0	2.03 ± 0.27
1	9.00 ± 0.97	135.6 ± 30.2	2.50 ± 0.41
2	7.48 ± 0.65	113.3 ± 27.8	2.17 ± 0.43
3	7.75 ± 0.70	95.9 ± 24.5	1.57 ± 0.32
4	8.88 ± 1.04	122.2 ± 13.1	1.74 ± 0.03
5	8.86 ± 1.17	128.9 ± 11.5	1.86 ± 0.05
6	10.25 ± 3.39	126.2 ± 65.2	1.69 ± 0.49

Table A.38. Mechanical properties of transverse 30% CF/PA6 composite specimens over 6 weeks of immersion in SAE 5W-30 motor oil at 70°C.

t (wk)	E (GPa)	UTS (MPa)	ε_b (%)
0	6.53 ± 0.80	96.4 ± 7.0	2.03 ± 0.27
1	8.23 ± 0.56	123.7 ± 5.9	2.28 ± 0.25
2	7.97 ± 0.64	112.5 ± 14.3	1.82 ± 0.15
3	10.00 ± 1.73	136.4 ± 29.9	1.66 ± 0.21
4	8.40 ± 1.03	113.6 ± 7.7	1.57 ± 0.13
5	9.30 ± 0.68	118.8 ± 10.2	1.41 ± 0.09
6	8.27 ± 1.43	105.8 ± 16.1	1.41 ± 0.00

Table A.39. Mechanical properties of transverse 30% CF/PA6 composite specimens over 6 weeks of immersion in windshield washer fluid at 70°C.

t (wk)	E (GPa)	UTS (MPa)	ε_b (%)
0	6.53 ± 0.80	96.4 ± 7.0	2.03 ± 0.27

1	4.90 ± 0.85	72.7 ± 6.6	2.80 ± 0.35
2	5.11 ± 0.71	67.1 ± 12.1	2.86 ± 0.45
3	4.52 ± 1.27	64.2 ± 11.7	2.66 ± 0.32
4	3.89 ± 0.87	49.8 ± 7.2	2.68 ± 0.57
5	4.76 ± 0.28	60.1 ± 5.1	2.47 ± 0.37
6	5.06 ± 0.58	66.9 ± 13.2	2.25 ± 0.18

Table A.40. Mechanical properties of transverse 30% CF/PA6 composite specimens over 6 weeks of immersion in E-20 gasoline at 50°C.

t (wk)	E (GPa)	UTS (MPa)	ε_b (%)
0	6.53 ± 0.80	96.4 ± 7.0	2.03 ± 0.27
1	6.21 ± 0.78	86.7 ± 15.2	1.93 ± 0.07
2	6.03 ± 0.96	74.4 ± 10.1	1.96 ± 0.67
3	5.97 ± 1.08	76.8 ± 24.4	1.71 ± 0.16
4	6.52 ± 0.70	85.5 ± 5.1	1.86 ± 0.29
5	6.52 ± 1.36	93.0 ± 23.3	2.17 ± 0.26
6	5.27 ± 0.51	65.9 ± 19.2	2.40 ± 0.88

Table A.41. Mechanical properties of transverse 50% CF/PA6 composite specimens over 6 weeks of immersion in antifreeze at 70°C.

t (wk)	E (GPa)	UTS (MPa)	ε_b (%)
0	8.36 ± 0.32	78.3 ± 9.2	1.27 ± 0.10
1	7.46 ± 0.58	65.7 ± 2.2	1.21 ± 0.16
2	7.45 ± 0.08	63.0 ± 5.3	1.20 ± 0.15
3	7.80 ± 1.16	63.2 ± 10.5	1.22 ± 0.06
4	6.58 ± 0.96	53.9 ± 9.73	1.18 ± 0.07
5	7.25 ± 0.41	64.6 ± 6.27	1.68 ± 0.98

6	6.81 ± 0.82	57.7 ± 5.9	1.49 ± 0.11

Table A.42. Mechanical properties of transverse 50% CF/PA6 composite specimens over 6 weeks of immersion in brake fluid at 70°C.

t (wk)	E (GPa)	UTS (MPa)	ε_b (%)
0	8.36 ± 0.32	78.3 ± 9.2	1.27 ± 0.10
1	8.42 ± 0.53	69.3 ± 4.7	1.32 ± 0.19
2	8.34 ± 0.34	82.5 ± 8.3	1.58 ± 0.36
3	8.38 ± 0.80	73.9 ± 8.8	1.24 ± 0.09
4	8.87 ± 0.51	75.0 ± 3.3	1.15 ± 0.10
5	8.22 ± 0.30	69.3 ± 10.9	1.14 ± 0.27
6	8.46 ± 0.45	65.8 ± 5.6	1.26 ± 0.40

Table A.43. Mechanical properties of transverse 50% CF/PA6 composite specimens over 6 weeks of immersion in powersteering fluid at 70°C.

t (wk)	E (GPa)	UTS (MPa)	ε_b (%)
0	8.36 ± 0.32	78.3 ± 9.2	1.27 ± 0.10
1	9.38 ± 0.25	78.4 ± 15.4	1.50 ± 0.55
2	8.83 ± 0.31	84.1 ± 17.0	1.54 ± 0.32
3	9.62 ± 0.01	84.8 ± 10.2	1.14 ± 0.15
4	9.58 ± 0.72	77.3 ± 9.1	1.05 ± 0.13
5	9.68 ± 0.13	73.9 ± 18.6	1.01 ± 0.21
6	10.77 ± 1.28	96.2 ± 15.6	1.25 ± 0.21

Table A.44. Mechanical properties of transverse 50% CF/PA6 composite specimens over 6 weeks of immersion in SAE 5W-30 motor oil at 70°C.

t (wk)	E (GPa)	UTS (MPa)	ε_b (%)
0	8.36 ± 0.32	78.3 ± 9.2	1.27 ± 0.10

1	8.87 ± 0.71	90.5 ± 15.4	1.62 ± 0.15
2	9.79 ± 0.49	91.1 ± 5.1	1.26 ± 0.11
3	10.84 ± 0.59	83.9 ± 9.4	1.00 ± 0.25
4	9.96 ± 0.26	86.2 ± 1.2	1.18 ± 0.04
5	10.08 ± 0.27	68.9 ± 16.6	1.01 ± 0.14
6	8.87 ± 0.81	90.5 ± 11.1	1.62 ± 0.12

Table A.45. Mechanical properties of transverse 50% CF/PA6 composite specimens over 6 weeks of immersion in windshield washer fluid at 70°C.

t (wk)	E (GPa)	UTS (MPa)	ε_b (%)
0	8.36 ± 0.32	78.3 ± 9.2	1.27 ± 0.10
1	4.39 ± 0.78	45.7 ± 6.8	2.16 ± 0.27
2	5.16 ± 0.27	53.9 ± 7.2	2.09 ± 0.35
3	5.43 ± 0.44	51.2 ± 8.4	1.83 ± 0.05
4	5.27 ± 0.18	51.4 ± 6.5	1.87 ± 0.40
5	5.30 ± 0.82	45.6 ± 1.7	1.71 ± 0.34
6	5.28 ± 0.62	54.4 ± 11.2	2.18 ± 0.74

Table A.46. Mechanical properties of transverse 50% CF/PA6 composite specimens over 6 weeks of immersion in E-20 gasoline at 50°C.

t (wk)	E (GPa)	UTS (MPa)	ε_b (%)
0	8.36 ± 0.32	78.3 ± 9.2	1.27 ± 0.10
1	7.69 ± 0.43	64.4 ± 8.4	1.14 ± 0.20
2	8.22 ± 0.73	63.6 ± 6.2	1.13 ± 0.16
3	7.73 ± 0.98	63.2 ± 13.0	1.15 ± 0.17
4	7.45 ± 0.90	61.5 ± 8.4	1.19 ± 0.14
5	7.03 ± 0.45	58.5 ± 5.5	1.20 ± 0.24

6	7.34 ± 0.69	66.3 ± 23.5	1.94 ± 0.82

Table A.47. Mechanical properties of 35% (F) CF/PA6/6 composite specimens over 10 weeks of immersion in windshield washer fluid at 23°C.

t (wk)	E (GPa)	UTS (MPa)	ε_b (%)
0	23.09 ± 2.33	195.5 ± 32.6	0.97 ± 0.15
1	22.39 ± 2.94	204.3 ± 18.9	1.42 ± 0.29
2	20.15 ± 1.50	200.3 ± 17.6	1.22 ± 0.18
3	20.31 ± 2.12	190.0 ± 21.8	1.06 ± 0.08
5	17.99 ± 0.16	175.0 ± 4.6	1.16 ± 0.06
10	16.62 ± 1.22	154.8 ± 6.9	1.08 ± 0.14

Table A.48. Mechanical properties of 35% (F) CF/PA6/6 composite specimens over 10 weeks of immersion in E-20 gasoline at 23°C.

t (wk)	E (GPa)	UTS (MPa)	ε_b (%)
0	23.09 ± 2.33	195.5 ± 32.6	0.97 ± 0.15
1	23.26 ± 0.76	202.0 ± 17.5	1.53 ± 0.86
2	21.92 ± 0.91	213.3 ± 17.9	1.62 ± 0.25
3	23.03 ± 2.37	230.0 ± 15.6	1.55 ± 0.43
5	19.88 ± 3.69	184.7 ± 59.5	1.02 ± 0.19
10	22.78 ± 1.39	235.0 ± 16.2	1.18 ± 0.13

Table A.49. Mechanical properties of 45% (F) CF/PA6/6 composite specimens over 10 weeks of immersion in windshield washer fluid at 23°C.

t (wk)	E (GPa)	UTS (MPa)	ε_b (%)
0	29.48 ± 3.65	164.0 ± 3.8	0.64 ± 0.12
1	29.44 ± 1.94	126.7 ± 33.8	0.78 ± 0.32
2	25.74 ± 2.43	149.0 ± 51.7	0.87 ± 0.44

3	26.33 ± 1.69	169.0 ± 11.3	0.84 ± 0.06
5	21.72 ± 3.26	151.7 ± 39.1	0.90 ± 0.15
10	16.79 ± 7.83	111.5 ± 72.1	0.88 ± 0.13

Table A.50. Mechanical properties of 45% (F) CF/PA6/6 composite specimens over 10 weeks of immersion in E-20 gasoline at 23°C.

t (wk)	E (GPa)	UTS (MPa)	ε_b (%)
0	29.48 ± 3.65	164.0 ± 3.8	0.64 ± 0.12
1	31.01 ± 1.38	169.0 ± 16.1	1.03 ± 0.17
2	29.19 ± 5.41	158.0 ± 35.4	0.99 ± 0.35
3	30.61 ± 1.03	174.0 ± 11.5	1.08 ± 0.29
5	27.52 ± 1.71	183.3 ± 17.1	0.78 ± 0.06
10	26.85 ± 1.55	156.5 ± 16.4	0.69 ± 0.06

Table A.51. Mechanical properties of fibre crossflow (left) and flow direction (right) 40% CF/PA6/6 composite specimens over 5 weeks of immersion in antifreeze at 23°C.

t (wk)	E (GPa)	UTS (MPa)	ε_b (%)	E (GPa)	UTS (MPa)	ε_b (%)
0	10.46 ± 1.21	94.0 ± 14.2	0.65 ± 0.14	28.81 ± 2.12	186.0 ± 0.59	0.83 ± 0.07
1	10.94 ± 2.15	99.6 ± 21.1	0.67 ± 0.08	23.60 ± 7.88	192.7 ± 42.4	1.14 ± 0.14
2	10.75 ± 1.57	102.2 ± 51.3	0.68 ± 0.28	27.71 ± 0.84	219.0 ± 10.4	1.11 ± 0.03
3	10.94 ± 1.15	106.7 ± 7.4	0.72 ± 0.04	24.04 ± 0.89	206.0 ± 23.3	1.15 ± 0.18
5	9.77 ± 1.68	117.4 ± 16.0	0.88 ± 0.06	24.71 ± 3.14	207.4 ± 23.6	1.10 ± 0.04

Table A.52. Mechanical properties of fibre crossflow (left) and flow direction (right) 40% CF/PA6/6 composite specimens over 5 weeks of immersion in brake fluid at 23°C.

t (wk)	E (GPa)	UTS (MPa)	ε_b (%)	E (GPa)	UTS (MPa)	ε_b (%)
0	10.46 ± 1.21	94.0 ± 14.2	0.65 ± 0.14	28.81 ± 2.12	186.0 ± 0.59	0.83 ± 0.07
1	10.40 ± 0.16	110.2 ± 13.7	0.81 ± 0.11	28.10 ± 2.26	224.3 ± 22.9	1.16 ± 0.10

2	11.07 ± 1.55	123.7 ± 18.0	0.82 ± 0.04	31.43 ± 4.04	234.0 ± 13.9	1.09 ± 0.18
3	10.41 ± 1.04	102.2 ± 14.9	0.66 ± 0.04	26.32 ± 2.47	215.9 ± 35.9	1.09 ± 0.07
5	10.15 ± 0.97	115.6 ± 28.3	0.89 ± 0.23	25.30 ± 2.31	198.9 ± 10.1	1.01 ± 0.06

Table A.53. Mechanical properties of fibre crossflow (left) and flow direction (right) 40% CF/PA6/6 composite specimens over 5 weeks of immersion in powersteering fluid at 23°C.

t (wk)	E (GPa)	UTS (MPa)	ε_b (%)	E (GPa)	UTS (MPa)	ε_b (%)
0	10.46 ± 1.21	94.0 ± 14.2	0.65 ± 0.14	28.81 ± 2.12	186.0 ± 0.59	0.83 ± 0.07
1	10.65 ± 1.96	108.3 ± 6.5	0.72 ± 0.09	28.05 ± 4.96	208.7 ± 27.3	1.00 ± 0.11
2	9.68 ± 0.90	111.2 ± 16.5	0.84 ± 0.13	27.40 ± 2.31	221.3 ± 31.8	1.17 ± 0.20
3	11.54 ± 1.55	131.3 ± 35.4	0.83 ± 0.18	26.84 ± 1.39	222.5 ± 41.5	1.08 ± 0.23
5	10.43 ± 0.83	105.5 ± 39.2	0.70 ± 0.25	28.15 ± 0.69	246.8 ± 24.9	1.19 ± 0.17

Table A.54. Mechanical properties of fibre crossflow (left) and flow direction (right) 40% CF/PA6/6 composite specimens over 5 weeks of immersion in SAE 5W-30 motor oil at 23°C.

t (wk)	E (GPa)	UTS (MPa)	ε_b (%)	E (GPa)	UTS (MPa)	ε_b (%)
0	10.46 ± 1.21	94.0 ± 14.2	0.65 ± 0.14	28.81 ± 2.12	186.0 ± 0.59	0.83 ± 0.07
1	11.84 ± 0.92	100.6 ± 24.2	0.67 ± 0.15	29.10 ± 3.11	211.3 ± 43.5	0.92 ± 0.19
2	10.63 ± 1.42	112.8 ± 15.1	0.80 ± 0.09	29.39 ± 1.31	228.0 ± 19.1	1.09 ± 0.09
3	10.49 ± 1.53	108.9 ± 12.1	0.76 ± 0.16	27.29 ± 1.03	237.5 ± 7.2	1.12 ± 0.12
5	10.12 ± 1.43	103.5 ± 10.7	0.79 ± 0.19	26.33 ± 1.02	216.5 ± 11.1	1.10 ± 0.04

Table A.55. Mechanical properties of fibre crossflow (left) and flow direction (right) 40% CF/PA6/6 composite specimens over 10 weeks of immersion in windshield washer fluid at 23°C.

t (wk)	E (GPa)	UTS (MPa)	ε_b (%)	E (GPa)	UTS (MPa)	ε_b (%)
0	10.46 ± 1.21	94.0 ± 14.2	0.65 ± 0.14	28.81 ± 2.12	186.0 ± 0.59	0.83 ± 0.07
1	8.74 ± 0.50	95.4 ± 17.2	0.83 ± 0.15	27.70 ± 3.55	155.7 ± 27.8	1.11 ± 0.20
2	7.68 ± 0.26	90.6 ± 8.2	0.98 ± 0.11	25.67 ± 1.40	167.3 ± 9.0	1.07 ± 0.12

3	6.84 ± 0.17	78.0 ± 7.1	0.96 ± 0.16	25.79 ± 0.50	163.3 ± 14.8	0.95 ± 0.27
5	6.56 ± 0.99	74.1 ± 9.3	1.11 ± 0.29	21.73 ± 0.33	167.7 ± 6.8	1.06 ± 0.10
10	X	X	X	22.25 ± 2.07	154.3 ± 18.6	0.94 ± 0.11

Table A.56. Mechanical properties of fibre crossflow (left) and flow direction (right) 40% CF/PA6/6 composite specimens over 10 weeks of immersion in E-20 gasoline at 23°C.

t (wk)	E (GPa)	UTS (MPa)	ε_b (%)	E (GPa)	UTS (MPa)	ε_b (%)
0	10.46 ± 1.21	94.0 ± 14.2	0.65 ± 0.14	28.81 ± 2.12	186.0 ± 0.59	0.83 ± 0.07
1	10.06 ± 0.24	115.0 ± 6.2	0.81 ± 0.05	30.31 ± 1.53	185.0 ± 20.0	1.25 ± 0.22
2	9.74 ± 0.47	96.5 ± 14.4	0.69 ± 0.10	28.48 ± 3.14	174.3 ± 85.1	0.99 ± 0.57
3	10.20 ± 0.41	109.8 ± 6.9	0.76 ± 0.09	32.05 ± 1.17	208.0 ± 32.9	1.04 ± 0.30
5	9.30 ± 1.01	97.7 ± 11.9	0.71 ± 0.09	27.83 ± 4.35	182.7 ± 26.7	0.89 ± 0.10
10	X	X	X	30.60 ± 2.19	214.2 ± 13.2	0.92 ± 0.04

Table A.57. Mechanical properties of fibre crossflow (left) and flow direction (right) 40% CF/PA6/6 composite specimens over 6 weeks of immersion in SAE 5W-30 motor oil at 70°C.

t (wk)	E (GPa)	UTS (MPa)	ε_b (%)	E (GPa)	UTS (MPa)	ε_b (%)
0	10.46 ± 1.21	94.0 ± 14.2	0.65 ± 0.14	28.81 ± 2.12	186.0 ± 0.59	0.83 ± 0.07
1	10.27 ± 0.84	102.6 ± 7.3	0.73 ± 0.05	25.88 ± 3.82	212.7 ± 8.0	0.98 ± 0.10
2	10.13 ± 0.55	94.6 ± 13.9	0.65 ± 0.09	26.38 ± 1.95	212.7 ± 21.1	1.00 ± 0.16
3	10.26 ± 1.92	106.4 ± 15.8	0.76 ± 0.16	25.56 ± 1.61	225.7 ± 21.0	1.02 ± 0.18
4	10.62 ± 1.31	105.8 ± 18.2	0.67 ± 0.09	26.20 ± 1.44	176.9 ± 12.6	0.89 ± 0.09
5	9.37 ± 0.91	98.5 ± 24.0	0.75 ± 0.15	26.53 ± 0.59	223.6 ± 15.7	1.11 ± 0.08
6	10.91 ± 0.37	101.7 ± 19.6	0.66 ± 0.16	26.23 ± 0.71	185.2 ± 8.5	0.89 ± 0.04

Table A.58. Mechanical properties of fibre crossflow (left) and flow direction (right) 40% CF/PA6/6 composite specimens over 6 weeks of immersion in windshield washer fluid at 70°C.

t (wk)	E (GPa)	UTS (MPa)	ε_b (%)	E (GPa)	UTS (MPa)	ε_b (%)

0	10.46 ± 1.21	94.0 ± 14.2	0.65 ± 0.14	28.81 ± 2.12	186.0 ± 0.59	0.83 ± 0.07
1	5.48 ± 0.35	69.1 ± 2.2	1.18 ± 0.11	17.05 ± 2.06	126.7 ± 30.4	1.00 ± 0.12
2	5.42 ± 0.76	60.2 ± 4.9	1.03 ± 0.09	17.82 ± 0.78	147.7 ± 9.5	1.08 ± 0.09
3	6.01 ± 1.17	65.3 ± 10.3	0.99 ± 0.17	18.27 ± 0.72	138.3 ± 22.2	0.97 ± 0.16
4	5.60 ± 0.59	52.6 ± 30.6	0.88 ± 0.42	17.12 ± 2.81	115.7 ± 43.8	0.86 ± 0.29
5	6.92 ± 1.03	70.9 ± 12.0	0.83 ± 0.12	18.45 ± 0.85	131.9 ± 1.9	1.01 ± 0.04
6	5.88 ± 1.92	52.6 ± 15.0	0.82 ± 0.12	16.80 ± 0.99	131.1 ± 6.2	1.02 ± 0.02

Table A.59. Mechanical properties of fibre crossflow (left) and flow direction (right) 40% CF/PA6/6 composite specimens over 6 weeks of immersion in E-20 gasoline at 50°C.

t (wk)	E (GPa)	UTS (MPa)	ε_b (%)	E (GPa)	UTS (MPa)	ε_b (%)
0	10.46 ± 1.21	94.0 ± 14.2	0.65 ± 0.14	28.81 ± 2.12	186.0 ± 0.59	0.83 ± 0.07
1	11.21 ± 1.06	108.3 ± 8.0	0.78 ± 0.05	27.04 ± 0.77	224.7 ± 31.8	1.11 ± 0.17
2	11.30 ± 0.91	113.9 ± 45.4	0.79 ± 0.29	29.74 ± 3.90	225.0 ± 14.7	1.24 ± 0.20
3	9.93 ± 0.91	106.3 ± 14.7	0.78 ± 0.08	24.27 ± 3.61	243.0 ± 12.3	1.22 ± 0.05
4	9.83 ± 0.57	99.2 ± 17.5	0.72 ± 0.14	24.53 ± 1.98	214.4 ± 24.4	1.16 ± 0.11
5	10.28 ± 0.57	104.3 ± 7.8	0.63 ± 0.03	24.05 ± 1.58	201.7 ± 28.1	1.11 ± 0.11
6	10.73 ± 0.41	112.3 ± 11.9	0.78 ± 0.02	25.94 ± 1.41	230.2 ± 11.9	0.78 ± 0.02